



**© Copyright by Ammar M. Aboalsaud 2016**  
**All Rights Reserved**

# **IMPACT OF POLYMER-GRAFTED NANOPARTICLES ON INTERFACIAL TENSION**

A Thesis

Presented to

the Faculty of the Department of Chemical and Biomolecular Engineering

University of Houston

In Partial Fulfillment

of the Requirements for the Degree

Master of Science

in Chemical Engineering

by

Ammar M. Aboalsaud

May 2016

# **Impact of Polymer-Grafted Nanoparticles on Interfacial Tension**

---

**Ammar M. Aboalsaud**

Approved:

---

Chair of the Committee:  
Dr. Ramanan Krishnamoorti,  
Professor, Department of Chemical  
and Biomolecular Engineering

Committee Members:

---

Dr. Megan Robertson  
Assistant Professor, Department of  
Chemical and Biomolecular  
Engineering

---

Dr. Haleh Ardebili,  
Assistant Professor, Department of  
Mechanical Engineering

---

Dr. Suresh K. Khator  
Associate Dean, Cullen  
College of Engineering

---

Dr. Michael P. Harold,  
Chair, Department of Chemical and  
Biomolecular Engineering

## Acknowledgments

First of all, I would like to express my deepest and sincerest gratitude to my loving and supportive family, without whom I would never have made it this far. At the top of the list are my parents, whom I thank for all the emotional, mental, and financial support throughout the years. I would also like to thank all my brothers, my sisters, my lovely nephew, and my beautiful niece. They have stood by me, helping me without any hesitation whenever I needed, no matter the situation. They have provided me with the courage and strength all those years. Thank you all for your unconditional love and support.

I would like to express my sincerest appreciation to my advisor, Professor Ramanan Krishnamoorti for all his encouragement and guidance. I also thank Professor Haleh Ardebili for serving on my committee, and Professor Megan Robertson for both serving on my committee and allowing me to use the equipment in her lab. Likewise, I thank Professor Gila Stein and Professor Jeffrey Rimer for allowing me to use the equipment in their labs.

Furthermore, I am grateful to all my research group members, both past and present, for all their help and support, as well as all their scientific discussions during my studies. Thank you Daehak, Ryan, Kim, Jack, Chinedu, Jialin, and Ruixuan. Moreover, I thank all my friends at the University of Houston for making it that much more fun to be there.

Last but not least, I would like to thank all my friends in Houston, both the ones still here and the ones who left already, who are truly a family to me. Thanks to you, Houston has become a second home to me.

# **IMPACT OF POLYMER-GRAFTED NANOPARTICLES ON INTERFACIAL TENSION**

An Abstract

of a

A Thesis

Presented to

the Faculty of the Department of Chemical and Biomolecular Engineering

University of Houston

In Partial Fulfillment

of the Requirements for the Degree

Master of Science

in Chemical Engineering

by

Ammar M. Aboalsaud

May 2016

## ABSTRACT

Emulsifiers have been extensively studied for various applications, the most common of which is possibly enhanced oil recovery (EOR). The use of polymer-grafted nanoparticles as emulsifiers has been gaining interest for their impressive interfacial tension (IFT) reduction capabilities due to their high interfacial activity. This thesis investigates the impact of polymer-grafted nanoparticles on the interfacial tension between alkane oils and water.

Two different types of polymer-grafted nanoparticles have been investigated in this study. The first is the SiO<sub>2</sub>-POEOMA, which is a type of hydrophilic homopolymer-grafted nanoparticles. The second is the SiO<sub>2</sub>-P(MA-*b*-OEOMA), which is a type of amphiphilic block copolymer-grafted nanoparticles.

The study concluded that both classes were able to reduce the interfacial tension to the same extent. This is due to the lack of interactions between PMA and either side of the interface because the PMA block is both hydrophobic and lyophobic to alkane oils, which caused the amphiphilic block copolymer to behave as hydrophilic homopolymer at the interface.

# Table of Contents

Acknowledgments.....	v
ABSTRACT .....	vii
Table of Contents .....	viii
List of Figures .....	xi
List of Tables.....	xvi
List of Schemes .....	xvii
<b>Chapter 1 Introduction .....</b>	<b>1</b>
<b>1.1 BACKGROUND.....</b>	<b>1</b>
<i>1.1.1 Emulsions.....</i>	<i>1</i>
<i>1.1.2 Colloidal Silica .....</i>	<i>3</i>
<i>1.1.3 Homopolymer Chains .....</i>	<i>8</i>
<i>1.1.4 Amphiphilic Block Copolymers.....</i>	<i>11</i>
<i>1.1.5 Atomic Transfer Radical Polymerization, ATRP .....</i>	<i>14</i>
<b>1.2 MOTIVATION.....</b>	<b>16</b>
<b>1.3 PREVIOUS WORK .....</b>	<b>18</b>
<b>1.4 OBJECTIVE .....</b>	<b>21</b>
<b>Chapter 2 Experimental Methods.....</b>	<b>24</b>
<b>2.1 PREPARATION OF POLYMER-GRAFTED NANOPARTICLES .....</b>	<b>24</b>
<i>2.1.1 Synthesis of 1-Chlorodimethylsilyl Propyl 2-Bromo-2-Methylpropionate.....</i>	<i>24</i>
2.1.1.1 Materials.....	24
2.1.1.2 Method .....	24
<i>2.1.2 Synthesis of 2-Bromoisobutyrate Initiator Functional Silica Nanoparticles .....</i>	<i>25</i>
2.1.2.1 Materials.....	25
2.1.2.2 Method .....	26

2.1.3 Synthesis of SiO <sub>2</sub> -POEOMA Hybrid Nanoparticles by Surface Initiated ATRP .....	28
2.1.3.1 Materials.....	28
2.1.3.2 Method .....	28
2.1.4 Synthesis of SiO <sub>2</sub> -PMA Hybrid Nanoparticles by Surface Initiated ATRP .....	30
2.1.4.1 Materials.....	30
2.1.4.2 Method .....	30
2.1.5 Synthesis of SiO <sub>2</sub> -P(MA- <i>b</i> -OEOMA) Hybrid Nanoparticles by POEOMA Chain Extension from SiO <sub>2</sub> -PMA Hybrid Nanoparticles.....	32
2.1.5.1 Materials.....	32
2.1.5.2 Method .....	32
<b>2.2 CHARACTERIZATION OF THE HYBRID NANOPARTICLES.....</b>	<b>34</b>
2.2.1 Gel Permeation Chromatography (GPC).....	34
2.2.1.1 Materials.....	34
2.2.1.2 Method .....	35
2.2.2 Thermal Gravimetric Analysis (TGA).....	37
2.2.3 Grafting Density .....	37
2.2.4 Small Angle X-Ray Scattering (SAXS) .....	38
2.2.5 Dynamic Light Scattering (DLS).....	39
<b>2.3 ANALYSIS OF OIL-WATER EMULSION .....</b>	<b>41</b>
<b>Chapter 3 Hydrophilic Homopolymer-Grafted Nanoparticles .....</b>	<b>46</b>
<b>3.1 METHODOLOGY .....</b>	<b>46</b>
3.1.1 Materials.....	46
3.1.2 Preparation.....	46
<b>3.2 CHARACTERIZATION .....</b>	<b>46</b>
3.2.1 Gel Permeation Chromatography (GPC).....	46
3.2.2 Thermal Gravimetric Analysis (TGA).....	49
3.2.3 Grafting Density .....	51
3.2.4 Small Angle X-Ray Scattering (SAXS) .....	51

3.2.5 <i>Dynamic Light Scattering (DLS)</i> .....	53
<b>3.3 EMULSION ANALYSIS</b> .....	57
<b>3.4 SUMMARY AND RESULTS</b> .....	60
<b>Chapter 4 Amphiphilic Block Copolymer-Grafted Nanoparticles</b> .....	<b>70</b>
<b>4.1 METHODOLOGY</b> .....	70
4.1.1 <i>Materials</i> .....	70
4.1.2 <i>Preparation</i> .....	70
<b>4.2 CHARACTERIZATION</b> .....	71
4.2.1 <i>Gel Permeation Chromatography (GPC)</i> .....	71
4.2.2 <i>Thermal Gravimetric Analysis (TGA)</i> .....	73
4.2.3 <i>Grafting Density</i> .....	75
4.2.4 <i>Small Angle X-Ray Scattering (SAXS)</i> .....	75
4.2.5 <i>Dynamic Light Scattering (DLS)</i> .....	77
<b>4.3 EMULSION ANALYSIS</b> .....	80
<b>4.4 SUMMARY AND RESULTS</b> .....	82
<b>Chapter 5 Conclusion</b> .....	<b>89</b>
<b>5.1 SUMMARY AND CONCLUSION</b> .....	89
<b>5.2 FUTURE WORK</b> .....	94
<b>References</b> .....	<b>97</b>

## List of Figures

Figure 1. 1: Formation of emulsions decreases the size of the droplets, thus increasing the interfacial area between the two fluids dramatically. ....	1
Figure 1. 2: The grafting of polymer chains on the surface of colloidal silica cores to synthesize hybrid nanoparticles through the process of atomic transfer radical polymerization, ATRP. ....	2
Figure 1. 3: Pickering emulsion created by the packing of solid spherical colloids at the interface between liquid A and liquid B. ....	3
Figure 1. 4: A spherical particle situated at the interface of oil and water. ....	7
Figure 1. 5: Two hybrid nanoparticles getting close together, which would cause the chains to overlap and interact causing an increase in the medium's viscosity. ....	9
Figure 1. 6: The geometry of a Janus particle at the interface between oil and water. <sup>14</sup> ..	12
Figure 1. 7: A computer simulation of an amphiphilic block copolymer-grafted nanoparticle dispersed in water (left) and at the interface between oil and water (right): the yellow part corresponds to the hydrophobic polymer block while the blue part corresponds to the hydrophilic polymer block. <sup>15</sup> .....	14
Figure 2. 1: General schematic depicting the separation based on size in a gel permeation chromatography column. ....	35
Figure 2. 2: General schematic depicting the cleaving of the polymer chains using HF.	36
Figure 2. 3: Optical contact angle instrument for interfacial tension measurements showing a pendent drop of hybrid nanoparticles solution suspended in Hexane-filled cuvette in front of a camera that is used to take the pictures. ....	42
Figure 2. 4: A picture of pendant drops of SiO <sub>2</sub> -POEOMA at: (a) 0 and (b) 30 minutes.	42

Figure 2. 5: The definition of the diameters used in the empirical equation for the pendant drop method. <sup>43</sup> .....	45
Figure 3. 1: GPC results showing SEC curve for sample A. ....	47
Figure 3. 2: GPC results showing SEC curve for sample B. ....	48
Figure 3. 3: GPC results showing SEC curve for sample C. ....	48
Figure 3. 4: TGA results showing weight change as temperature is increasing from 25 °C to 800 °C for sample A. ....	49
Figure 3. 5: TGA results showing weight change as temperature is increasing from 25 °C to 800 °C for sample B. ....	50
Figure 3. 6: TGA results showing weight change as temperature is increasing from 25 °C to 800 °C for sample C. ....	50
Figure 3. 7: SAXS results showing the scattering intensity as a function of the scattering vector for sample A.....	52
Figure 3. 8: SAXS results showing the scattering intensity as a function of the scattering vector for sample B.....	52
Figure 3. 9: SAXS results showing the scattering intensity as a function of the scattering vector for sample C.....	53
Figure 3. 10: DLS results showing scattering intensity as a function of time for sample A; used for fitting in the autocorrelation function. ....	54
Figure 3. 11: DLS results showing scattering intensity as a function of time for sample B; used for fitting in the autocorrelation function. ....	54
Figure 3. 12: DLS results showing scattering intensity as a function of time for sample C; used for fitting in the autocorrelation function. ....	55

Figure 3. 13: Plotting gamma vs the squared of the scattering vector to get the diffusivity of sample A. ....	56
Figure 3. 14: Plotting gamma vs the squared of the scattering vector to get the diffusivity of sample B. ....	56
Figure 3. 15: Plotting gamma vs the squared of the scattering vector to get the diffusivity of sample C. ....	57
Figure 3. 16: The reduction of the interfacial tension between Hexane and DI-Water using the hybrid nanoparticles of sample A. ....	58
Figure 3. 17: The reduction of the interfacial tension between Hexane and DI-Water using the hybrid nanoparticles of sample B.....	58
Figure 3. 18: The reduction of the interfacial tension between Hexane and DI-Water using the hybrid nanoparticles of sample C.....	59
Figure 3. 19: The polymer weight fraction is increasing as the molecular weight of the grafted polymer chains is increased.....	61
Figure 3. 20: The increase in the inverse of amount of residue with molecular weight of grafted polymer chains is linear. This linearity is indicative of the similar grafting densities in all three samples. ....	62
Figure 3. 21: The dry state diameter of the hybrid nanoparticles is increasing as the molecular weight of the grafted polymer chains is increasing. ....	63
Figure 3. 22: The change in the hydrodynamic diameter as we increase the molecular weight of the grafted polymer chains.....	64
Figure 3. 23: A graph showing the largest polymer end-to-end distance and the definition of the angle $\theta$ used in the equation of $R_{\max}$ . <sup>44</sup> ....	66

Figure 3. 24: The effect of the SiO <sub>2</sub> -POEOMA molecular weight (M <sub>n</sub> ) on the reduction of the interfacial tension between Hexane and DI-Water. ....	68
Figure 3. 25: The effect of the hybrid nanoparticle concentration on the stability of the emulsion between Hexane and DI-Water. ....	69
Figure 4. 1: GPC results showing SEC curve for sample D. ....	72
Figure 4. 2: GPC results showing SEC curve for sample E.....	73
Figure 4. 3: TGA results showing weight change as temperature is increased from 25 °C to 800 °C for sample D. ....	74
Figure 4. 4: TGA results showing weight change as temperature is increased from 25 °C to 800 °C for sample E.....	74
Figure 4. 5: SAXS results showing the scattering intensity as a function of the scattering vector for sample D.....	76
Figure 4. 6: SAXS results showing the scattering intensity as a function of the scattering vector for sample E. ....	76
Figure 4. 7: DLS results showing scattering intensity as a function of time for sample D; used for fitting in the autocorrelation function. ....	77
Figure 4. 8: DLS results showing scattering intensity as a function of time for sample E; used for fitting in the autocorrelation function. ....	78
Figure 4. 9: Plotting gamma vs the squared of the scattering vector to get the diffusivity of sample D. ....	79
Figure 4. 10: Plotting gamma vs the squared of the scattering vector to get the diffusivity of sample E. ....	79

Figure 4. 11: The reduction of the interfacial tension between Hexane and DI-Water using the hybrid nanoparticles of sample D. ....	80
Figure 4. 12: The reduction of the interfacial tension between Hexane and DI-Water using the hybrid nanoparticles of sample E.....	81
Figure 4. 13: The polymer weight fraction is increasing as the molecular weight of the grafted polymer chains is increased.....	83
Figure 4. 14: The dry state diameter of the hybrid nanoparticles in increasing as the molecular weight of the grafted polymer chains in increasing. ....	84
Figure 4. 15: The change in the hydrodynamic diameter as we increase the molecular weight of the hydrophilic part of the grafted polymer chains.....	86
Figure 4. 16: The effect of the SiO <sub>2</sub> -P(MA-b-OEOMA) molecular weight (M <sub>n</sub> ) on the reduction of the interfacial tension between Hexane and DI-Water.....	87
Figure 5. 1: A figure comparing the ability of the two different classes of polymer-grafted nanoparticles to reduce the interfacial tension between hexane and water. ....	92

## List of Tables

Table 3. 1: Table summarizing the characterization of the SiO <sub>2</sub> -POEOMA samples.....	60
Table 3. 2: Table summarizing the IFT data of the SiO <sub>2</sub> -POEOMA samples.....	68
Table 4. 1: Table summarizing the characterization of the SiO <sub>2</sub> -P(MA-b-OEOMA) samples. ....	82
Table 4. 2: Table summarizing the IFT data of the SiO <sub>2</sub> -P(MA-b-OEOMA) samples....	88

## List of Schemes

Scheme 2. 1: General scheme for the synthesis reaction of 1-Chlorodimethylsilyl Propyl 2-Bromo-2-Methylpropionate.....	25
Scheme 2. 2: General scheme for the synthesis reaction of 2-Bromoisobutyrate initiator functional silica nanoparticles.....	27
Scheme 2. 3: General scheme for the synthesis reaction of SiO <sub>2</sub> -POEOMA hybrid nanoparticles by surface initiated ATRP.....	29
Scheme 2. 4: General scheme for the synthesis reaction of SiO <sub>2</sub> -PMA hybrid nanoparticles by surface initiated ATRP.....	31
Scheme 2. 5: General scheme for the synthesis reaction of SiO <sub>2</sub> -P(MA-b-OEOMA) hybrid nanoparticles by surface initiated ATRP.....	34

# Chapter 1 Introduction

## 1.1 Background

### 1.1.1 Emulsions

It is a well-known fact that oil and water are immiscible fluids. When the two are mixed, they create a highly unstable emulsion, and they rapidly separate into two distinct phases. This phenomenon is dictated by thermodynamics. During an emulsification process, the interfacial area between the two fluids is increased dramatically due to the decrease in the diameter of the droplets as shown in the figure below.

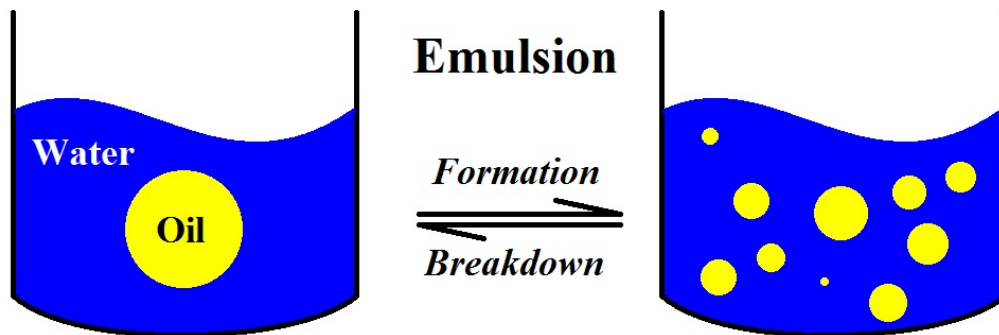


Figure 1. 1: Formation of emulsions decreases the size of the droplets, thus increasing the interfacial area between the two fluids dramatically.

This dramatic increase in the interfacial area, combined with the high interfacial tension between oil and water, increase the interfacial energy. The increase in the interfacial energy, in turn, increases the free energy of emulsion formation according to the Gibbs free energy equation expressed as<sup>1</sup>

$$\Delta G_{form.} = \Delta A\gamma_{12} - T\Delta S, \quad (1.1)$$

where:

$\Delta G_{form.}$  = the change in the free energy of emulsion formation;

$\Delta A$  = the change in the interfacial area;

$\gamma_{12}$  = the interfacial tension between fluids one and two;

$T$  = the temperature of the system; and

$\Delta S$  = the change in the entropy of the system.

Increasing the free energy is a thermodynamically unfavorable process. Therefore, the emulsion between oil and water always automatically breaks down. That is why the introduction of emulsifiers is important to maintain a stable emulsion.<sup>2</sup> This study investigates the effect of a class of emulsifiers known as polymer-grafted nanoparticles. The idea behind this class of emulsifiers is the combination of polymer chains and colloidal silica cores. The figure below shows the grafting of polymer chains on colloidal silica cores to create hybrid nanoparticles.

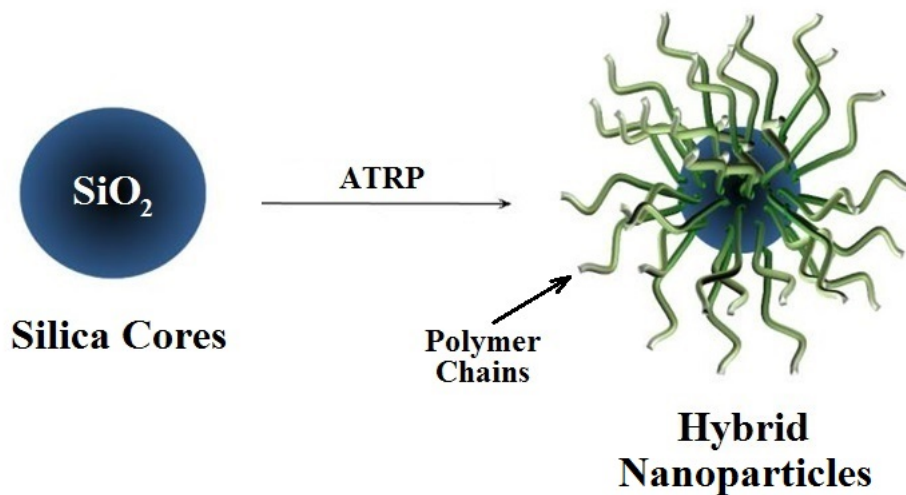
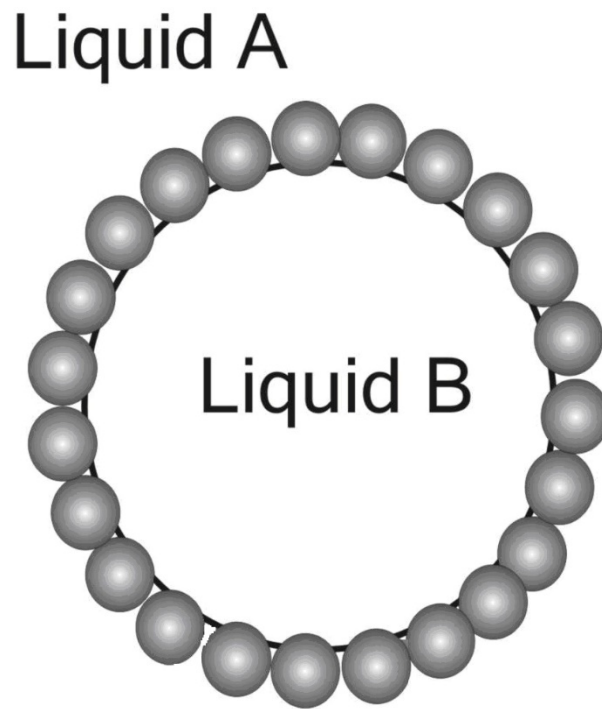


Figure 1. 2: The grafting of polymer chains on the surface of colloidal silica cores to synthesize hybrid nanoparticles through the process of atomic transfer radical polymerization, ATRP.

### 1.1.2 Colloidal Silica

The solid spherical silica cores are used to create a Pickering Emulsion. When those nanoparticles are dissolved in the solution, they travel to the interface between oil and water, where they pack and structure. This packing at the interface lowers the interfacial tension between the two immiscible fluids creating a stable emulsion. Emulsions stabilized by the adsorption of solid colloidal particles at the interface are called Pickering Emulsion, an example of which is shown in the figure below.<sup>3</sup>



*Figure 1. 3: Pickering emulsion created by the packing of solid spherical colloids at the interface between liquid A and liquid B.*

The driving force that causes the travel of those colloidal silica cores from the bulk water phase to the interface is an entropic force. The structuring of the nanoparticles at the interface reduces their number of microstates and possible configurations,  $\Omega$ , thus decreasing the entropy of those particles according to the Boltzmann's entropy equation expressed as<sup>4</sup>

$$S = k_B \ln \Omega, \quad (1.2)$$

where:

$S$  = entropy; and

$k_B$  = Boltzmann's constant.

Although the structuring of those nanoparticles at the interface reduces their entropy, it increases the overall entropy of the system. By structuring at the interface, they are replacing the smaller sized, larger quantity, water molecules that are at the interface. This replacement increases the overall number of microstates and possible configurations, thus, increasing the overall entropy of the system. The increase in the entropy of the system is greater in magnitude than the decrease in the entropy of the nanoparticles. When the overall entropy of the system is increased, the free energy of the system decreases. Therefore, the system's free energy with those colloidal particles situated at the interface is lower than the system's free energy with the colloidal particles situated in the bulk water phase. The increase in the entropy of the system lowers the free energy of the system according to Gibbs free energy equation expressed as

$$\Delta G = \Delta H - T\Delta S, \quad (1.3)$$

where:

$\Delta G$  = the change in the free energy of the system;

$\Delta H$  = the change in the enthalpy of the system;

$\Delta S$  = the change in the entropy of the system; and

$T$  = the temperature of the system.

The increase in the entropy of the system causes a decrease in the free energy of the system. The state of the system with the lower free energy is thermodynamically more favorable than the state of the system with the higher free energy.

When those nanoparticles are driven to structure at the interface due to entropic forces, they reduce the interfacial tension causing a stable Pickering Emulsion between the oil and water. Therefore, the nanoparticles' ability to reduce the interfacial tension relies on how well they move to, and structure at the interface. There are multiple variables that can affect the adsorption of the nanoparticles at the interface, and they are related through the free energy associated with the placement of the nanoparticles at the interface.

The free energy of the particles at the interface,  $F_{P,int}$ , is often described as the difference between the free energy of the system with the particles situated at the interface,  $F_{S,f}$ , and the free energy of the system with the nanoparticles dispersed in the bulk water phase,  $F_{S,i}$  as in<sup>5,6</sup>

$$F_{P,int} = F_{S,f} - F_{S,i}, \quad (1.4)$$

where the subscript “ $P, int$ ” refers to the particle at the interface, the subscript “ $S, f$ ” refers to the final state of the system when the particles situate themselves at the interface, and the subscript “ $S, i$ ” refers to the initial state of the system when the particles are still at the bulk water phase. The  $F_{S,f}$  and  $F_{S,i}$  can be expressed as

$$F_{S,f} = \gamma_{12} A_{12} + \gamma_{P1} A_{P1} + \gamma_{P2} A_{P2} + \tau L + \gamma_{12} A_{st} \text{ and} \quad (1.5)$$

$$F_{S,i} = \gamma_{12} A_{12} + \gamma_{P1} A_P, \quad (1.6)$$

where:

1 = oil;

2 = water;

$P$  = particle;

$\gamma_{ij}$  = the interfacial tension between  $i$  and  $j$ ;

$A_{ij}$  = the contact area between  $i$  and  $j$ ;

$A_{st}$  = the contact area removed by nanoparticles from original interface;

$A_P$  = the particle's surface area;

$\tau$  = the line tension; and

$L$  = length of the three-phase contact line.

Taking the difference between the two free energies, and simplifying the equation according to the fact that  $A_P = A_{P1} + A_{P2}$ , allows us to express the free energy of the particles at the interface as

$$F_{P,int} = (\gamma_{P2} - \gamma_{P1}) A_{P2} - \gamma_{12} A_{st} + \tau L. \quad (1.7)$$

Assuming solid spheres situated at the interface as in the figure below

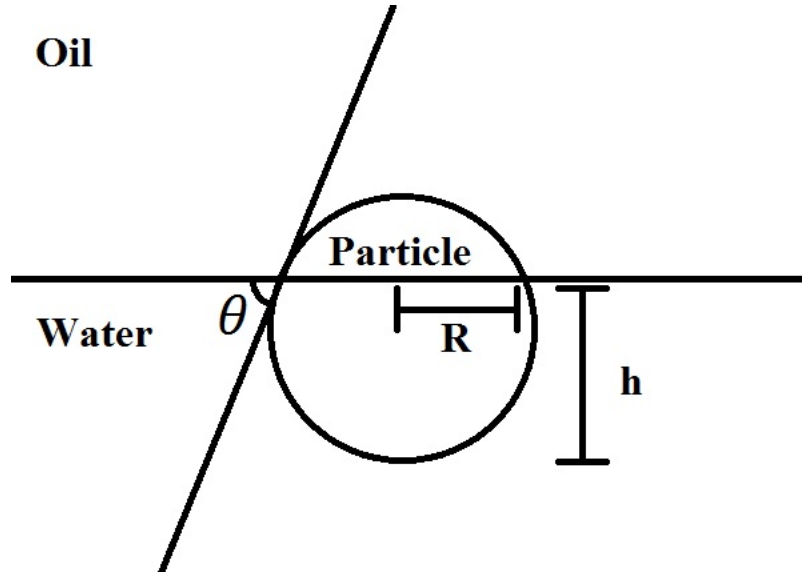


Figure 1. 4: A spherical particle situated at the interface of oil and water.

we can express the areas in the equation as

$$A_{P2} = 2\pi R h = 2\pi R^2 (1 - \cos \theta) \text{ and} \quad (1.8)$$

$$A_{st} = \pi R^2 \sin^2 \theta = \pi R^2 (1 - \cos^2 \theta), \quad (1.9)$$

where:

$R$  = the radius of the nanoparticles;

$\theta$  = the contact angle of the water on the particle surface; and

$h$  = the depth to which the particle is immersed in water.

Also, since the effects of both the gravity, and the line tension, are very small, they can be neglected. Finally, if we combine all the above with Young's equation expressed as

$$\gamma_{P1} - \gamma_{P2} = \gamma_{12} \cos \theta, \quad (1.10)$$

we can express the free energy of the particle at the interface as

$$F_{P,int} = -\pi R^2 \gamma_{12} (\cos \theta - 1)^2. \quad (1.11)$$

The better the adsorption at the interface is, the larger the drop in the free energy of the system due to the adsorption of the particles at the interface, and the higher the energy needed to detach those particles from the interface. Meaning, the larger the drop in the free energy, the more stable the emulsion is, and the lower the interfacial tension achieved is. This is why we will work on trying to increase the adsorption energy of those particles.

According to equation 1.11 above, the contact angle, as well as the radius of the particle, are both important in determining the free energy associated with the particle's adsorption at the interface. The radius of the particle can be varied by synthesizing larger particles. That brings us to the contact angle. The contact angle depends on the interactions between the particles and the molecules present at the interface of oil and water. Meaning, the more prone the particles are to interact with the two fluids, the better the adsorption, thus the lower the interfacial tension. Therefore, we will work with increasing the interfacial activity of those particles. This is where the polymer chains come into play.

### *1.1.3 Homopolymer Chains*

The idea of introducing polymer chains to the colloidal silica has many purposes. The most important purpose behind the addition of those polymer chains, however, and the one most relating to this study, is the increase in the interfacial activity.<sup>3</sup> By introducing polymer chains to the interface, we're introducing molecules that would interact with water and oil molecules. Those interactions lower the interfacial tension by increasing the adsorption energy of the hybrid nanoparticles at the interface. As explained by equation

1.11 above, the interfacial activity affects the contact angle, which affects the interfacial adsorption, which lowers the interfacial tension.

Among those purposes of introducing polymer chains is also the effect they have on the viscosity of the medium. Polymer chains extend and take a brush-like conformation in a good solvent. Due to this, as well as the fact that those polymer chains are attached to the silica cores, and are not free chains, they overlap between adjacent particles. This overlapping of the polymer chains lead to interparticle interactions. The interparticle interactions, in turn, contribute to the increase in the viscosity of the medium. Free polymer chains, however, are not believed to overlap, or interact, in the medium in the same manner, and thus do not cause the same increase in the viscosity. This increase in the viscosity of the medium contributes to the stability of the emulsion by preventing demulsification due to coalescence. Coalescence is a process in which small emulsion droplets combine together forming one large droplet.<sup>7-9</sup> The figure below shows a sketch of how those hybrid nanoparticles would come together causing an overlap between the polymer chains, which would cause the increase in the viscosity of the medium.

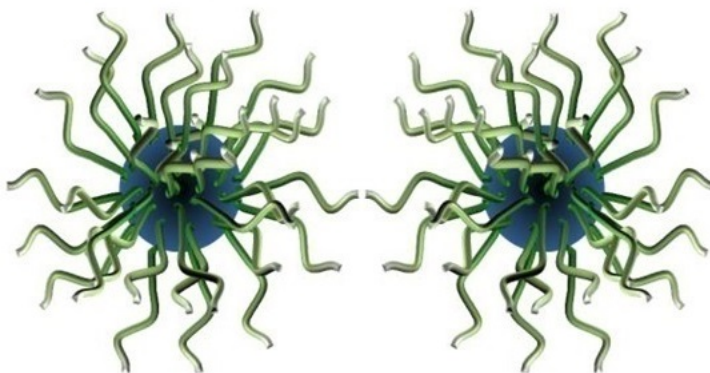


*Figure 1. 5: Two hybrid nanoparticles getting close together, which would cause the chains to overlap and interact causing an increase in the medium's viscosity.*

Another purpose that those polymer chains play is the stability against Ostwald Ripening Effect. Polymer brushes at the interface are believed to provide Surface Dilatational Modulus to the system. This modulus provides resistance to the change in the interfacial area. Ostwald Ripening Effect is where larger droplets grow on the expense of the smaller ones. The pressure inside the smaller droplets is usually larger than the pressure inside the larger droplets. To equate those two different pressures, and achieve pressure equilibrium, mass transfers through diffusion from the smaller droplets to the larger ones. As the smaller droplets become even smaller, their pressure increases further, and as the larger droplets become larger, their pressure decreases further. This causes the mass transfer to continue until the smaller ones disappear and the larger ones become larger. This means that the larger droplets will always grow at the expense of the smaller droplets. To prevent this, we need to prevent the pressure inside the smaller droplets from increasing as the radius of those droplets decrease.<sup>7,10-13</sup> This is satisfied when

$$E = \frac{d\gamma}{d \ln A} \geq \frac{\gamma}{2}, \quad (1.12)$$

where:

$E$  = Surface Dilatational Modulus;

$\gamma$  = Interfacial Tension; and

$A$  = surface area of an oil droplet.

Meaning, when this inequality is satisfied, Ostwald Ripening Effect is thermodynamically unfavorable. The addition of polymer chains provide dilatational modulus to the system by resisting the change in the interfacial area once the emulsion is

created and the hybrid nanoparticles are structured at the interface. Therefore, the presence of those polymer chains is highly helpful in the prevention of the Ostwald Ripening Effect.

#### *1.1.4 Amphiphilic Block Copolymers*

The idea that the interfacial activity can be enhanced using polymer chains that are grafted on the surface of the colloidal silica cores, led to the introduction of amphiphilic block copolymer chains grafted on those colloidal silica cores. When we have homopolymer chains, they are able to interact with the water molecules at the interface if the chains were of a hydrophilic polymer, or interact with the oil molecules if they were of a hydrophobic polymer. Therefore, the addition of amphiphilic block copolymers was introduced.

Amphiphilic block copolymers are composed of a hydrophobic block of polymer and a hydrophilic block of polymer. This allows the amphiphilic block copolymer to interact with both sides of the interface; the hydrophobic block would interact with oil molecules while the hydrophilic block would react with water molecules. This interaction with both sides of the interface increases the interfacial activity of the hybrid nanoparticles dramatically.

The idea behind using an amphiphilic block copolymer started with the introduction of a Janus particle. Janus particles are particles that have two different regions each with its own unique characteristics, contact angle, and wettability.<sup>14</sup> In the case of utilizing a Janus particle to create an emulsion between oil and water, those two regions would be a hydrophilic region and a hydrophobic regions, each with its own contact angle. The figure below shows a geometry of a Janus particle situated at the interface between oil and water.

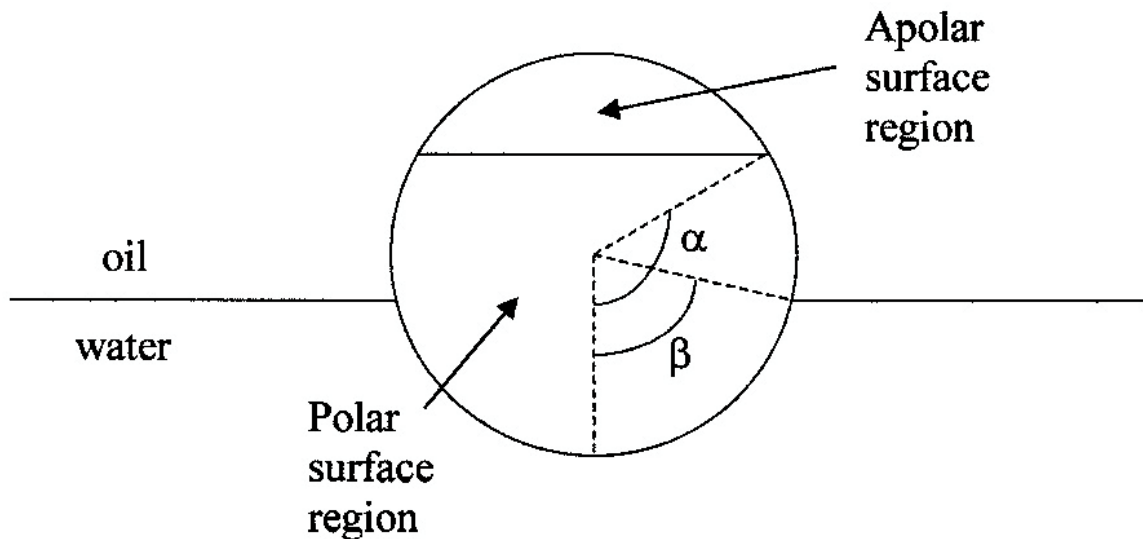


Figure 1. 6: The geometry of a Janus particle at the interface between oil and water.<sup>14</sup>

Binks *et al.* conducted a study that investigates the adsorption of a Janus particle at the interface between oil and water. In their study, Binks *et al.* showed multiple calculations to prove that the free energy associated with the adsorption of the particles at the interface increased when the amphiphilicity of the particle was increased over the whole range of contact angles.<sup>14</sup> This means that the desorption, or detachment, energy needed to remove the particles from the interface is greater in the case of the Janus-like particles than it is in the case of the homogenous particles. This, in turn, means that the Janus-like particles are able to adsorb more strongly to the interface than the homogenous particles, which would mean better packing and structuring at the interface, which would mean better interfacial reduction capabilities. In fact, they showed that the interfacial activity increased three folds using a Janus particle compared to homogenous particles, and that this interfacial activity increased as the extent of amphiphilicity increased. Binks *et al.* tuned the extent of amphiphilicity by changing  $\Delta\theta$ , which was define as

$$\Delta\theta = \frac{(\theta_\beta - \theta_\alpha)}{2}, \quad (1.13)$$

where the angles are defined as shown in the figure of the Janus particle shown above.

According to Binks *et al.*, the free energy of the system,  $E$ , with the Janus particles situated at the interface is as follow:<sup>14</sup>

For  $\beta \leq \alpha$ ,

$$E(\beta) = 2\pi R^2 \left[ \gamma_{AO}(1 + \cos \alpha) + \gamma_{PO}(\cos \beta - \cos \alpha) + \gamma_{PW}(1 - \cos \beta) - \frac{1}{2}\gamma_{OW}(\sin^2 \beta) \right] \text{ and} \quad (1.14)$$

for  $\beta \geq \alpha$ ,

$$E(\beta) = 2\pi R^2 \left[ \gamma_{AO}(1 + \cos \beta) + \gamma_{AW}(\cos \alpha - \cos \beta) + \gamma_{PW}(1 - \cos \alpha) - \frac{1}{2}\gamma_{OW}(\sin^2 \beta) \right], \quad (1.15)$$

where the subscripts are as follow:

$A$  = apolar surface region;

$P$  = polar surface region;

$O$  = oil bulk phase; and

$W$  = water bulk phase.

$\beta$  and  $\alpha$  are the angles  $\beta$  and  $\alpha$  as shown above.

Synthesizing a Janus particle, however, is a tedious process.<sup>3</sup> Instead, we're able to utilize this segregation at the interface due to the double functionality of a Janus particle, and thus achieve this enhanced adsorption at the interface, using the relatively easier process of synthesizing an amphiphilic block copolymer. A computer simulation study

predicted that this double interaction at the interface is due to a segregation of the hybrid nanoparticles at the interface. They were also able to show, using the computer simulation, how those particles would look like at the interface compared to the bulk water phase. This is shown in the figure below.<sup>15</sup>

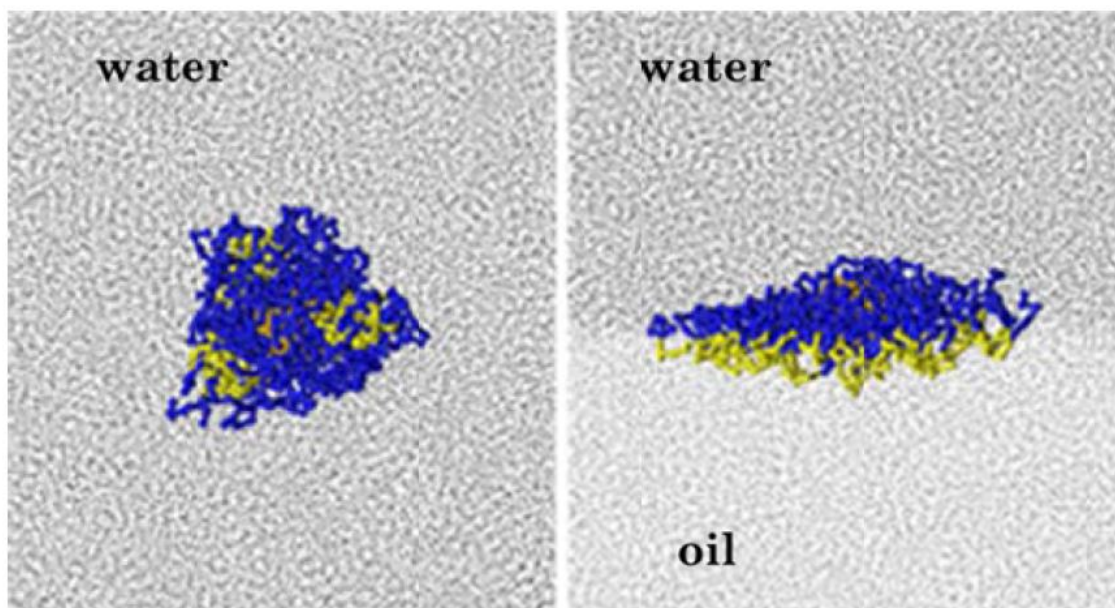


*Figure 1. 7: A computer simulation of an amphiphilic block copolymer-grafted nanoparticle dispersed in water (left) and at the interface between oil and water (right): the yellow part corresponds to the hydrophobic polymer block while the blue part corresponds to the hydrophilic polymer block.<sup>15</sup>*

### *1.1.5 Atomic Transfer Radical Polymerization, ATRP*

As mentioned earlier, we plan to use polymer-grafted nanoparticles in our study. The way we would synthesize those hybrid nanoparticles is by grafting polymer chains on colloidal silica cores. To graft those polymer chains, we plan to use the process of atomic transfer radical polymerization, ATRP.

One of the objectives of this investigation is to study the effect of the molecular weight of those grafted polymer chains on the ability to reduce the interfacial tension (IFT) between oil and water. In order to do so, we need to synthesize polymer chains that are as monodisperse as possible. The idea behind this is to have a narrow distribution of molecular

weights so we can relate the results we achieve to this particular molecular weight. When we have a polydisperse population of polymer chains with a wide distribution of molecular weights, we cannot relate the results we achieve with that specific molecular weight and truly test the effect of the molecular weight on the reduction of the interfacial tension. Therefore, we plan to use a controlled radical polymerization process because it can yield narrow distributions and low values of the polydispersity index (PDI).

We plan to use controlled radical polymerization as opposed to step growth polymerization because the polymerization proceeds at a much faster rate when using the former as opposed to the latter. We also ruled out the use of free chain radical polymerization because this type of polymerization yields a wide distribution with large values of PDI. There are other types of controlled radical polymerizations other than ATRP, but we plan to ATRP for many different reasons, such as its amenability to both types of polymerizations conducted in this study, its tolerant to many different end functional groups, and its need for relatively less aggressive conditions than other types of controlled radical polymerization.

The mechanism in which the ATRP proceeds differ from that of the free chain radical polymerization primarily in that the polymer in ATRP has a dormant state in which the radical is not active. In free chain radical polymerization, after the initiating the radical, it is very difficult to stop the propagation steps. It can be done using irreversible termination reactions, which could affect the PDI drastically. In the case of the ATRP, however, we can stop the propagation without an irreversible termination step. This is true because the polymer with the free radical on the end group has a dormant state where the radical is bonded to a halide, and is unable to proceed with the polymerization. When the halide is

removed from the radical, it acts as an unreactive inert, and cannot propagate and proceed with its own polymerization reaction. When the radical goes back and forth between its dormant and active state, it gives a better control over the PDI because it is more likely to polymerize a limited smaller number of repeat units per active state than to proceed with a burst of polymerization with high number of repeat units before going back to its dormant state. When this occurs to every radical we have in the system, the polymerization is better controlled and the result is a narrow distribution with low PDI. The existence of this dormant state also reduces the rate of the irreversible termination steps.

In our synthesis, we use Br as the halide attached to the polymer in the dormant state. The catalyst we use in our synthesis is CuBr, which is able to detach the Br group from the polymer, becoming CuBr<sub>2</sub>, and activating the radical polymer to proceed with the polymerization reaction. In order for the catalyst to become active, however, we need a ligand to combine with it, forming a complex that allows it to detach the Br and become CuBr<sub>2</sub>.<sup>16</sup>

## **1.2 Motivation**

The motivation for this research area stemmed from two main topics: cleaning oil spills, and enhanced oil recovery (EOR). When an oil spill occurs, the oil forms an oil slick layer at the surface of the water. This layer is highly dangerous to the marine environment and lifeforms for many reasons, for example: it prevents light from penetrating deep into the water, and it prevents gas exchange between the marine environment and its surroundings. Not only is it dangerous to the marine life, but it is also dangerous to lifeforms at the shore. Oil can stick to the skin and feathers of various lifeforms. It can also be toxic to the environment and lifeforms.<sup>17,18</sup> Many different methods were developed and

studied to remove those oil slicks and clean the spills, such as: booming, skimming, combustion, and in situ burning.<sup>19,20</sup> The idea of using bacteria and microorganisms to clean oil spills then led to the development of different dispersants.<sup>21,22</sup>

Biodegradation refers to the process in which bacteria and other microorganisms use hydrocarbons as a source of food and nutrition.<sup>22</sup> Oil slicks are rich with hydrocarbons. Those hydrocarbons, however, are inaccessible to the bacteria and microorganism. This could be thought of as adjacent to the following analogy. Human beings need food to live, but they are unable to live in food. They live in their natural surroundings, air, and consume food. Bacteria and microorganisms are more or less the same. They are unable to live in their food, the oil slick. They need to live in their natural surroundings, water in the case of marine environments, and access and consume their food, the hydrocarbons.

Using dispersants, we are able to disperse oil droplets in the surrounding water, making hydrocarbons accessible to bacteria and microorganisms. This way, they would be able to clean the oil spill using the process of biodegradation. Many dispersants were developed to serve this need, but the concern for dispersion stability and toxicity of such dispersants kept rising.<sup>3,17,23–25</sup>

Those nanoparticle dispersants can also be used for enhanced oil recovery, EOR. When oil is recovered from an oil reservoir, often up to or even more than, 60% of the original oil in place (OOIP) remains behind even after primary and secondary recoveries. This is because the remaining amount of oil is heavier than the amount recovered. Different techniques have been implemented to try and recover the rest of this oil, such as: steam, carbon dioxide, and chemicals. Nanoparticle dispersants are able to reduce the interfacial tension between oil and water. By reducing the interfacial tension, they are able to disperse

the oil droplets into the water phase, as mentioned earlier. This, in turn, alters the wettability, solubility, and mobility of the remaining oil inside the reservoir.<sup>3,26,27</sup> By altering those properties, we would be able to recover larger amounts of oil. In a study done by Wasan and Nikolov, a solution with silica nanoparticles was able to recover 55% of the crude oil, compared to only 17% recovered by a solution of brine.<sup>28</sup>

### **1.3 Previous Work**

Many different studies have been conducted in order to reduce the Interfacial Tension (IFT) between oil and water. As we mentioned, there are numerous different types of emulsifiers that can disperse oil and water in each other creating an emulsion. Therefore, several have investigated the interfacial tension capabilities of different emulsifiers.

One of those studies used charged polyelectrolyte-grafted silica nanoparticles to investigate their ability to reduce the interfacial tension between oil and water. The study used poly (styrene sulfonate)-grafted silica nanoparticles, SiO<sub>2</sub>-PSS. During the investigation, they found that those charged particles favor the adsorption to the interface despite their large negative charge. This was due to the fact that the poly (styrene sulfonate) backbone of the hybrid nanoparticles is hydrophobic. The adsorption to the interface facilitated the ability to reduce the interfacial tension. In fact, those charged SiO<sub>2</sub>-PSS nanoparticles were able to reduce the interfacial tension between Trichloroethylene and water from 30 mN/m to 14.5 mN/m at 5 mg/mL nanoparticles concentration.<sup>29</sup>

Another study was conducted by Alvarez *et al.* using poly (2-(dimethyl amino) ethyl methacrylate)-grafted silica nanoparticles, SiO<sub>2</sub>-PDMAEMA. The investigators were able to reduce the interfacial tension of xylene and water from around 38 mN/m to around

10 mN/m. Those results were gathered using 0.05wt% particles solution with a grafting density of 1,600 chains per particle and polymer chains of 19.4 kDa molecular weight.<sup>10</sup>

The same polymer-grafted nanoparticles, SiO<sub>2</sub>-PDMAEMA, were used by Saigal *et al.* to reduce the interfacial tension between oil and water. In the case of cyclohexane and water, they were able to reduce the interfacial tension from 48.5 mN/m to around 10 mN/m. In the case of xylene and water, on the other hand, they were able to reduce the interfacial tension from 30 mN/m to around 4 mN/m. This value of 4 mN/m is lower than the one Alvarez *et al.* was able to reach even though both studies used the same polymer and the same oil. The reason for this is the difference in the molecular weight of the polymer chains. Alvarez's study used 19.4 kDa polymer chains, while Saigal's study used 36.15 kDa.<sup>30</sup>

While those studies used homopolymer-grafted nanoparticles, Kim investigated the effect of switching between homopolymer and block copolymer-grafted nanoparticles. He used poly (oligo (ethylene oxide) mono methyl ether methacrylate) (POEOMA) as the hydrophilic homopolymer, and poly (oligo (ethylene oxide) mono methyl ether methacrylate – b – styrene) (P(OEOMA-b-Sty)) as the amphiphilic block copolymer. Using SiO<sub>2</sub>-POEOMA at a concentration of 500 ppm, polymer chains molecular weight of 208 kDa, and grafting density of 0.1 chains/nm<sup>2</sup>, he was able to reduce the interfacial tension between hexane and water from 50 mN/m to 20 mN/m. He was also able to reduce the interfacial tension between Toluene and water, using the same hydrophilic homopolymer-grafter nanoparticles, SiO<sub>2</sub>-POEOMA, from 30 mN/m to 5 mN/m. Using SiO<sub>2</sub>-P(OEOMA-b-Sty), on the other hand, he was able to reduce the interfacial tension between toluene and water from 30 mN/m to as low as 0.2 mN/m. This means that using the same oil and water,

the addition of the hydrophobic block, and converting the hybrid nanoparticles into amphiphilic block copolymers, he was able to enhance the interfacial reduction ability by 25 folds.<sup>3,31</sup>

Foster *et al.* also investigated the effect of POEOMA polymer chains on the interfacial tension between oil and water, but they didn't use silica as the nanoparticle cores. Instead, they used Iron Oxide. Using those IO-POEOMA hybrid nanoparticles, they were able to reduce the interfacial tension between dodecane and water from 52.5 mN/m to 17 mN/m.<sup>7</sup>

All the studies mentioned so far used polymer-grafted nanoparticles. Yoon *et al.*, on the other hand, used polymer-coated particles instead. They investigated the oil/water interfacial tension reduction capabilities of iron oxide coated with amphiphilic block copolymers. In their investigation, they used poly (acrylic acid-b-butyl acrylate), (PAA-b-PBA) as the amphiphilic block copolymer, and dodecane as the oil. Using particles concentrations of 0.125wt%, they were able to reduce the interfacial tension from 52.8 mN/m to 27.85 mN/m.<sup>12</sup>

This means that by adding the hydrophobic block PBA, which converted the hybrid nanoparticles into amphiphilic block copolymer-coated nanoparticles, and switching to coating the polymer chains instead of grafting them, the ability of the hybrid nanoparticles to reduce the interfacial tension was decreased. Instead of increasing the interfacial activity and enhancing the interfacial reduction capabilities as we discussed in section 1.1.4, the exact opposite occurred.

At the beginning of this study, we mentioned that there are many types of emulsifiers, and that polymer-grafted nanoparticles is one of them. Among the other types

are surfactants and carbon black (CB) particles. In an attempt to understand the stability and rheology of tricaprylin oil-in-water emulsions, Binks *et al.* used surfactants to reduce the interfacial tension and disperse the oil in water creating the emulsion. Using surfactant concentrations as high as 1wt%, they were able to reduce the interfacial tension between tricaprylin and water from 31 mN/m to 1.7 mN/m.<sup>32</sup>

As this study has shown, surfactants have the ability to reduce the interfacial tension. Katepalli *et al.* tested the effect of having both surfactants and carbon black (CB) particles at the same time. They also investigated having different types of surfactants. In their study, they used Octane as the oil, which has an interfacial tension of 51.2 mN/m with water. This interfacial tension, however, was reduced, using CB particles, to 16.8 mN/m in the presence of sodium octyl sulfate (SOS) surfactants, 8 mN/m in the presence of sodium dodecyl sulfate (SDS) surfactants, 3 mN/m in the presence of Triton X-100 surfactants, and to 8.42 mN/m in the presence of octyl trimethyl ammonium bromide (OTAB) and dodecyl trimethyl ammonium bromide (DTAB) surfactants. It was concluded in this study that the CB particle-surfactant interactions strongly influence the interfacial tension reduction capabilities.<sup>33</sup>

## **1.4 Objective**

As we just discussed in section 1.3, when using a hydrophilic homopolymer-grafted nanoparticles with an alkane oil and water, the interfacial tension was reduced from 52.5 mN/m to 17 mN/m. Using the same alkane oil and water, but adding a hydrophobic block and switching to coating instead of grafting, however, decreased the ability to reduce the interfacial tension, and was able to reduce it to around 28 mN/m instead of 17 mN/m.

This is a highly curious case because the hydrophobic block used in that study was PBA, which is not only a hydrophobic block, but also a lyophobic block to alkane oils. This means that this block would not interact with either side of the interface. This lack of interaction could be the cause of the decrease in the interfacial activity, and thus the decrease in the ability to reduce the interfacial tension. On the other hand, however, the two cases cannot be compared as is to make an informed conclusion because the addition of this block was not the only thing done differently between the two studies. In the first study, the polymer chains were grafted on the colloidal cores, while in the second study, they were coated on the colloidal cores.

The objective of our study is to investigate whether the ability to reduce the interfacial tension was affected due to the coating process, or due to the fact that the hydrophobic block chosen in the study is lyophobic to alkane oils, which are the type of oil used in that study. In order to imitate that study, we plan to use both a hydrophobic block that's lyophobic to alkane oils, and an alkane oil. To imitate the study even further, we plan to use a hydrophobic block similar in structure to the one they used. That study used poly(butyl acrylate), and we plan to use poly(methyl acrylate). The oil they used was dodecane, and the one we plan to use is Hexane. In order to arrive at an answer, however, we plan to graft those polymer chains on our colloidal nanoparticles.

In our study, we will investigate the interfacial tension reduction capabilities of both hydrophilic homopolymer-grafted nanoparticles, and amphiphilic block copolymer-grafted nanoparticles. For the hydrophilic homopolymer-grafted nanoparticles case, we will use poly(p(ethylene glycol) methyl ether methacrylate))-grafted silica nanoparticles, SiO<sub>2</sub>-POEOMA. For the amphiphilic block copolymer-grafted nanoparticles case, we will use

poly(methyl acrylate-co-p(ethylene glycol) methyl ether methacrylate)-grafted silica nanoparticles, SiO<sub>2</sub>-P(MA-b-OEOMA). In order to graft those polymer chains on the colloidal silica cores, we will use the process of atomic transfer radical polymerization (ATRP). Both the effect of changing the hybrid nanoparticle solution concentration, as well as the effect of changing the molecular weight of the grafted polymer chains will be investigated as well in this study.

## Chapter 2 Experimental Methods

### 2.1 Preparation of Polymer-Grafted Nanoparticles

#### 2.1.1 Synthesis of 1-Chlorodimethylsilyl Propyl 2-Bromo-2-Methylpropionate

##### 2.1.1.1 Materials

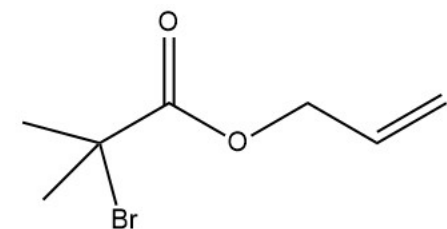
Platinum on Carbon (Sigma-Aldrich), Chlorodimethylsilane (98%, Sigma-Aldrich), and Allyl 2-bromo-2-methylpropionate (98%, Sigma-Aldrich).

##### 2.1.1.2 Method

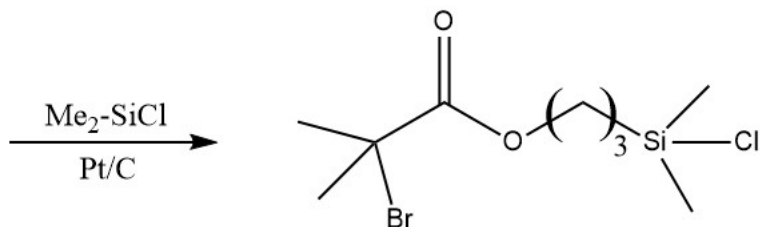
The synthesis method was carried out by modifying an already published literature procedure.<sup>3,9,29,34,35</sup> 220 mg (1.13 mmol) of Platinum on Carbon, Pt\_C (10% Pt) catalyst were added to a 250 mL round-bottom flask (A) along with a stirrer, then sealed with a rubber septum and covered with Aluminum foil to avoid light exposure. In another 250 mL round-bottom flask (B), 100 g (1.06 mol) of Chlorodimethylsilane were added along with a stirrer, then sealed with a septum. Using a syringe, 10 g (48.3 mmol) of Allyl 2-bromo-2-methylpropionate was slowly added to flask (B), containing the Chlorodimethylsilane. After adding the Allyl 2-bromo-2-methylpropionate, the mixture was allowed to stir.

Both flasks were connected with a Cannula tube, and purged with Nitrogen gas for 20 minutes. The solution in flask (B) was transferred to flask (A) under Nitrogen pressure through the cannula tube. Then, the entire mixture was allowed to stir.

The mixture was left to react, while stirring, for 1 hour at a temperature of 40 °C. After that, the mixture was allowed to cool back down to room temperature, and react, at room temperature, for another 2 days, while stirring. Scheme 2.1 shows the synthesis reaction of 1-Chlorodimethylsilyl Propyl 2-Bromo-2-Methylpropionate.



Allyl 2-bromo-2-methylpropionate



1-Chlorodimethylsilyl Propyl 2-Bromo-2-Methylpropionate

*Scheme 2. 1: General scheme for the synthesis reaction of 1-Chlorodimethylsilyl Propyl 2-Bromo-2-Methylpropionate.*

Using rubber-less syringes, the mixture was then ran through syringe filters equipped with 0.2  $\mu\text{m}$  Polytetrafluoroethylene (PTFE) membranes to remove the catalyst.

After filtering out the catalyst, the excess solvent was evaporated using a rotary evaporator leaving only the 1-Chlorodimethylsilyl Propyl 2-Bromo-2-Methylpropionate behind, which was collected in an amber bottle, sealed with a PTFE cap, and stored in the refrigerator.

### 2.1.2 Synthesis of 2-Bromoisobutyrate Initiator Functional Silica Nanoparticles

#### 2.1.2.1 Materials

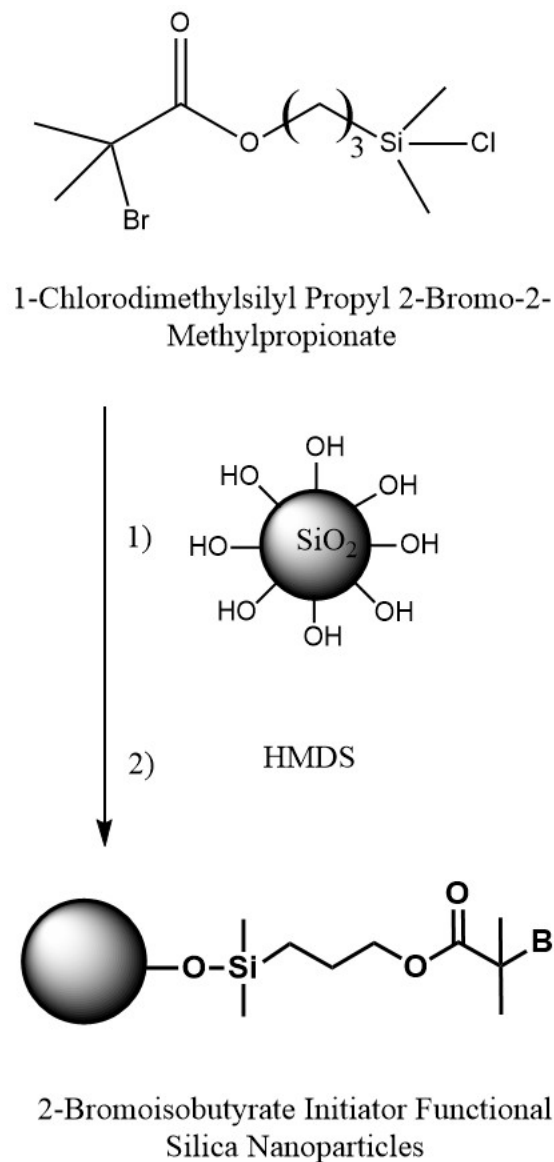
Platinum on Carbon (Sigma-Aldrich), Chlorodimethylsilane (98%, Sigma-Aldrich), Allyl 2-bromo-2-methylpropionate (98%, Sigma-Aldrich), MIBK-ST (Nissan Chemical), Hexamethyldisilazane (99.9%, Sigma-Aldrich), Methanol (Methyl Alcohol,

Macron), Tetrahydrofuran (99+%, VWR), Hexanes (Macron), and Deionized Water (DI-Water).

#### 2.1.2.2 Method

The synthesis method was carried out by modifying an already published literature procedure.<sup>3,9,29,36,37</sup> 25 g of silica dispersion (30-31wt% silica in methyl isobutyl ketone, MIBK-ST) was added, along with a stirrer, to a 125 mL round-bottom flask, then refluxed at 85 °C. While refluxing, various amounts (0.25 g to 2.5 g - 0.829 mmol to 8.29 mmol) of the 1-Chlorodimethylsilyl Propyl 2-Bromo-2-Methylpropionate were added to the MIBK-ST (depending on the targeted weight fraction of initiator to silica). The entire mixture was left to reflux at 85 °C overnight.

The mixture was then allowed to cool back down to room temperature. After that, 3 mL (2.32 g, 14.4 mmol) of Hexamethyldisilazane was added to the mixture, and was allowed to stir for 3 hours at room temperature. After that, the entire mixture was refluxed at 60 °C overnight. Scheme 2.2 shows the synthesis reaction of 2-Bromoisobutyrate initiator functional silica nanoparticles.



*Scheme 2. 2: General scheme for the synthesis reaction of 2-Bromoisobutyrate initiator functional silica nanoparticles.*

The mixture was then allowed to cool back down to room temperature. After that, it was centrifuge, and only the liquid phase was collected. The solid phase consists of the non-functionalized silica nanoparticles. The liquid phase was precipitated in a 4 to 1 Methanol to Deionized Water (DI-Water) by volume. This mixture was centrifuged, and only the solid phase, which consists of functionalized silica nanoparticles, was collected.

The collected functionalized silica nanoparticles were dispersed in minimal amounts of Tetrahydrofuran (THF), washed in excess amounts of Hexane 10-15 times to

remove any unattached initiators, then dried in a vacuum oven at 60 °C until they were completely dried.

### *2.1.3 Synthesis of SiO<sub>2</sub>-POEOMA Hybrid Nanoparticles by Surface Initiated ATRP*

#### 2.1.3.1 Materials

Platinum on Carbon (Sigma-Aldrich), Chlorodimethylsilane (98%, Sigma-Aldrich), Allyl 2-bromo-2-methylpropionate (98%, Sigma-Aldrich), MIBK-ST (Nissan Chemical), Hexamethyldisilazane (99.9%, Sigma-Aldrich), Methanol (Methyl Alcohol, Macron), Tetrahydrofuran (99+%, VWR), Hexanes (Macron), Deionized Water (DI-Water), Poly(ethylene glycol) methyl ether methacrylate (POEOMA, Average Mn 300, Sigma-Aldrich), Copper(I) bromide (98%, Sigma-Aldrich), 2,2'-Bipyridyl (99+%, Sigma-Aldrich), Aluminum oxide (Sigma-Aldrich), and Inhibitor removers (Sigma-Aldrich).

#### 2.1.3.2 Method

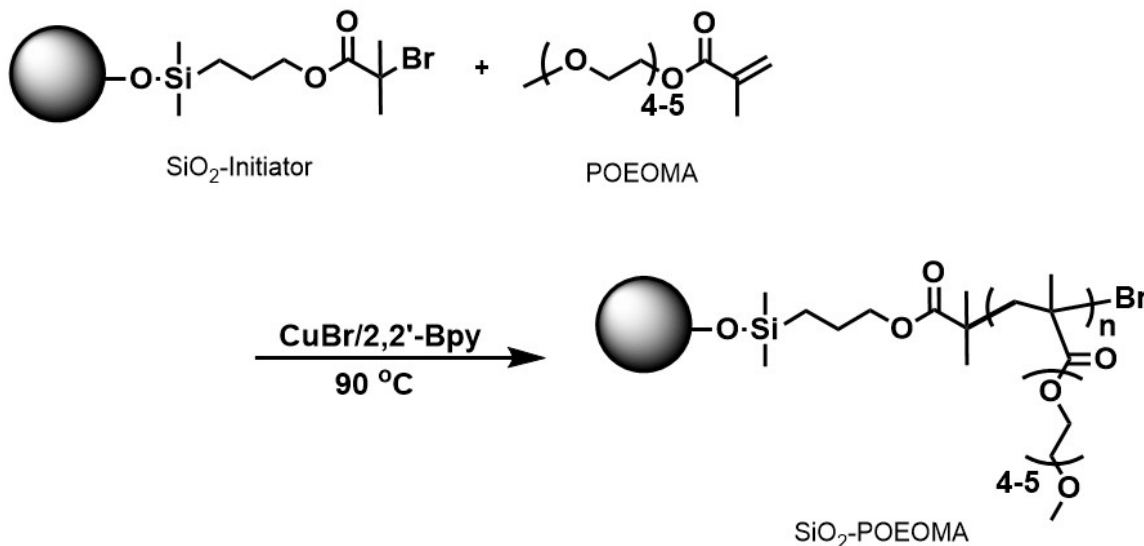
At first, the inhibitors needed to be removed from the monomers. This was done by packing a chromatography column with 10 alternating layers (5 layers of each) of aluminum oxide and inhibitor removers, starting with the aluminum oxide at the bottom. The monomers were then run through this column, and air pressure was added to speed up the process.<sup>3,31</sup>

The synthesis method was carried out by modifying an already published literature procedure.<sup>3,9</sup> 0.5 g of initiator functional silica nanoparticles, and 25 g (83.33 mmol) Poly(ethylene glycol) methyl ether methacrylate (POEOMA) were added to a 125 mL round-bottom flask (A). 49 mg (0.34 mmol) Copper (I) bromide, and 106 mg (0.68 mmol)

2,2'-Bipyridyl were added to round-bottom flask (B). A stirrer was added to each flask, and then both flasks were sealed with rubber septum.

Please note that those amount were based on 9.67wt% initiator in silica nanoparticles, which means 0.17 mmol initiators per 0.5 g of initiator functional silica nanoparticles. This makes the molar ratios as follow: 1 to 2 to 4 to 490 (initiator to catalyst to ligand to monomers).

The two flasks were connected to each other using a cannula tube, and purged with nitrogen gas for 1 hour. The contents of flask (A) were then transferred to flask (B) under nitrogen pressure. After that, the whole mixture was stirred for 5 minutes to ensure homogenous mixing of the solution during the polymerization. Scheme 2.3 shows the synthesis reaction of SiO<sub>2</sub>-POEOMA hybrid nanoparticles by surface initiated ATRP.



*Scheme 2. 3: General scheme for the synthesis reaction of SiO<sub>2</sub>-POEOMA hybrid nanoparticles by surface initiated ATRP.*

Flask (B) was then placed in an oil bath at temperature 90 °C, and left to react for various amounts of times (5-20 minutes, depending on the target molecular weight). After

that, the reaction was stopped by exposing the mixture to air. The mixture was then diluted with THF, and ran through a column packed with activated neutral Aluminum Oxide.

After that, the mixture was concentrated using a rotary evaporator, precipitated with Hexane, and left to dry in a vacuum oven at room temperature.

#### *2.1.4 Synthesis of SiO<sub>2</sub>-PMA Hybrid Nanoparticles by Surface Initiated ATRP*

##### 2.1.4.1 Materials

Platinum on Carbon (Sigma-Aldrich), Chlorodimethylsilane (98%, Sigma-Aldrich), Allyl 2-bromo-2-methylpropionate (98%, Sigma-Aldrich), MIBK-ST (Nissan Chemical), Hexamethyldisilazane (99.9%, Sigma-Aldrich), Methanol (Methyl Alcohol, Macron), Tetrahydrofuran (99+%, VWR), Hexanes (Macron), Deionized Water (DI-Water), Methyl Acrylate (99%, Sigma-Aldrich), N,N,N',N',N'-Pentamethyl diethylene triamine (PMDETA, 99%, Sigma-Aldrich), Copper (I) bromide (98%, Sigma-Aldrich), Aluminum oxide (Sigma-Aldrich), and Inhibitor removers (Sigma-Aldrich).

##### 2.1.4.2 Method

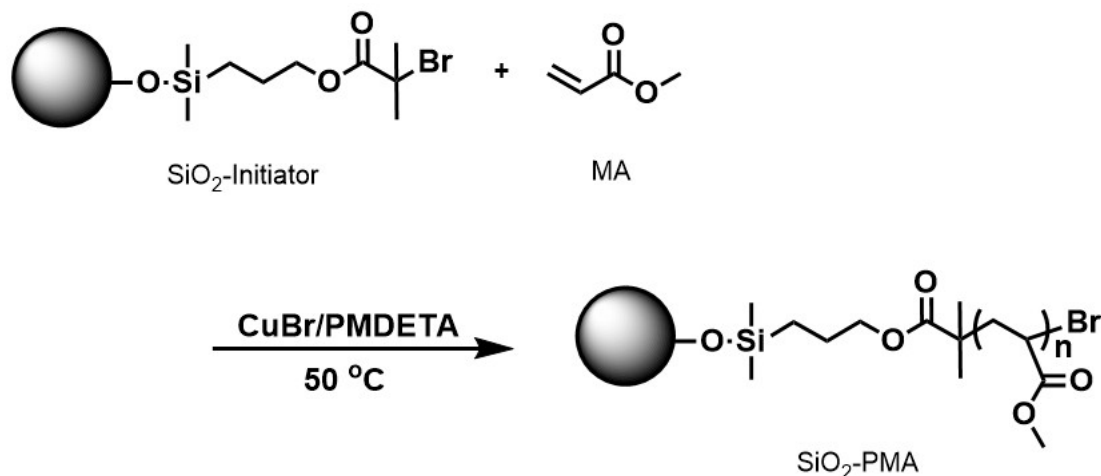
At first, the inhibitors needed to be removed from the monomers. This was done by packing a chromatography column with 10 alternating layers (5 layers of each) of aluminum oxide and inhibitor removers, starting with the aluminum oxide at the bottom. The monomers were then run through this column, and air pressure was added to speed up the process.<sup>3,31</sup>

The synthesis method was carried out by modifying an already published literature procedure.<sup>38</sup> 1 g of initiator functional silica nanoparticles, 50 g (580.88 mmol) Methyl Acrylate, and 70  $\mu$ L (0.34 mmol) of N,N,N',N',N'-Pentamethyl diethylene triamine (PMDETA) of were added to a 125 mL round-bottom flask (A). 49 mg (0.34

mmol) Copper (I) bromide was added to round-bottom flask (B). A stirrer was added to each flask, and then both flasks were sealed with rubber septum.

Please note that those amount were based on 9.67wt% initiator in silica nanoparticles, which means 0.34 mmol initiators per 1 g of initiator functional silica nanoparticles. This makes the molar ratios as follow: 1 to 1 to 1 to 1708 (initiator to catalyst to ligand to monomers).

The two flasks were connected to each other using a cannula tube, and purged with nitrogen gas for 40 minutes. The contents of flask (A) were then transferred to flask (B) under nitrogen pressure. After that, the whole mixture was stirred for 5 minutes to ensure homogenous mixing of the solution during the polymerization. Scheme 2.4 shows the synthesis reaction of SiO<sub>2</sub>-PMA hybrid nanoparticles by surface initiated ATRP.



*Scheme 2. 4: General scheme for the synthesis reaction of SiO<sub>2</sub>-PMA hybrid nanoparticles by surface initiated ATRP.*

Flask (B) was then placed in an oil bath at temperature 50 °C, and left to react for various amounts of times (1-3 hours, depending on the target molecular weight). After that, the reaction was stopped by exposing the mixture to air. The mixture was then diluted with THF, and ran through a column packed with activated neutral Aluminum Oxide.

After that, the mixture was concentrated using a rotary evaporator, precipitated with 70vol% Methanol in DI-Water, and left to dry in a vacuum oven at room temperature.

### *2.1.5 Synthesis of SiO<sub>2</sub>-P(MA-*b*-OEOMA) Hybrid Nanoparticles by POEOMA Chain Extension from SiO<sub>2</sub>-PMA Hybrid Nanoparticles*

#### 2.1.5.1 Materials

Platinum on Carbon (Sigma-Aldrich), Chlorodimethylsilane (98%, Sigma-Aldrich), Allyl 2-bromo-2-methylpropionate (98%, Sigma-Aldrich), MIBK-ST (Nissan Chemical), Hexamethyldisilazane (99.9%, Sigma-Aldrich), Methanol (Methyl Alcohol, Macron), Tetrahydrofuran (99+%, VWR), Hexanes (Macron), Deionized Water (DI-Water), Methyl Acrylate (99%, Sigma-Aldrich), Poly(ethylene glycol) methyl ether methacrylate (POEOMA, Average Mn 300, Sigma-Aldrich), N,N,N',N',N'-Pentamethyl diethylene triamine (PMDETA, 99%, Sigma-Aldrich), Copper (I) bromide (98%, Sigma-Aldrich), 2,2'-Bipyridyl (99+%, Sigma-Aldrich), Aluminum oxide (Sigma-Aldrich), and Inhibitor removers (Sigma-Aldrich).

#### 2.1.5.2 Method

At first, the inhibitors needed to be removed from the monomers. This was done by packing a chromatography column with 10 alternating layers (5 layers of each) of aluminum oxide and inhibitor removers, starting with the aluminum oxide at the bottom. The monomers were then run through this column, and air pressure was added to speed up the process.<sup>3,31</sup>

1 g of initiator functional silica nanoparticles, 50 g (580.88 mmol) Methyl Acrylate, and 70  $\mu$ L (0.34 mmol) of N,N,N',N',N'-Pentamethyl diethylene triamine (PMDETA) of were added to a 125 mL round-bottom flask (A). 49 mg (0.34 mmol)

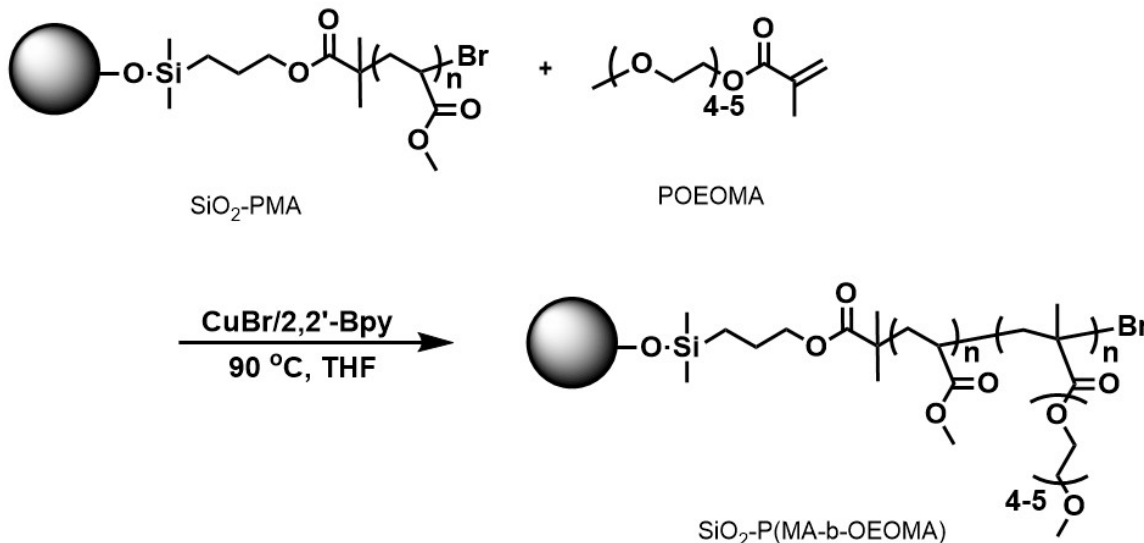
Copper (I) bromide was added to round-bottom flask (B). A stirrer was added to each flask, and then both flasks were sealed with rubber septum.

The two flasks were connected to each other using a cannula tube, and purged with nitrogen gas for 1 hour. The contents of flask (A) were then transferred to flask (B) under nitrogen pressure. After that, the whole mixture was stirred for 5 minutes to ensure homogenous mixing of the solution during the polymerization. Scheme 2.4 shows the synthesis reaction of SiO<sub>2</sub>-PMA hybrid nanoparticles by surface initiated ATRP.

Flask (B) was then placed in an oil bath at temperature 50 °C, and left to react for various amounts of times (1-3 hours, depending on the target molecular weight of the PMA block of the copolymer). After that, the reaction was stopped by exposing the mixture to air. After that, the mixture was precipitated with 70vol% Methanol in DI-Water, and the precipitants were dispersed in minimal amount of THF.

50 g (166.67 mmol) Poly(ethylene glycol) methyl ether methacrylate (POEOMA) were added to a 125 mL round-bottom flask (A). The dispersed SiO<sub>2</sub>-PMA in THF solution was then added to the POEOMA in flask (A). 49 mg (0.34 mmol) Copper (I) bromide, and 106 mg (0.68 mmol) 2,2' -Bipyridyl were added to round-bottom flask (B). A stirrer was added to each flask, and then both flasks were sealed with rubber septum.

The two flasks were connected to each other using a cannula tube, and purged with nitrogen gas for 1 hour. The contents of flask (A) were then transferred to flask (B) under nitrogen pressure. After that, the whole mixture was stirred for 5 minutes to ensure homogenous mixing of the solution during the polymerization. Scheme 2.5 shows the synthesis reaction of SiO<sub>2</sub>-P(MA-b-OEOMA) hybrid nanoparticles by POEOMA chain extension from SiO<sub>2</sub>-PMA hybrid nanoparticles.



Scheme 2. 5: General scheme for the synthesis reaction of  $\text{SiO}_2\text{-P(MA-b-OEOMA)}$  hybrid nanoparticles by surface initiated ATRP.

Flask (B) was then placed in an oil bath at temperature  $90\text{ }^\circ\text{C}$ , and left to react for various amounts of times (0.5-2 hours, depending on the target molecular weight of the POEOMA block of the copolymer). After that, the reaction was stopped by exposing the mixture to air. The mixture was then diluted with THF, and ran through a column packed with activated neutral Aluminum Oxide.

After that, the mixture was concentrated using a rotary evaporator, precipitated with Hexane, and left to dry in a vacuum oven at room temperature.

## 2.2 Characterization of the Hybrid Nanoparticles.

### 2.2.1 Gel Permeation Chromatography (GPC)

#### 2.2.1.1 Materials

Tetrahydrofuran (99+%, VWR), Hydrofluoric acid (HF, 48%, Sigma-Aldrich), Sodium hydroxide (NaOH, 97%, Sigma-Aldrich), Magnesium sulfate (97%, Sigma-Aldrich), and Deionized Water (DI-Water).

### 2.2.1.2 Method

The molecular weights of the polymer chains, both the number-average molecular weight ( $M_n$ ) and the weight-average molecular weight ( $M_w$ ), were measured using gel permeation chromatography (GPC). Both molecular weights were measured using triple detection method using a Viscotek 270 instrument.

Gel permeation chromatography is a type of size exclusion chromatography, where particles are separated according to size. The instrument has columns which the particles pass through. The small particles are trapped in channels that have pores designed specifically to increase the distance traveled by the particles that fit into those pores. The larger particles, on the other hand, that do not fit into those pores, pass around them, which decreases the distance traveled. This means that the larger particles would come out of the column before the smaller ones, which is how the instrument separated based on size. The figure below shows a schematic of how this process works.

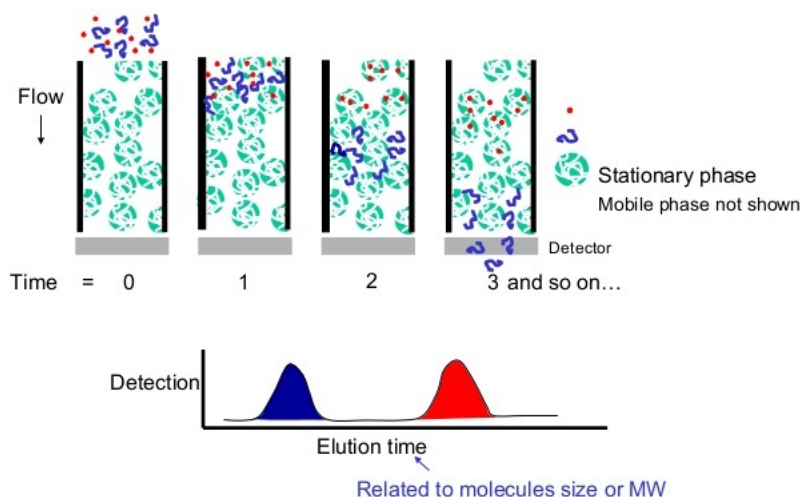


Figure 2. 1: General schematic depicting the separation based on size in a gel permeation chromatography column.

In order to measure the molecular weights, the polymer chains had to be cleaved from the silica cores on which they were grafted, however. This was done by dissolving the hybrid nanoparticles in minimal amount of THF, then adding an equal volume amount of 2% HF solution. The HF solution obtained was a 48% solution, so it was diluted to 2% using DI-Water prior to using it. The mixture was allowed to stir for at least an hour, then it was neutralized using a saturated NaOH solution. The water in the solution was dried by adding magnesium sulfates. The cleaved polymer chains in the remaining THF solution were precipitated using Hexane in the case of both POEOMA and P(MA-b-OEOMA), and using 70vol% Methanol in DI-Water in the case of PMA as the non-solvents. After precipitating and drying the cleaved polymer chains, they were dissolved in inhibitor-stabilized THF, and ran through GPC to measure the molecular weights.<sup>3,9,31</sup> The figure below shows a schematic of the cleaving of the polymer chains using HF.

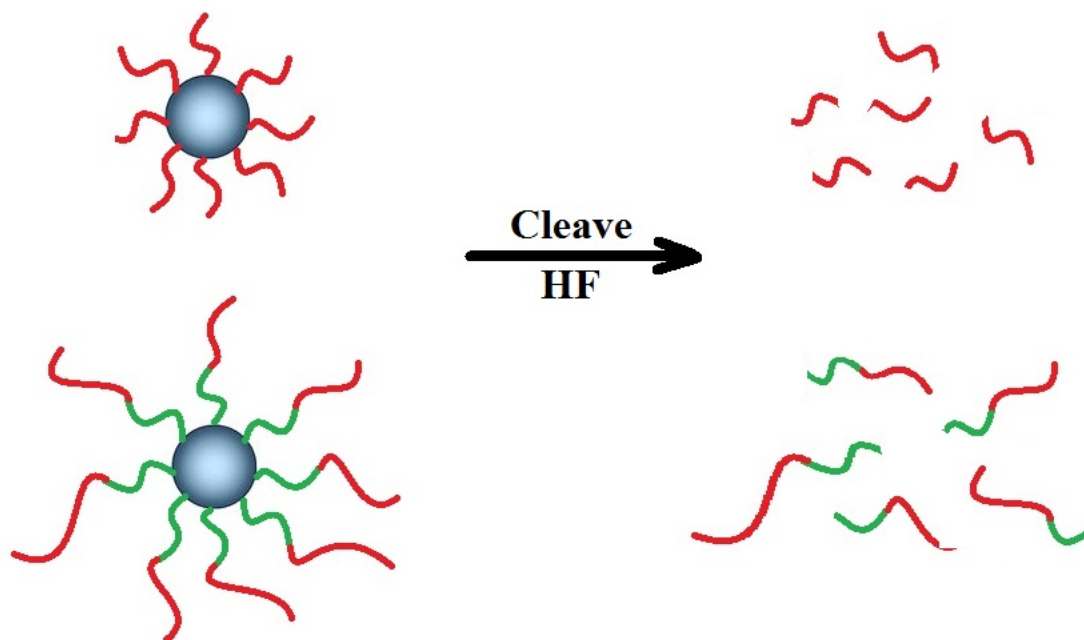


Figure 2. 2: General schematic depicting the cleaving of the polymer chains using HF.

### 2.2.2 Thermal Gravimetric Analysis (TGA)

The weight percentage of polymer present in the hybrid nanoparticles was measured using thermal gravimetric analysis (TGA Q500, TA Instruments). The instrument heats the sample from 25 °C to 800 °C with increments of 10 °C per minute, in nitrogen atmosphere. As the sample is being heated, the bonds break down causing the polymer to degrade and decompose. This changes the weight of the sample. TGA measures the change in weight of the sample as this is happening. Using this technique, we can get both the weight percentage of the polymer, as well as the thermal degradation temperature of the polymer. In this study, we are only interested in the weight percentage of the polymer, which we will use to calculate the grafting density of the hybrid nanoparticles.

### 2.2.3 Grafting Density

Grafting density is a measure of how many polymer chains are on the silica nanoparticles. It can be expressed in two different methods; either as number of chains per silica core, or number of chains per surface area of silica cores. The equations determining those two methods as expressed as

$$\frac{Chains}{SiO_2} = \frac{(Polymer\ wt\%) (N_A) \left(\frac{4}{3}\pi r^3\right) (\rho_{SiO_2})}{(M_{n_{polymer}}) (SiO_2\ wt\%) 10^{21}} \text{ and} \quad (2.1)$$

$$\frac{Chains}{nm^2} = \frac{(Polymer\ wt\%) (N_A) \left(\frac{1}{3}r\right) (\rho_{SiO_2})}{(M_{n_{polymer}}) (SiO_2\ wt\%) 10^{21}}, \quad (2.2)$$

where:

$Polymer\ wt\%$  = weight percentage of polymer; measured using TGA;

$N_A$  = Avogadro's number =  $6.022 \times 10^{23}$ ;

$r$  = radius of the silica cores (in nm);

$\rho_{SiO_2}$  = density of the silica cores (in g/ml);

$M_{n_{polymer}}$  = number average molecular weight (in g/mol); measured using GPC;

$SiO_2\ wt\%$  =  $100\% - Polymer\ wt\% - Initiator\ wt\%$  = weight percentage of silica;

$Initiator\ wt\%$  = weight percent of initiators; measured using TGA; and

$10^{21}$  accounts for unit conversions.

The silica cores used in this study have an average radius of 6 nm (measured using SAXS), and a density of 2.2 g/mL.

#### 2.2.4 Small Angle X-Ray Scattering (SAXS)

The diameter of the hybrid nanoparticle in the dry state was obtained by small angle x-ray scattering (SAXS) using Rigaku SMax3000 with a MicroMax-007HF rotating anode X-ray generator. This technique gives the center-to-center distance between the adjacent silica cores. Taking into account both the fact that there is no solvent present in the SAXS measurements, as well as the assumption that the hybrid particles are packed in an ordered manner, this center-to-center distance is equal to the average diameter of the hybrid nanoparticles at the dry state.<sup>3,9,31</sup>

After collecting the scattering data, it was corrected for the background scattering from the kapton tape. The correction follows

$$\begin{aligned}
& I(q)_{\text{Particles,corrected}} \\
& = I(q)_{\text{Particles,uncorrected}} - \left( \frac{T_{\text{Particles}}}{T_{\text{Kapton}}} \right) I(q)_{\text{Kapton}},
\end{aligned} \tag{2.3}$$

where:

$I$  = scattering intensity; and

$T$  = transmittance.

The value of the scattering vector ( $q$ ) that corresponds to the first peak, maximum  $I(q)$ , is what determines the center-to-center distance, and thus the diameter. Then, the diameter ( $d$ ) is determined according to<sup>39-41</sup>

$$d = \frac{2 \pi}{q}. \tag{2.4}$$

### 2.2.5 Dynamic Light Scattering (DLS)

When the hybrid nanoparticles are dissolved in a good solvent, such as DI-Water in the case of this study, the hydrophilic portion of the polymer chains expand. This expansion changes the diameter of the hybrid nanoparticles. The new diameter was measured by dynamic light scattering (DLS) using Brookhaven Instrument, BI-200SM. DLS utilizes the Stokes-Einstein equation that relates the radius of the sphere to its diffusivity. DLS measures the diffusion of colloidal particles through a unit volume. When those colloids enter this volume, they start to scatter light, and the scattering ends when they diffuse out of this volume. The intensity of this scattering also relies on the angle at which the scattering occurs.

In our study, this hydrodynamic diameter ( $d_h$ ) was measured by creating a 100 ppm solution of the hybrid nanoparticles in DI-Water, and proceeding with the following process:<sup>39,42</sup>

1. Run multiple DLS experiments on the sample with the detector positioned at a different angle,  $\theta$  each run.
2. Fit the data gathered from each run into the autocorrelation function expressed as<sup>42</sup>

$$g(\tau) = B + \beta \exp(-2\bar{\Gamma}\tau) \left(1 + \frac{\mu_2}{2!}\tau^2 - \frac{\mu_3}{3!}\tau^3 \dots\right)^2, \quad (2.5)$$

where:

$B$ ,  $\beta$ ,  $\bar{\Gamma}$ , and  $\mu_i$  ( $i=2,3,\dots$ ) = fitting parameters.

$\tau$  = delay time.

3. Plot  $\bar{\Gamma}$  vs. the squared of the Scattering Vector,  $q^2$ .<sup>39,42</sup> Since

$$\bar{\Gamma} = D * q^2, \quad (2.6)$$

the slope of the  $\bar{\Gamma}$  vs.  $q^2$  plot gives the Diffusivity,  $D$ ,<sup>39</sup> where

$$q = \frac{4\pi n_0}{\lambda_0} \sin\left(\frac{\theta}{2}\right); \quad (2.7)$$

$n_0$  = the refractive index of the solvent;

$\lambda_0$  = the wavelength of the laser in vacuum; and

$\theta$  = the angles at which the scattering data were collected.

4. Using the Stokes-Einstein relation below, one can obtain the hydrodynamic radius,  $R_h$  expressed as<sup>39</sup>

$$R_h = \frac{k_B T}{6\pi\eta D}, \quad (2.8)$$

where:

$k_B$  = the Boltzmann's constant;

$T$  = the absolute temperature; and

$\eta$  = the dynamic viscosity of the solution.

5. Once we have the hydrodynamic radius, we can calculate the hydrodynamic diameter as

$$d_h = 2 R_h. \quad (2.9)$$

### 2.3 Analysis of Oil-Water Emulsion

The interfacial tension between oil and water was measured using a literature procedure called the Pendant Drop Method.<sup>3,31,43</sup> Different amounts of polymer-grafted nanoparticles were dissolved in DI-Water (depending on the target concentration). Then, using an Optical Contact Angle measuring instrument (OCA 15EC, DataPhysics), 3-5  $\mu\text{L}$  of the nanoparticles-water solution were injected using a syringe into a cuvette filled with hexane. This is shown in the figure below.

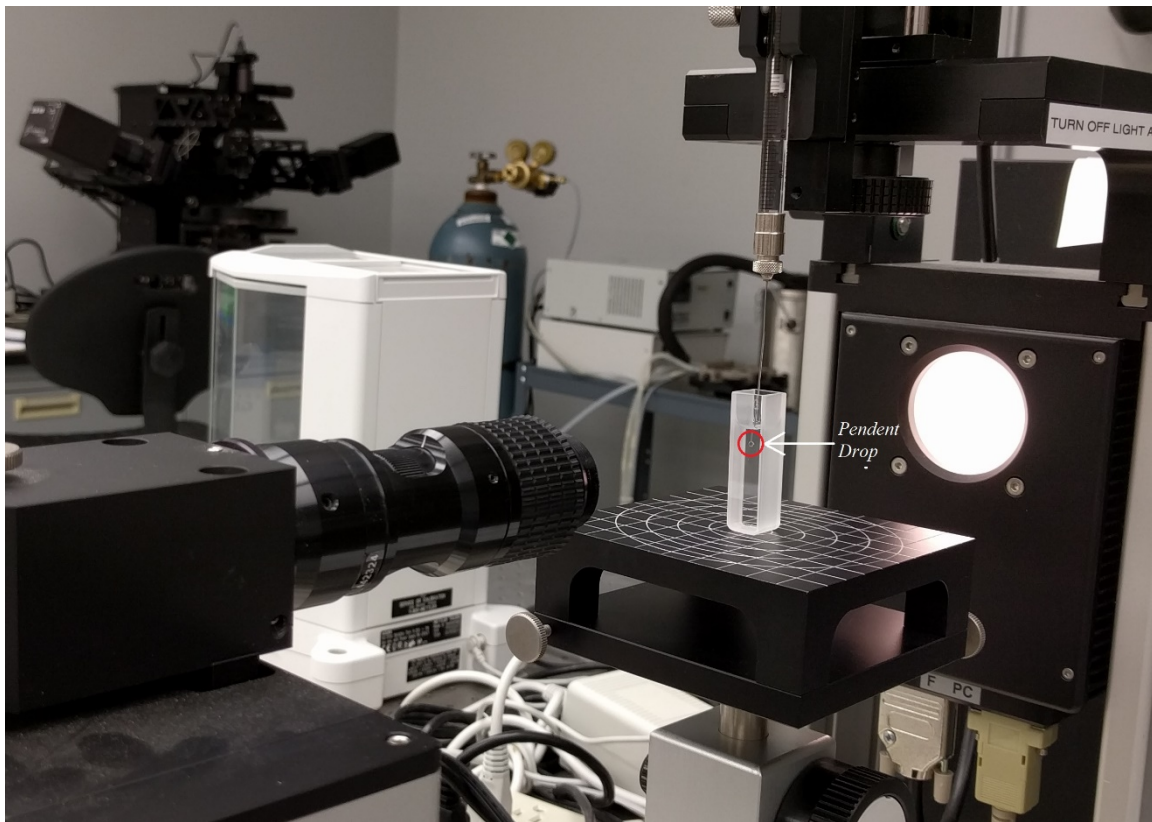


Figure 2. 3: Optical contact angle instrument for interfacial tension measurements showing a pendent drop of hybrid nanoparticles solution suspended in Hexane-filled cuvette in front of a camera that is used to take the pictures.

Pictures at different time intervals were taken using the instrument for analysis, as in the figures shown below.

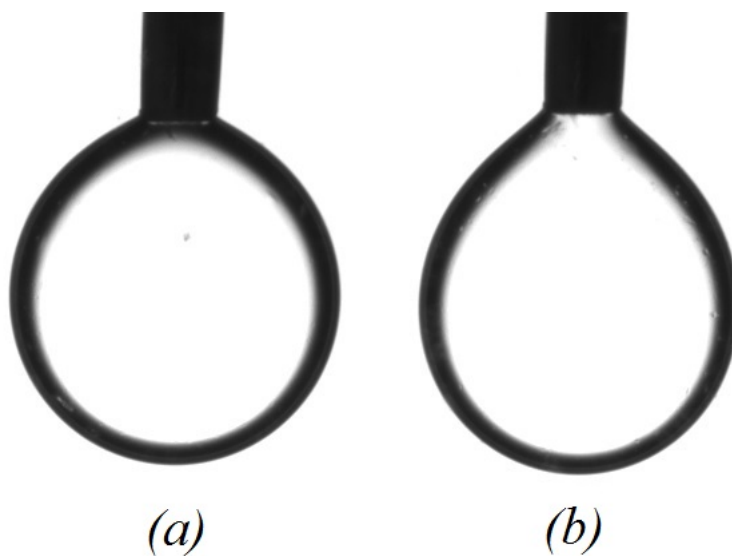


Figure 2. 4: A picture of pendant drops of SiO<sub>2</sub>-POEOMA at: (a) 0 and (b) 30 minutes.

Those pictures were analyzed using Matlab, and since the computer measures the dimensions of a picture in pixels, a calibration was needed to obtain a conversion factor between pixels and length units. The Matlab algorithm that was developed to analyze the pictures and calculate the interfacial tension between the oil and water, was developed according to the pendent drop method from the literature. The interfacial tension in that method was expressed as

$$\gamma = \frac{g \Delta\rho d_e^2}{H}, \text{ where} \quad (2.10)$$

$$\Delta\rho = |\rho_{\text{water}} - \rho_{\text{oil}}| \text{ and} \quad (2.11)$$

$$S = \frac{d_s}{d_e}, \quad (2.12)$$

where:

$\gamma$  = interfacial tension;

$g$  = gravitational acceleration;

$\rho$  = density;

$d_e$  and  $d_s$  are the diameters defined as in the figure below; and

$H$  depends on the value of  $S$  as follows:

$$0.401 \leq S \leq 0.46,$$

$$\begin{aligned} 1/H = & \left(0.32720/S^{2.56651}\right) - 0.97553 \times S^2 + 0.84059 \times S \\ & - 0.18069, \end{aligned} \quad (2.13a)$$

$$0.46 < S \leq 0.59,$$

$$\begin{aligned} 1/H = & \left(0.31968/S^{2.59725}\right) - 0.46898 \times S^2 + 0.50059 \times S \\ & - 0.13261, \end{aligned} \quad (2.13b)$$

$$0.59 < S \leq 0.68,$$

$$\begin{aligned} 1/H = & \left(0.31522/S^{2.62435}\right) - 0.11714 \times S^2 + 0.15756 \times S \\ & - 0.05285, \end{aligned} \quad (2.13c)$$

$$0.68 < S \leq 0.90,$$

$$\begin{aligned} 1/H = & \left(0.31345/S^{2.64267}\right) - 0.09155 \times S^2 + 0.14701 \times S \\ & - 0.05877, \text{ and} \end{aligned} \quad (2.13d)$$

$$0.90 < S \leq 1.00,$$

$$\begin{aligned} 1/H = & \left(0.30715/S^{2.84636}\right) - 0.69116 \times S^3 + 1.08315 \times S^2 \\ & - 0.18341 \times S - 0.20970. \end{aligned} \quad (2.13e)$$

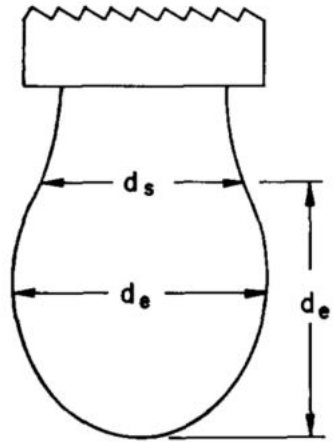


Figure 2. 5: The definition of the diameters used in the empirical equation for the pendant drop method.<sup>43</sup>

## **Chapter 3 Hydrophilic Homopolymer-Grafted Nanoparticles**

### **3.1 Methodology**

#### *3.1.1 Materials*

Platinum on Carbon (Sigma-Aldrich), Chlorodimethylsilane (98%, Sigma-Aldrich), Allyl 2-bromo-2-methylpropionate (98%, Sigma-Aldrich), MIBK-ST (Nissan Chemical), Hexamethyldisilazane (99.9%, Sigma-Aldrich), Methanol (Methyl Alcohol, Macron), Tetrahydrofuran (99+%, VWR), Hexanes (Macron), Deionized Water (DI-Water), Poly(ethylene glycol) methyl ether methacrylate (POEOMA, Average Mn 300, Sigma-Aldrich), Copper(I) bromide (98%, Sigma-Aldrich), 2,2'-Bipyridyl (99+%, Sigma-Aldrich), Aluminum oxide (Sigma-Aldrich), Inhibitor removers (Sigma-Aldrich), Hydrofluoric acid (HF, 48%, Sigma-Aldrich), Sodium hydroxide (NaOH, 97%, Sigma-Aldrich), and Magnesium sulfate (97%, Sigma-Aldrich).

#### *3.1.2 Preparation*

The hydrophilic homopolymer-grafted nanoparticles used in this study were poly(p(ethylene glycol) methyl ether methacrylate))-grafted silica nanoparticles, SiO<sub>2</sub>-POEOMA. Three different batches of the SiO<sub>2</sub>-POEOMA were synthesized. Both the amounts of monomers added to each synthesis reaction, and the length of each reaction were changed according to the target molecular weight. The preparation of the particles followed the synthesis method described in section 2.1.3.

### **3.2 Characterization**

#### *3.2.1 Gel Permeation Chromatography (GPC)*

After the synthesis procedure was completed, the polymer-grafted nanoparticles were dried at room temperature in a vacuum oven overnight. The polymer chains on the

nanoparticle hybrid were cleaved using the procedure described in section 2.2.1. The cleaved polymer chains were then run in the GPC instrument. Below are the gathered GPC results showing the Size Exclusion Chromatography (SEC) curves for each sample.

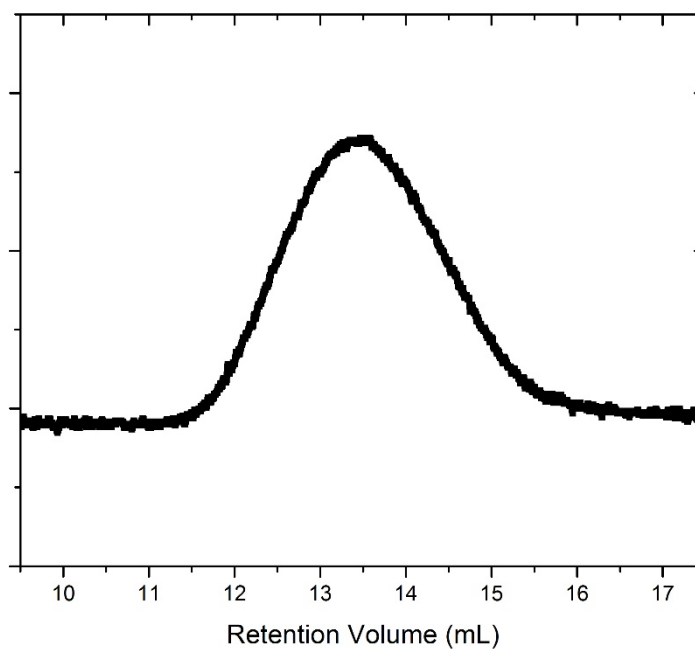


*Figure 3. 1: GPC results showing SEC curve for sample A.*

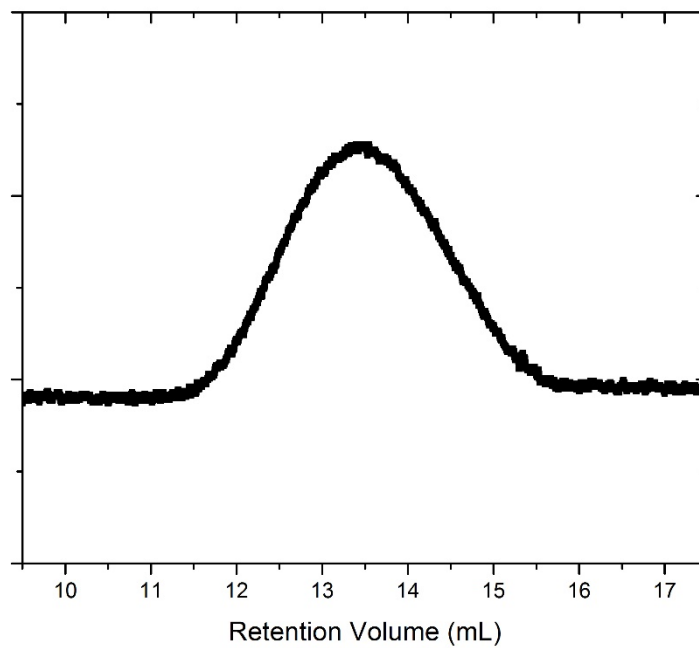


Figure 3. 2: GPC results showing SEC curve for sample B.

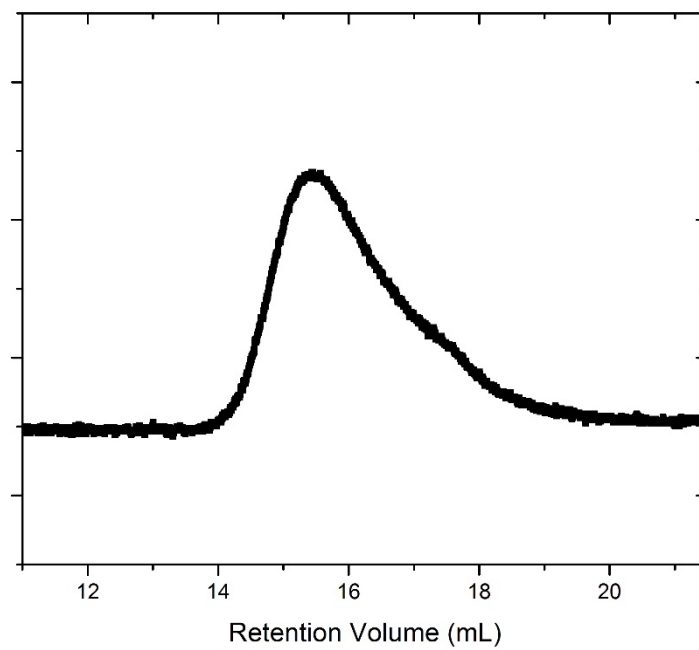


Figure 3. 3: GPC results showing SEC curve for sample C.

Upon analysis of the data using triple detection method in the Viscotek 270 instrument, both the number average molecular weight ( $M_n$ ), and the weight average molecular weight ( $M_w$ ) were determined for each sample. Using both  $M_n$  and  $M_w$ , the polydispersity Index (PDI) of the polymer chains was determined as<sup>16</sup>

$$PDI = M_w/M_n. \quad (3.1)$$

The number average molecular weight,  $M_n$ , and the poly dispersity index, PDI, for each sample is summarized in table 3.1 below.

### 3.2.2 Thermal Gravimetric Analysis (TGA)

A small amount of each sample of the hybrid nanoparticles was used to run TGA as described in section 2.2.2. Following are the results obtained for samples A, B, and C:

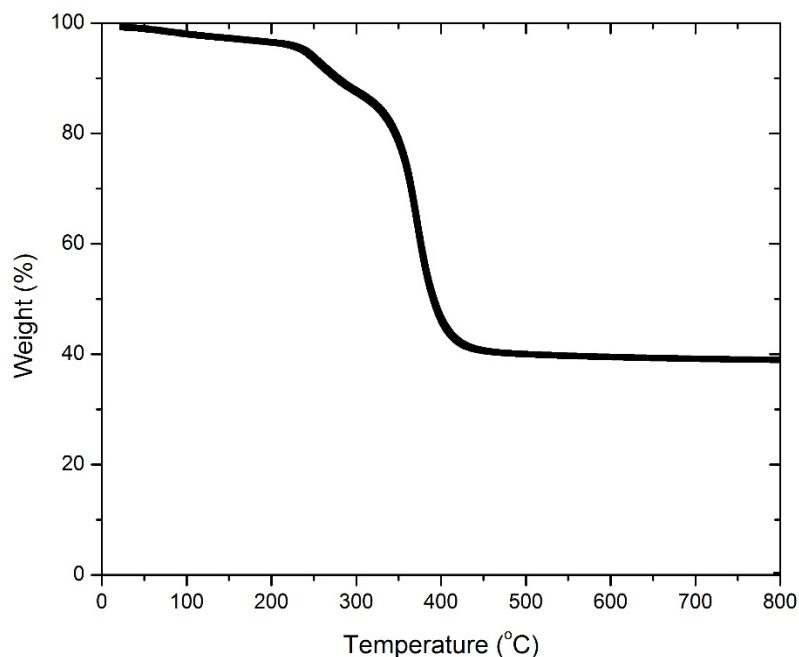


Figure 3. 4: TGA results showing weight change as temperature is increasing from 25 °C to 800 °C for sample A.

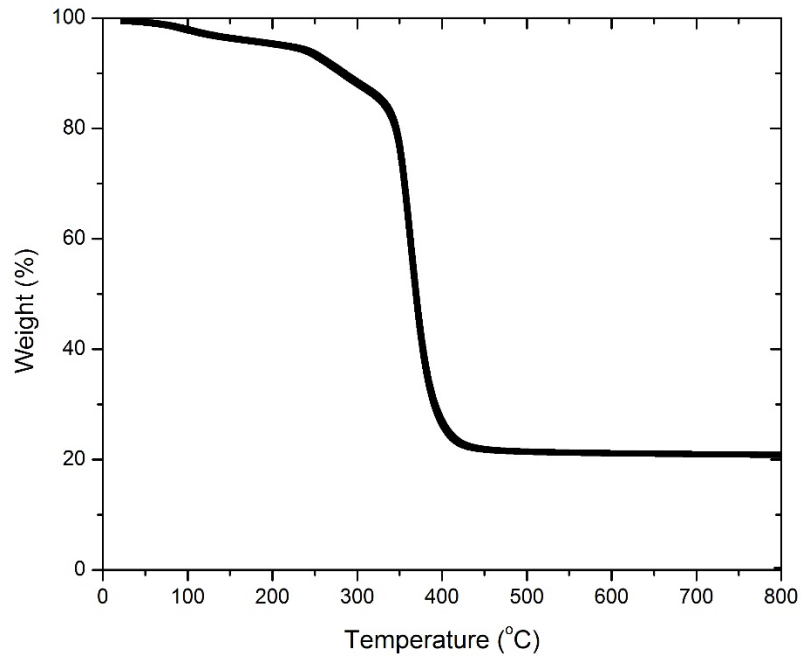


Figure 3. 5: TGA results showing weight change as temperature is increasing from 25 °C to 800 °C for sample B.

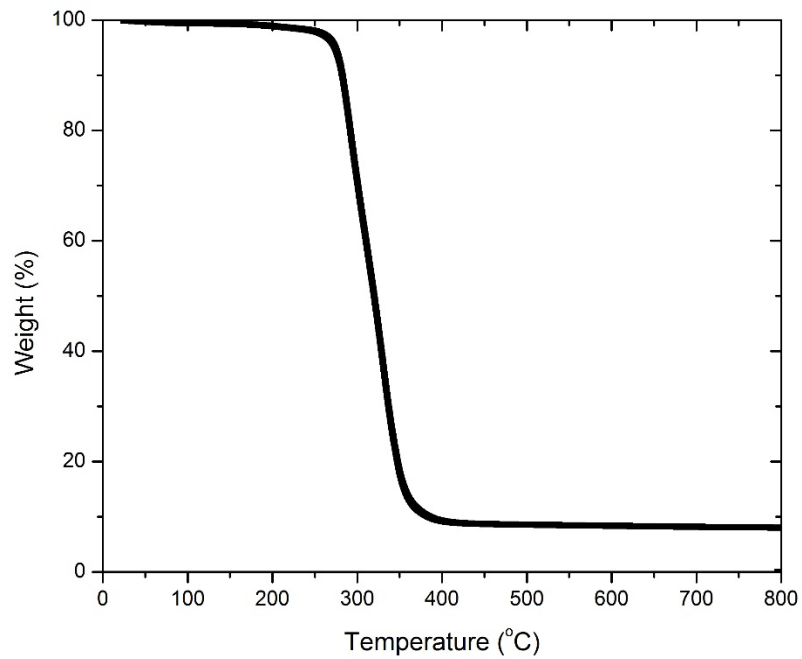


Figure 3. 6: TGA results showing weight change as temperature is increasing from 25 °C to 800 °C for sample C.

The first weight drop, starting from the beginning up to around 100 °C, corresponds to residual solvent that was left in the sample due to incomplete drying. The second weight drop, starting from around 100 °C up to 300-350 °C, corresponds to the initiators in the sample. The final weight drop, starting from 300-350 °C, corresponds to the polymer chains in the sample. The rest of the mass of the sample corresponds to the silica cores in the samples. The polymer weight percent for samples A, B, and C are 47%, 64%, and 90%.

### *3.2.3 Grafting Density*

Using the results obtained from both GPC and TGA, the grafting densities of the polymer chains on the silica cores were calculated. The equations used for those calculations are equations 2.1 and 2.2 in section 2.2.3. By controlling the amount of initiators to silica, as described in section 2.1.2, the grafting densities can be controlled. This study did not attempt to control the grafting density, nor did it investigate the effect of grafting densities on IFT measurements. The values for the grafting densities are summarized in table 3.1 below.

### *3.2.4 Small Angle X-Ray Scattering (SAXS)*

A small amount of each sample of the hybrid nanoparticles was used to run SAXS measurements as described in section 2.2.4. When running SAXS, the scattering intensity and transmittance of the sample covered with kapton tape were gathered as well as those of the kapton tape alone so that we can correct for scattering from the tape according to equation 2.3 in section 2.2.4. The dry state diameter was then calculated according to equation 2.4 in section 2.2.4. Following are the results for the corrected data for samples A, B, and C in order:

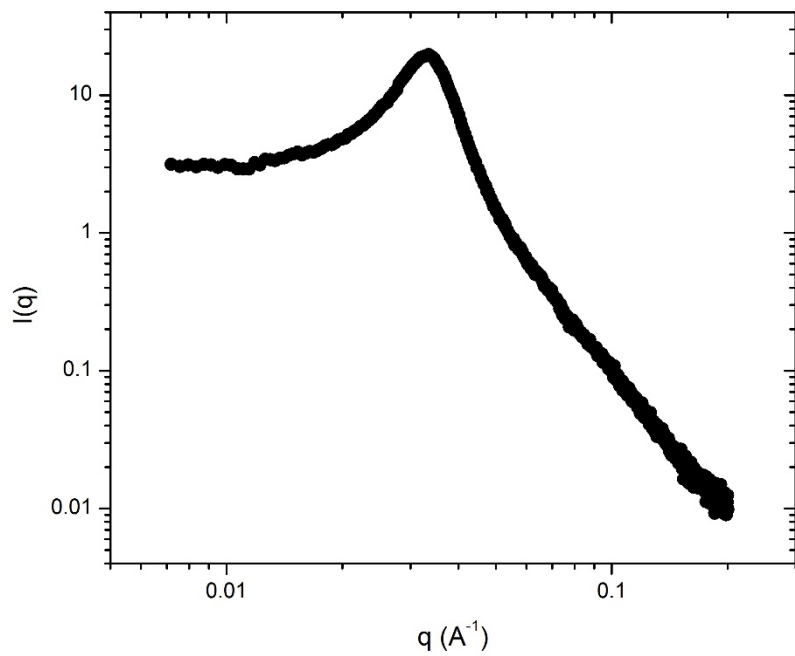


Figure 3. 7: SAXS results showing the scattering intensity as a function of the scattering vector for sample A.

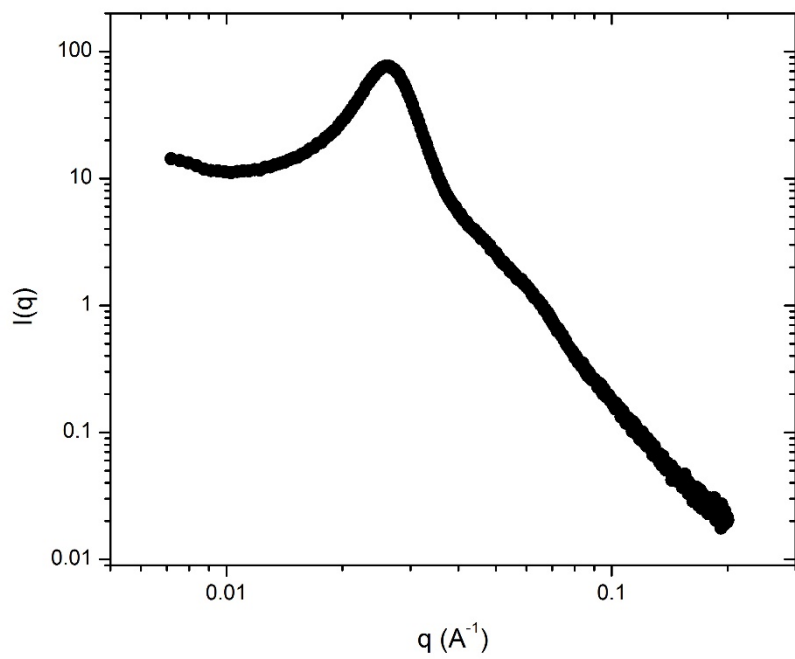


Figure 3. 8: SAXS results showing the scattering intensity as a function of the scattering vector for sample B.

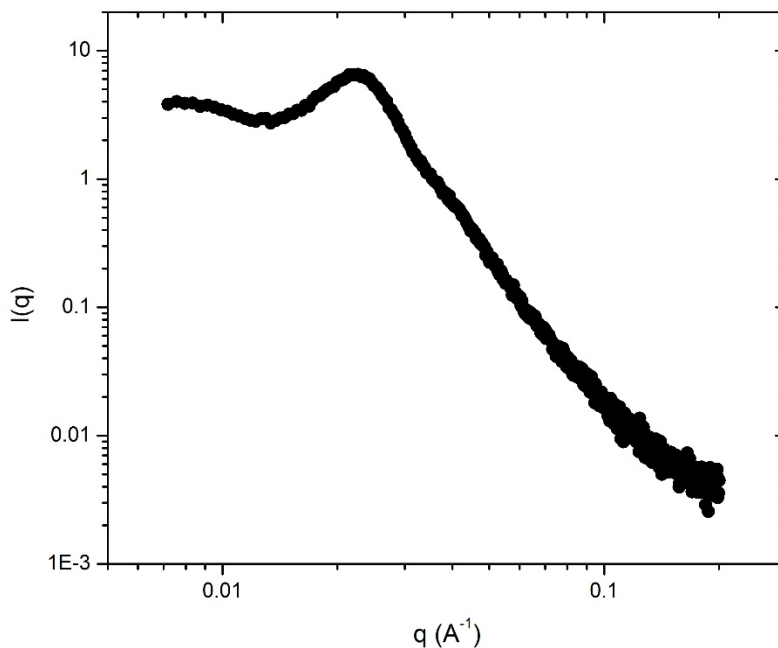


Figure 3. 9: SAXS results showing the scattering intensity as a function of the scattering vector for sample C.

The dry state diameter values for these samples are summarized in table 3.1 below.

### 3.2.5 Dynamic Light Scattering (DLS)

For DLS analysis, 100 ppm solutions of each of the hybrid nanoparticle samples in DI-Water were prepared. Then, DLS was run according the procedure described in section 2.2.5. After running DLS on them, the following results were obtained for samples A,B, and C in order:

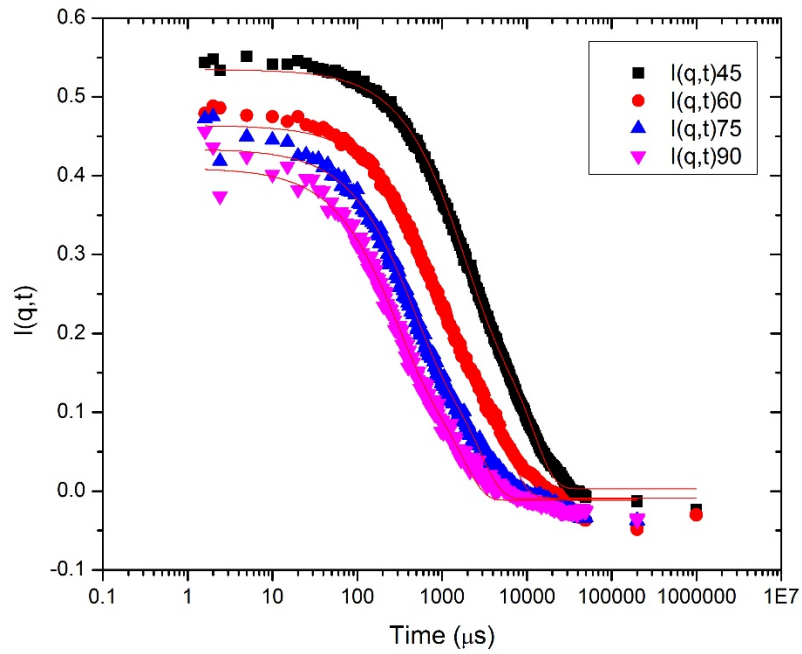


Figure 3. 10: DLS results showing scattering intensity as a function of time for sample A; used for fitting in the autocorrelation function.

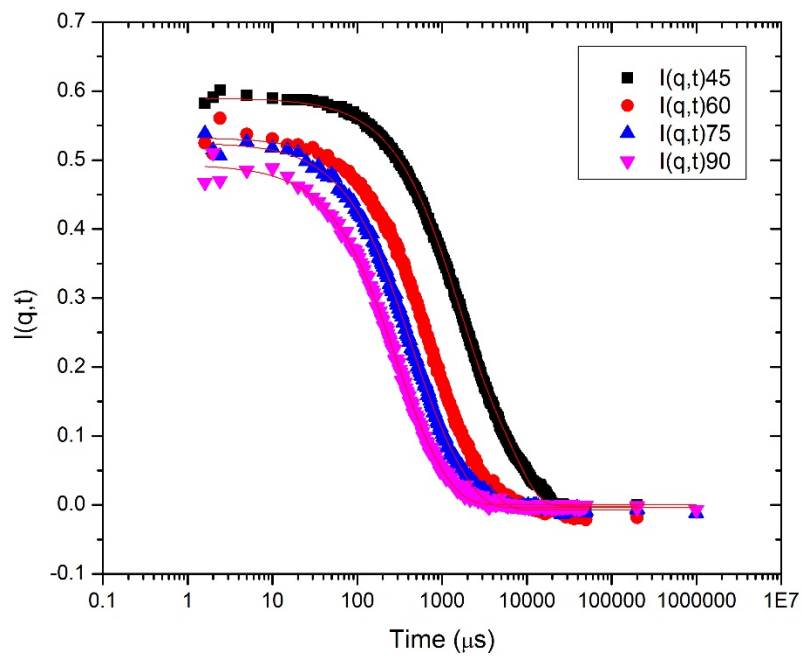


Figure 3. 11: DLS results showing scattering intensity as a function of time for sample B; used for fitting in the autocorrelation function.

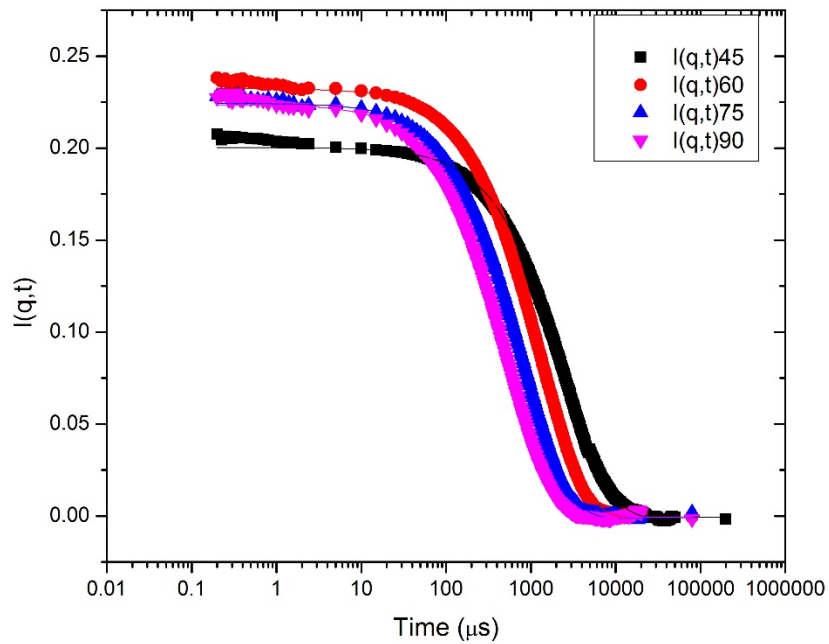


Figure 3. 12: DLS results showing scattering intensity as a function of time for sample C; used for fitting in the autocorrelation function.

Using a data analysis software, the data shown above for each sample were fitted to the autocorrelation function shown in equation 2.5 to obtain  $\bar{\Gamma}$ . As shown above, the angles used were 45°, 60°, 75°, and 90°. Those angles were used to calculate  $q^2$  according to equation 2.7. The following were obtained by plotting  $\bar{\Gamma}$  vs.  $q^2$ .

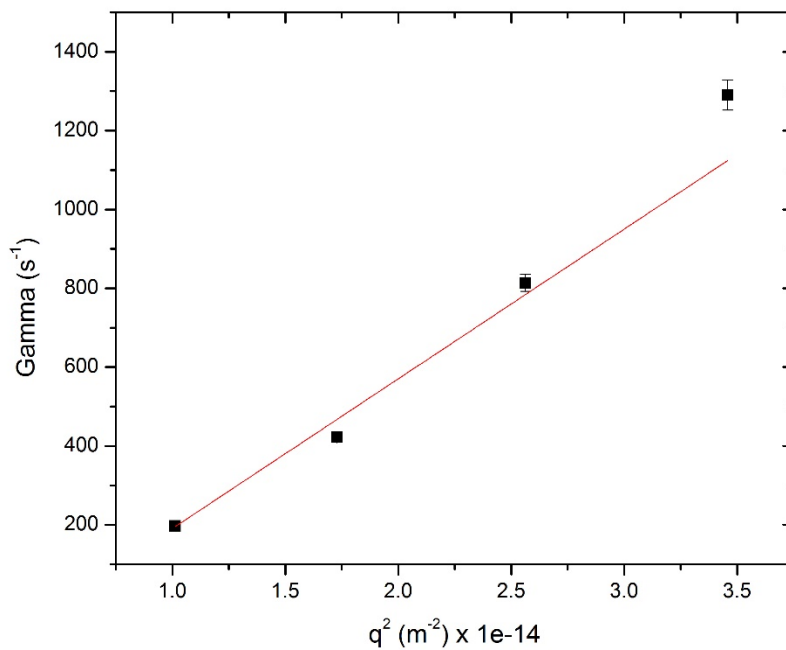


Figure 3. 13: Plotting gamma vs the squared of the scattering vector to get the diffusivity of sample A.

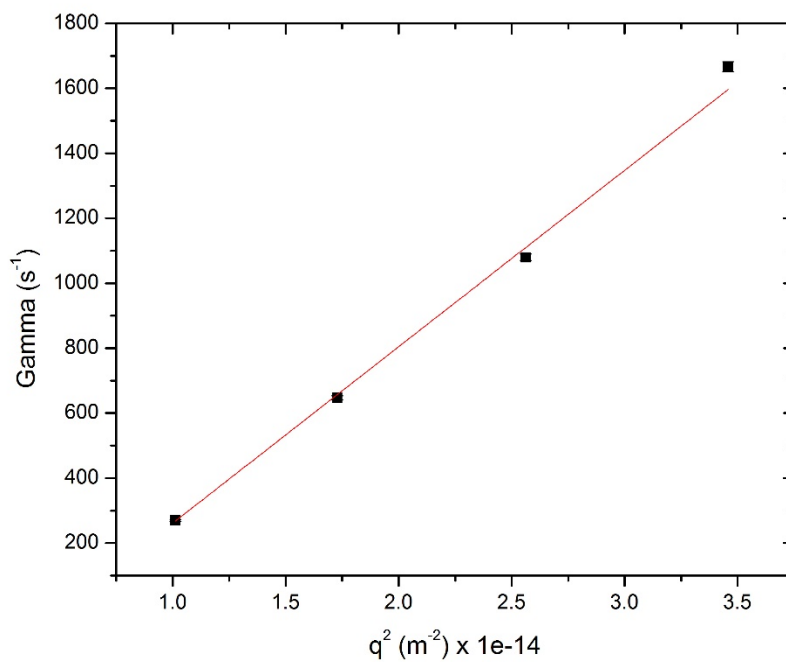


Figure 3. 14: Plotting gamma vs the squared of the scattering vector to get the diffusivity of sample B.

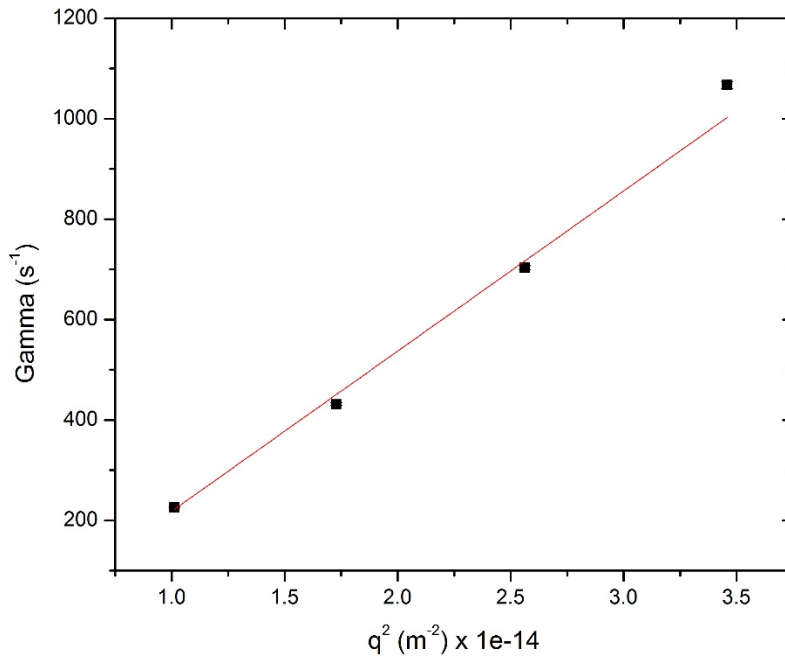


Figure 3. 15: Plotting gamma vs the squared of the scattering vector to get the diffusivity of sample C.

The slope of each line above is the diffusivity,  $D$ . Using equations 2.8 and 2.9, we can calculate the hydrodynamic diameter,  $d_h$ . The results are discussed in section 3.4.

### 3.3 Emulsion Analysis

Different concentration solutions of the hybrid nanoparticles in DI-Water were prepared. Those solutions were used for both the calculation of the interfacial tension (IFT) between oil and water, and for making oil and water dispersions. For the IFT measurements, the method described in section 2.3 was followed. For making oil and water dispersions, equal volumes of the nanoparticle solution and oil were mixed together using a vortex mixer. For the purposes of this study, Hexane was used as the oil in both IFT measurements and oil and water dispersions.

Following the method described in section 2.3, the following IFT results were obtained for samples A, B, and C in order.

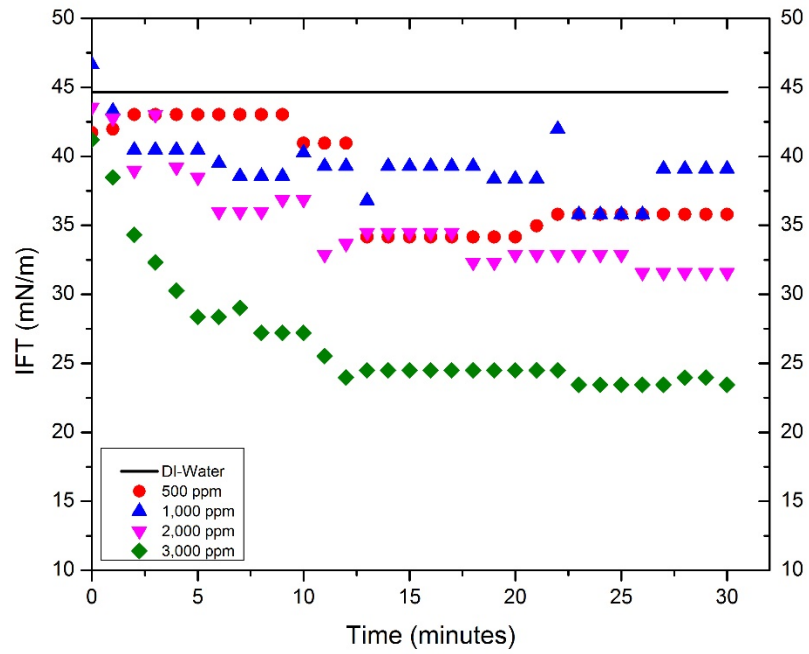


Figure 3. 16: The reduction of the interfacial tension between Hexane and DI-Water using the hybrid nanoparticles of sample A.

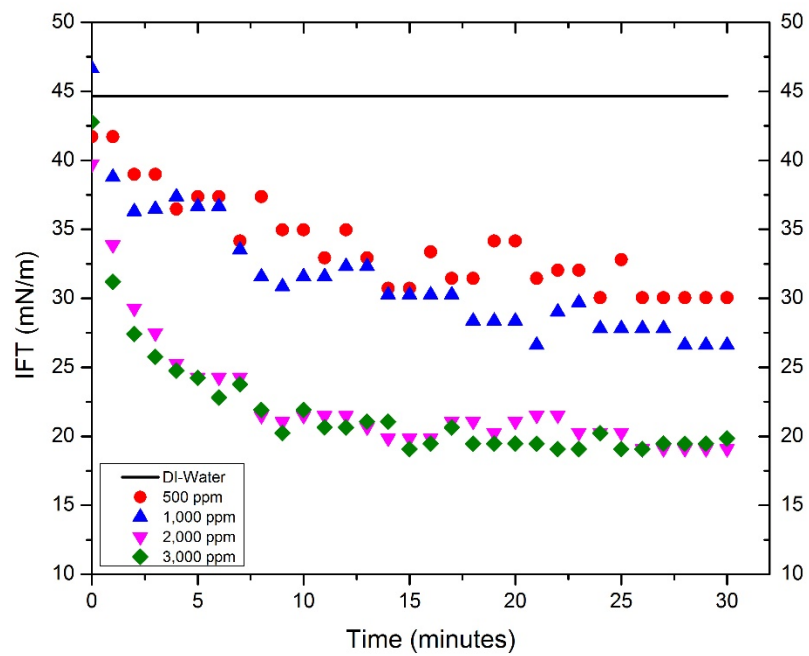


Figure 3. 17: The reduction of the interfacial tension between Hexane and DI-Water using the hybrid nanoparticles of sample B.

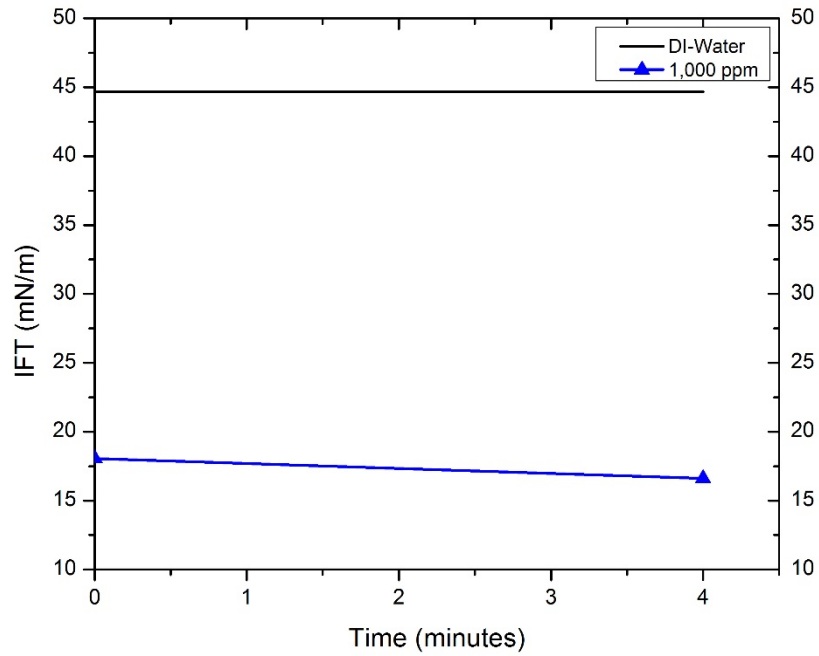


Figure 3. 18: The reduction of the interfacial tension between Hexane and DI-Water using the hybrid nanoparticles of sample C.

The black solid line on the top of each plot corresponds to the IFT between pure DI-Water and Hexane, and has a value of 44.7 mN/m. Also, the plots above show that as the concentration of the sample increases, the IFT is reduced faster and to lower levels.

### 3.4 Summary and Results

Table 3.1, shown below, summarizes the characterization of each of the samples mentioned above.

Table 3. 1: Table summarizing the characterization of the SiO<sub>2</sub>-POEOMA samples.

Sample	Reaction Time (minutes)	Mn (kDa)	PDI	Grafting Density		Dry State Diameter, d (nm)	Hydrodynamic Diameter, d <sub>h</sub> (nm)
				$\frac{chains}{SiO_2}$	$\frac{chains}{nm^2}$		
A	5	92	1.9	14	0.03	19	65
B	10	107	1.7	27	0.06	23	51
C	40	672	1.3	18	0.04	26	79

The molecular weight data obtained using GPC showed an increase in the molecular weight as the polymerization reaction time increased. This is consistent with what we had anticipated. TGA data were also consistent with what we had expected since the polymer weight fraction increased with increasing molecular weight. The figure below compares the TGA results for all three samples, and shows a clear increase in the polymer weight fraction as the molecular weight of the grafted polymer chains is increased.

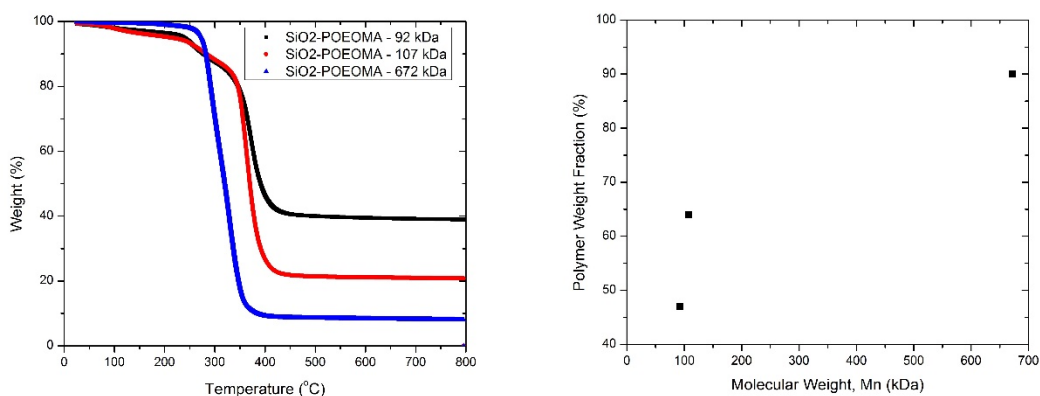


Figure 3. 19: The polymer weight fraction is increasing as the molecular weight of the grafted polymer chains is increased.

When the molecular weight of the polymer chains is increased, the length and weight of those chains are increased. Given that the grafting densities of those samples are relatively similar to each other, we have similar amounts of polymer chains in each sample, and so increasing the polymer chain length and weight would increase the polymer weight fraction in the sample. This is precisely what we see in the figure above. As the molecular weight of the polymer chains is increased, the drop in the weight corresponding to the polymer fraction increases reflecting the increase in the polymer weight fraction in the sample. The figure below shows the relationship between the inverse of the amount of residue in the samples and the molecular weight of the polymer chains in the samples. As shown in the figure, the increase is linear. This linearity indicates the constant grafting density of the hybrid nanoparticles. Increasing the molecular weight of the polymer chains without increasing the number of chains significantly, should increase the polymer weight fraction in the sample. This is precisely what the TGA data are showing us, as we just explained. Also, the figure below proves what we already summarized in table 3.1 above. As the table shows, the number of chains per squared nanometer is almost exactly the same for all three samples.

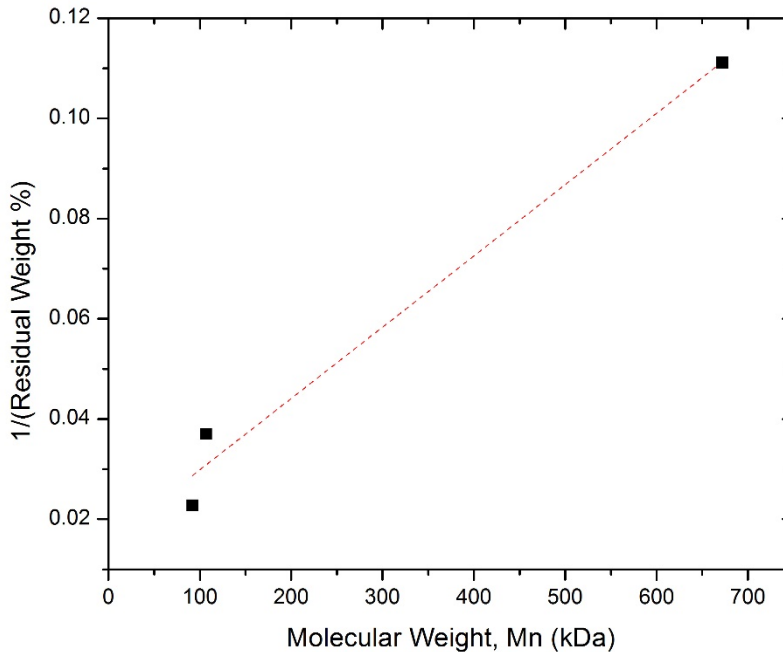


Figure 3. 20: The increase in the inverse of amount of residue with molecular weight of grafted polymer chains is linear. This linearity is indicative of the similar grafting densities in all three samples.

The dry state diameters obtained using SAXS data are also consistent with the increase in the molecular weight of the polymer chains stemming from increasing the polymerization reaction times from one sample to the other, as expected. When the molecular weight of the polymer chains is increased, the size of those chains increase, which in turn means that the overall size of the hybrid nanoparticles would also increase. As described earlier, the dry state diameter measured using SAXS is determined by the position of the first peak. As we can see in the figure below, the position of this peak is shifted the left, smaller  $q$  values, as the molecular weight of the polymer chains is increased. The smaller the  $q$  value, the larger the dry state diameter is since the size is inversely proportional to  $q$ .

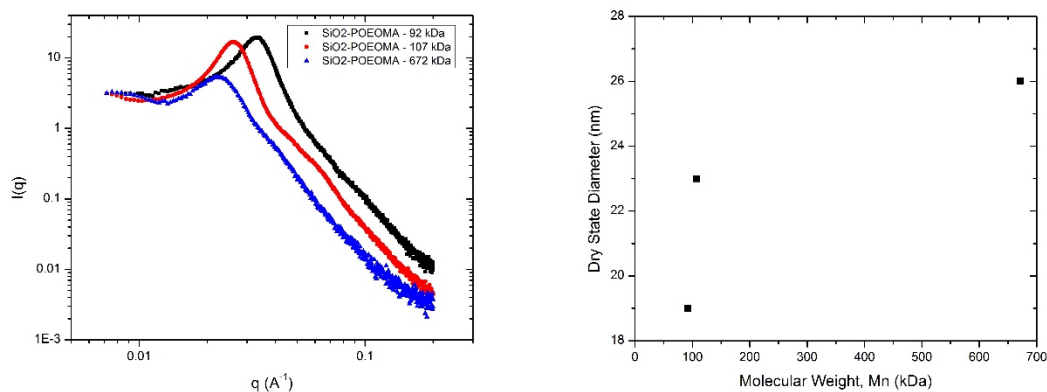


Figure 3. 21: The dry state diameter of the hybrid nanoparticles is increasing as the molecular weight of the grafted polymer chains is increasing.

The polymer chains investigated in this chapter of the study are hydrophilic polymer chains, which means that the polymer chains should extend when dissolved in DI-Water. The extension of the polymer chains would lead to a larger hydrodynamic diameters than their corresponding dry state diameters. As shown in table 3.1, the hydrodynamic diameter is larger than the corresponding dry state diameter. This proves that the polymer is indeed hydrophilic.

As the molecular weight of the polymer chains increases, the hydrodynamic diameter of the sample should increase. This is not the case here, however. As shown in table 3.1, the hydrodynamic diameter increases with molecular weight if we considered only samples B and C. It does not increase with molecular weight when sample A is added into consideration. Even though sample A has a smaller molecular weight than sample B, it has a larger hydrodynamic diameter. This is shown in the figure below.

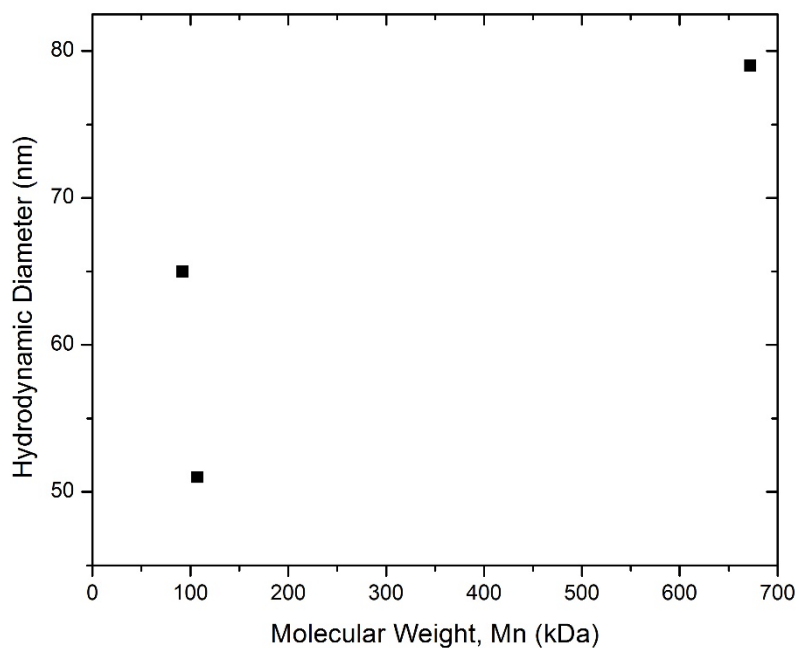


Figure 3. 22: The change in the hydrodynamic diameter as we increase the molecular weight of the grafted polymer chains.

The fact that the hydrodynamic diameter of the first sample was larger than that of the second sample even though the molecular weight of the grafted polymer chains in that sample is smaller led us to believe that this inconsistency either came from the GPC molecular weight results, or from the DLS hydrodynamic results. Taking into account that both the dry state diameter, and the polymer weight fraction are both increasing with the increase in the molecular weight is proof that the molecular weight is indeed increasing. This led us to believe that the GPC result is correct, while the DLS result for that sample is not.

At first, the hydrodynamic diameter for each sample was calculated using the method described in section 2.2.5. The values calculated from that were very high. Also, they were inconsistent with the increase in the molecular weight, as just mentioned. The hydrodynamic diameter for sample A, for example, was calculated to be 130 nm compared

to only 90 nm for sample B. This led us to calculate the maximum possible diameters for each sample just to double check.

The maximum possible diameters for the hybrid nanoparticles were calculated based on the length of the polymer chains, assuming fully extended polymer chains, and based on the diameter of the silica cores. The length of the fully extended polymer chains was calculated using<sup>44</sup>

$$R_{max} = n l \cos\left(\frac{\theta}{2}\right), \quad (3.2)$$

where:

$n$  = the number of skeleton bonds in the polymer chain; and

$l \cos\left(\frac{\theta}{2}\right)$  = the projected length of the skeleton bonds.

The figure below shows the parameters used in the above equation.

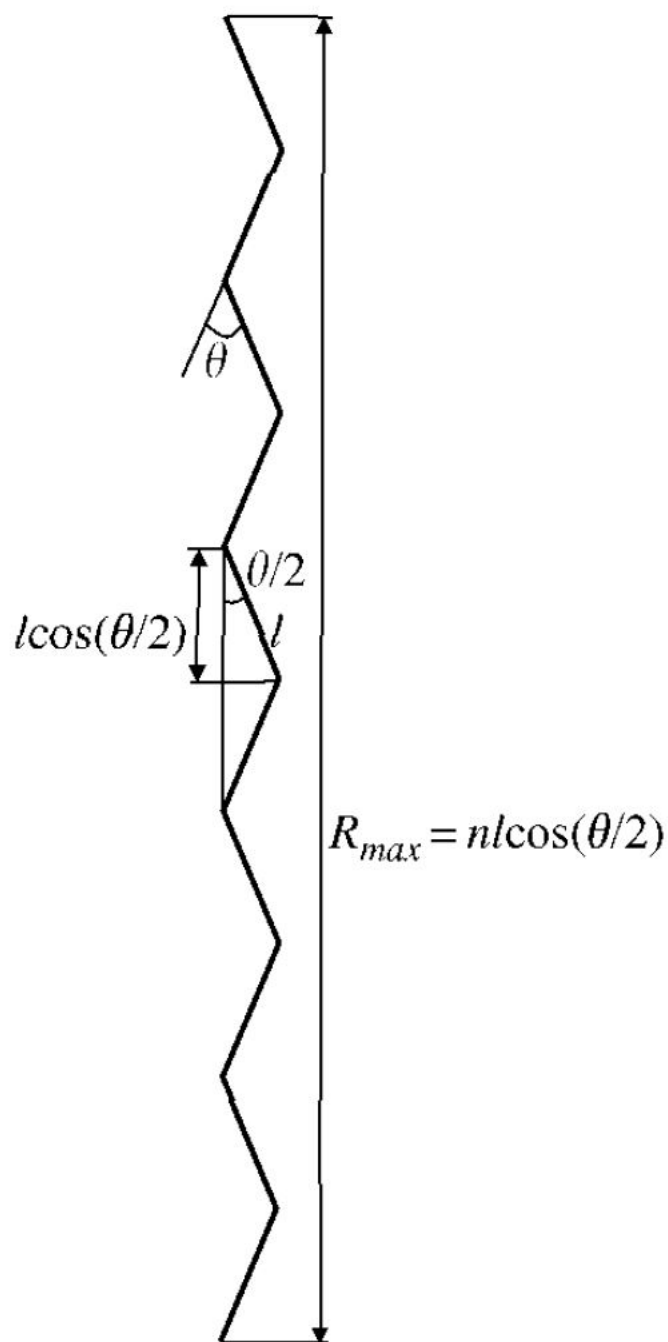


Figure 3. 23: A graph showing the largest polymer end-to-end distance and the definition of the angle  $\theta$  used in the equation of  $R_{max}$ .<sup>44</sup>

Based on the equation above, and the diameter of the silica cores, the maximum possible diameters for the hybrid nanoparticles, assuming fully extended polymer chains, are as follow: 140, 190, and 1,140 nm for samples A, B, and C in order.

As mentioned earlier, the hydrodynamic diameter of sample A, calculated using DLS, is 130 nm while the maximum possible diameter is 140 nm. Meaning, sample A is 93% of the maximum possible diameter for it. This led us to believe that the hydrodynamic diameter measured using DLS for sample A is incorrect. We believe that the hybrid nanoparticles in this sample aggregated prior to running DLS.

The fact that using the method described in section 2.2.5 showed that the hydrodynamic diameter for sample A is highly unreasonable led us to adjust our method of calculating the hydrodynamic diameter. Instead of using the slope to get the diffusivity, we used the diffusivity based on one of the angles. In our calculations, we used the gamma and the squared of the scattering vector values at the 90° angle to calculate the diffusivity. This gives us the diffusivity at that angle. We used this diffusivity, and the Stokes-Einstein equation, to get the hydrodynamic diameters for each sample. It is important to note that this method gives us an apparent hydrodynamic diameter that can only be used to compare different samples, not the actual hydrodynamic diameter. For the purposes of this investigation, this apparent hydrodynamic comparison is sufficient enough.

When investigating the IFT measurements, it was shown that the IFT values decreased both faster and to lower values with two parameter; concentration of the sample, and molecular weight of the polymer chains in the hybrid nanoparticles. Figures 3.16 and 3.17 show the effect of concentration on the IFT at constant molecular weights. The figure below shows the effect of the molecular weight on the IFT at constant concentrations, and table 3.2 below summarizes the IFT data for the different samples.

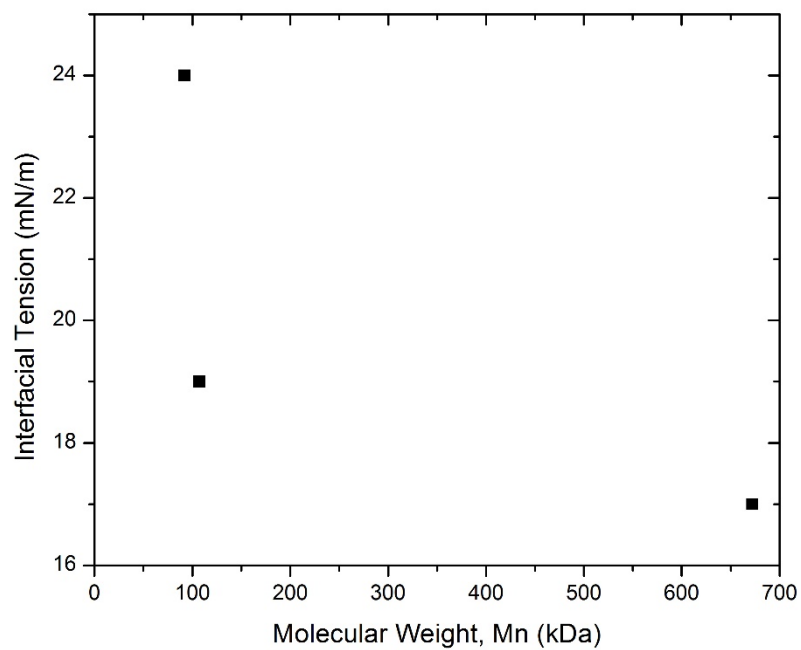
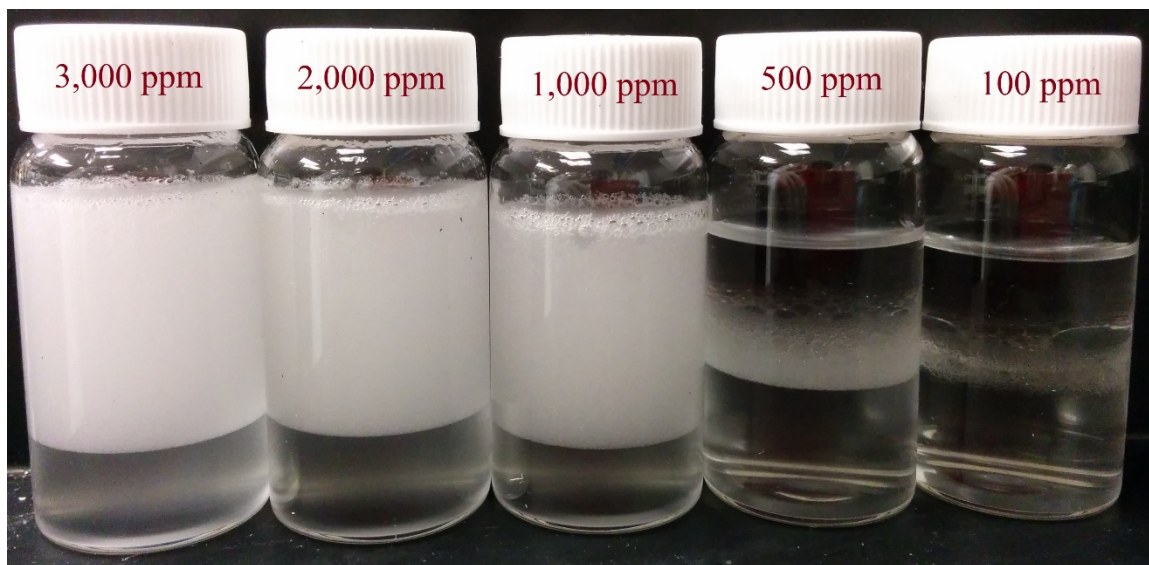


Figure 3. 24: The effect of the SiO<sub>2</sub>-POEOMA molecular weight (Mn) on the reduction of the interfacial tension between Hexane and DI-Water.

Table 3. 2: Table summarizing the IFT data of the SiO<sub>2</sub>-POEOMA samples.

Sample	Mn (kDa)	Interfacial Tension Between Hexane and DI-Water (mN/m)			
		at			
		500 ppm	1,000 ppm	2,000 ppm	3,000 ppm
A	92	36	36	32	24
B	107	30	27	19	19
C	672	N/A	17	N/A	N/A
Pure DI-Water		45			

We showed above that both the concentration and the molecular weight are important factors in the process of the IFT reduction. The increase in the concentration helps by providing more particles that can structure at the interface and reduce the IFT until saturation is reached at the interface.<sup>45</sup> That is why we believe the higher the concentration, the more stable the emulsion would be. This stability dependence on the concentration has also been proven in our study. As mentioned earlier, when we reduce the interfacial tension, we are able to create an emulsion of oil and water. Therefore, after proving that we can reduce the interfacial tension, we performed a dispersion test using different concentration solutions of the same molecular weight polymer chains. The figure below shows water in oil emulsions for different concentrations solutions; 100 ppm, 500 ppm, 1,000 ppm, 2,000 ppm, and 3,000 ppm from right to left. As the figure shows, the higher the concentration, the better the emulsion is and the more stable it is.



*Figure 3. 25: The effect of the hybrid nanoparticle concentration on the stability of the emulsion between Hexane and DI-Water.*

# Chapter 4 Amphiphilic Block Copolymer-Grafted Nanoparticles

## 4.1 Methodology

### 4.1.1 Materials

Platinum on Carbon (Sigma-Aldrich), Chlorodimethylsilane (98%, Sigma-Aldrich), Allyl 2-bromo-2-methylpropionate (98%, Sigma-Aldrich), MIBK-ST (Nissan Chemical), Hexamethyldisilazane (99.9%, Sigma-Aldrich), Methanol (Methyl Alcohol, Macron), Tetrahydrofuran (99+%, VWR), Hexanes (Macron), Deionized Water (DI-Water), Methyl Acrylate (99%, Sigma-Aldrich), Poly(ethylene glycol) methyl ether methacrylate (POEOMA, Average Mn 300, Sigma-Aldrich), N,N,N',N'',N''-Pentamethyl diethylene triamine (PMDETA, 99%, Sigma-Aldrich), Copper (I) bromide (98%, Sigma-Aldrich), 2,2'-Bipyridyl (99+%, Sigma-Aldrich), Aluminum oxide (Sigma-Aldrich), Inhibitor removers (Sigma-Aldrich), Hydrofluoric acid (HF, 48%, Sigma-Aldrich), Sodium hydroxide (NaOH, 97%, Sigma-Aldrich), and Magnesium sulfate (97%, Sigma-Aldrich).

### 4.1.2 Preparation

The amphiphilic block copolymer-grafted nanoparticles used in this study were poly(methyl acrylate-co-p(ethylene glycol) methyl ether methacrylate)-grafted silica nanoparticles, SiO<sub>2</sub>-P(MA-b-OEOMA). Two different batches of the SiO<sub>2</sub>-P(MA-b-OEOMA) were synthesized. Both the amounts of monomers added to each synthesis reaction, and the length of each reaction were changed according to the target molecular weight. The preparation of the particles followed the synthesis method described in section 2.1.5.

## 4.2 Characterization

### 4.2.1 Gel Permeation Chromatography (GPC)

After the first polymerization during the synthesis procedure, the SiO<sub>2</sub>-PMA polymerization, an aliquot was taken for GPC analysis. Then, after the whole synthesis procedure was completed, both the aliquot and the overall polymer-grafted nanoparticles, SiO<sub>2</sub>-P(MA-*b*-OEOMA), were dried at room temperature in a vacuum oven overnight. The polymer chains on the nanoparticle hybrid were cleaved using the procedure described in section 2.2.1. The cleaved polymer chains were then run in the GPC instrument. Below are the gathered GPC results showing the Size Exclusion Chromatography (SEC) curves for each sample. The graphs below only show the SEC curves for the overall block copolymer.

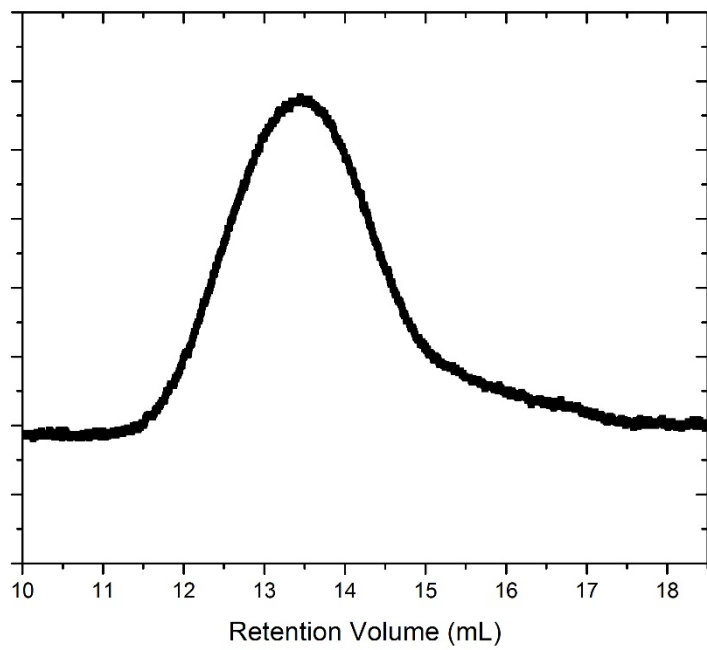


*Figure 4. 1: GPC results showing SEC curve for sample D.*

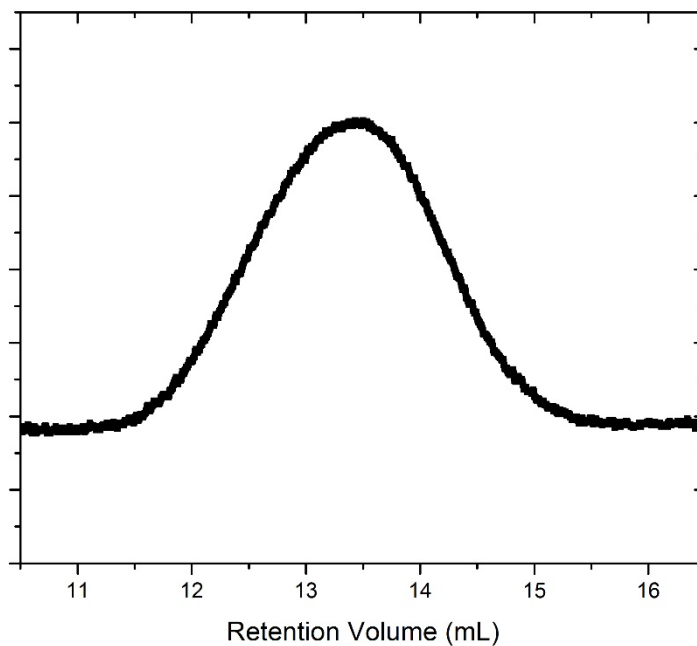


Figure 4. 2: GPC results showing SEC curve for sample E.

Upon analysis of the data using triple detection method in the Viscotek 270 instrument, both the number average molecular weight ( $M_n$ ), and the weight average molecular weight ( $M_w$ ) were determined for each sample. Using both  $M_n$  and  $M_w$ , the polydispersity Index (PDI) of the polymer chains was determined as<sup>16</sup>

$$PDI = M_w/M_n. \quad (4.1)$$

The GPC results, summarized in table 4.1, showed that  $M_n$  increased as the polymerization time was increased during the synthesis, which was as expected.

#### 4.2.2 Thermal Gravimetric Analysis (TGA)

A small amount of each sample of the overall hybrid nanoparticles was used to run TGA as described in section 2.2.2. Following are the results obtained for samples D and E:

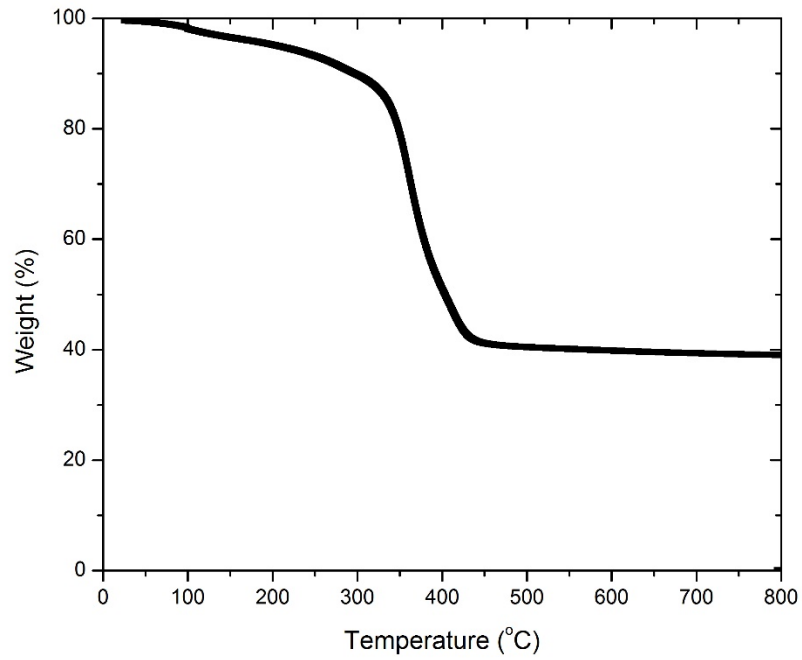


Figure 4. 3: TGA results showing weight change as temperature is increased from 25 °C to 800 °C for sample D.

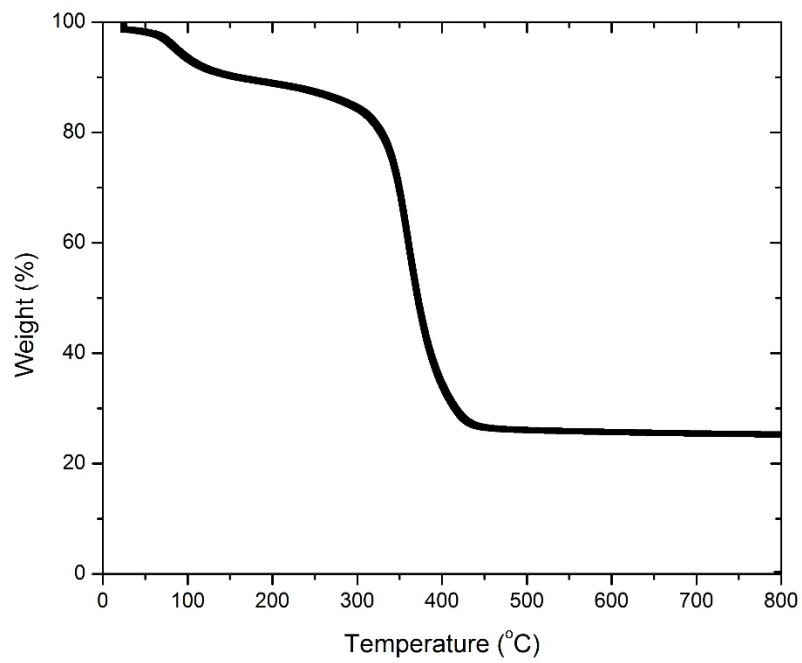


Figure 4. 4: TGA results showing weight change as temperature is increased from 25 °C to 800 °C for sample E.

The first weight drop, starting from the beginning up to around 100 °C, corresponds to residual solvent that was left in the sample due to incomplete drying. The second weight drop, starting from around 100 °C up to 300-350 °C, corresponds to the initiators in the sample. The final weight drop, starting from 300-350 °C, corresponds to the polymer chains in the sample. The rest of the mass of the sample corresponds to the silica cores in the samples. The polymer weight fractions obtained from TGA for samples D and E are 54% and 62%.

#### *4.2.3 Grafting Density*

Using the results obtained from both GPC and TGA, the grafting densities of the polymer chains on the silica cores were calculated. The equations used for those calculations are equations 2.1 and 2.2 in section 2.2.3. By controlling the amount of initiators to silica, as described in section 2.1.2, the grafting densities can be controlled. This study did not attempt to control the grafting density, nor did it investigate the effect of grafting densities on IFT measurements. The values for the grafting densities are summarized in table 4.1 below.

#### *4.2.4 Small Angle X-Ray Scattering (SAXS)*

A small amount of each sample of the overall hybrid nanoparticles was used to run SAXS measurements as described in section 2.2.4. When running SAXS, the scattering intensity and transmittance of the sample covered with kapton tape were gathered as well as those of the kapton tape alone so that we can correct for scattering from the tape according to equation 2.3 in section 2.2.4. The dry state diameters were then calculated according to equation 2.4 in section 2.2.4. Following are the results for the corrected data, as well as the fitted graph for samples D and E in order:

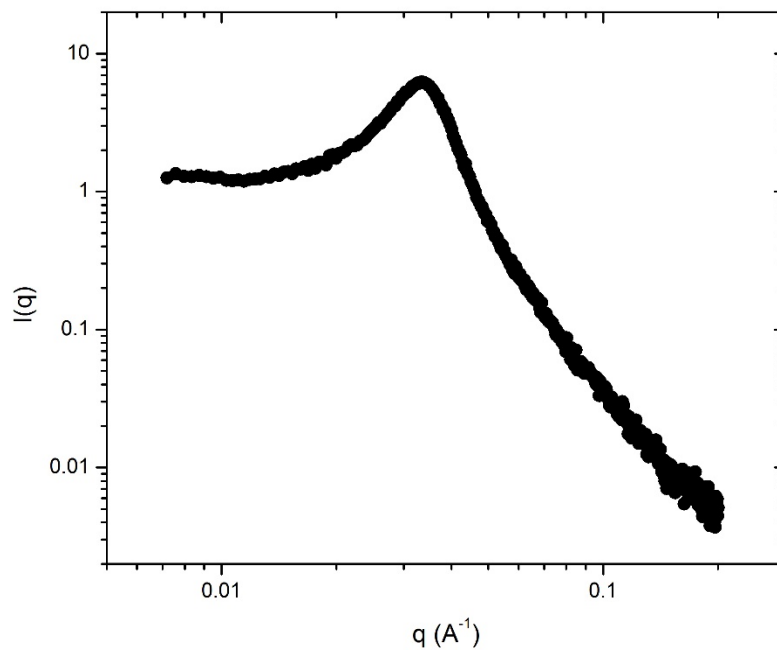


Figure 4. 5: SAXS results showing the scattering intensity as a function of the scattering vector for sample D.

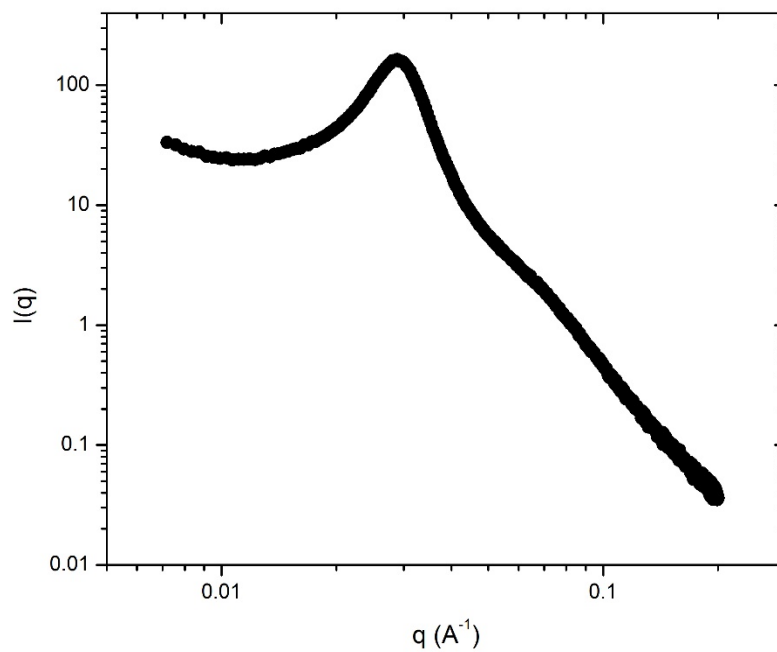


Figure 4. 6: SAXS results showing the scattering intensity as a function of the scattering vector for sample E.

The dry state diameter values for these samples are summarized in table 4.1 below.

#### 4.2.5 Dynamic Light Scattering (DLS)

For DLS analysis, 100 ppm solutions of each of the overall hybrid nanoparticle samples in DI-Water were prepared. Then, DLS was run according the procedure described in section 2.2.5. After running DLS on them, the following results were obtained for samples D and E in order:

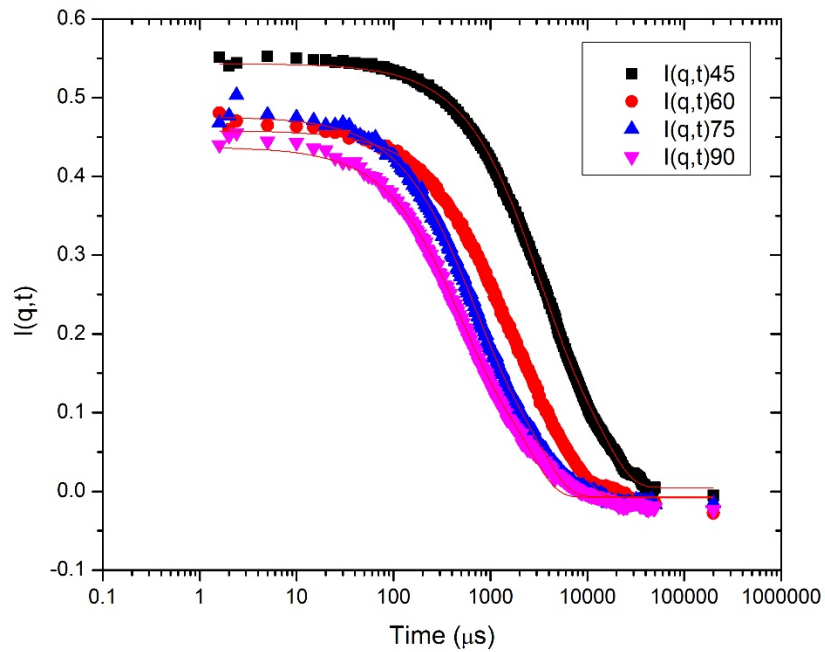


Figure 4. 7: DLS results showing scattering intensity as a function of time for sample D; used for fitting in the autocorrelation function.

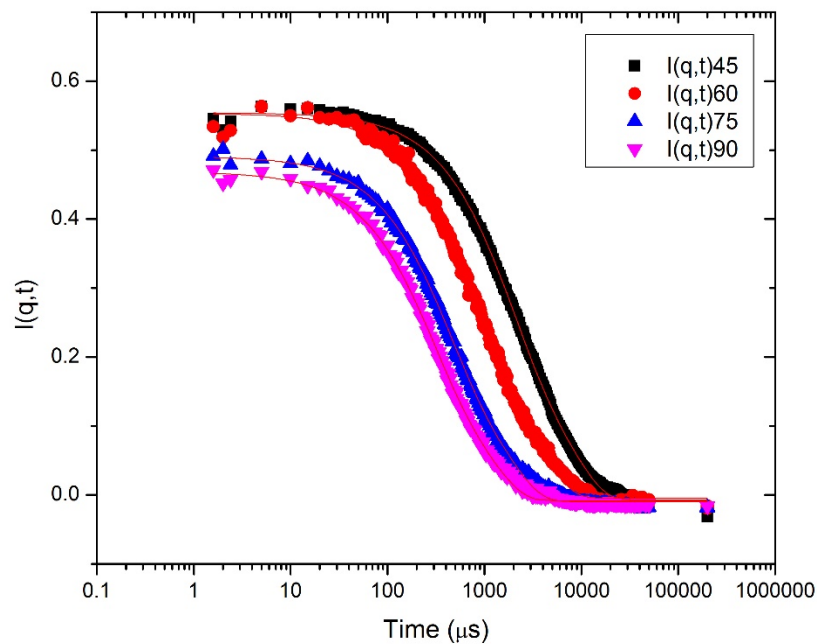


Figure 4. 8: DLS results showing scattering intensity as a function of time for sample E; used for fitting in the autocorrelation function.

Using a data analysis software, the data shown above for each sample were fitted to the autocorrelation function shown in equation 2.5 to obtain  $\bar{\Gamma}$ . As shown above, the angles used were 45°, 60°, 75°, and 90°. Those angles were used to calculate  $q^2$  according to equation 2.7. The following were obtained by plotting  $\bar{\Gamma}$  vs.  $q^2$ .

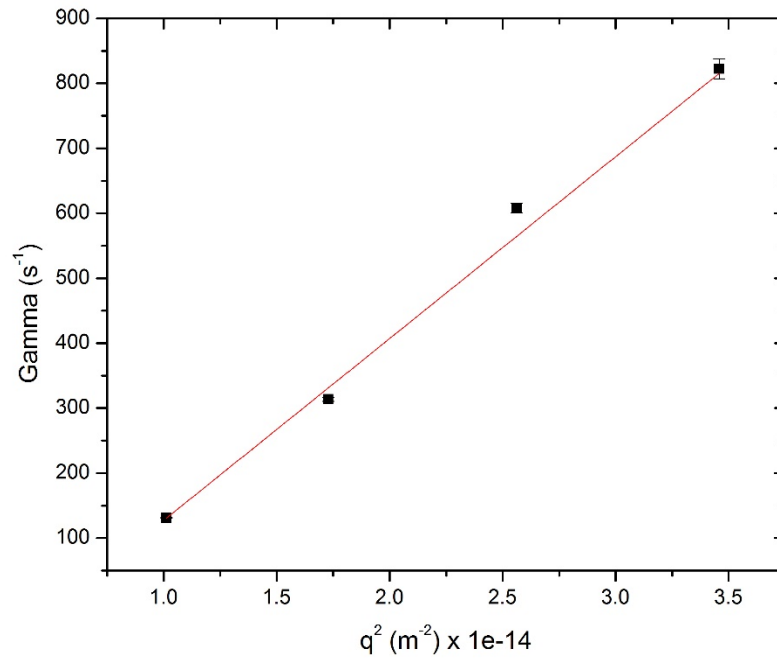


Figure 4. 9: Plotting gamma vs the squared of the scattering vector to get the diffusivity of sample D.

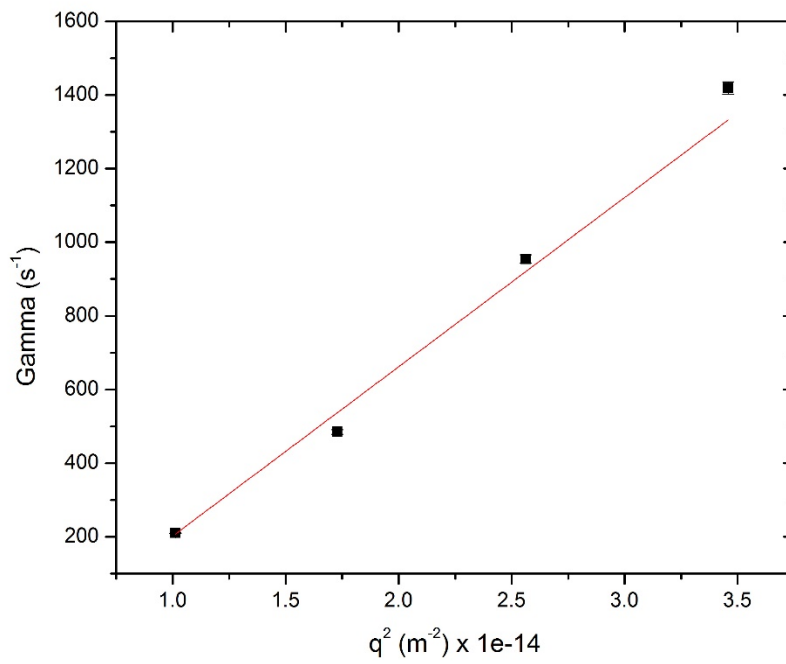


Figure 4. 10: Plotting gamma vs the squared of the scattering vector to get the diffusivity of sample E.

The slope of each line above is the diffusivity,  $D$ . Using equations 2.8 and 2.9, we can calculate the hydrodynamic diameter,  $d_h$ . The results are discussed in section 4.4.

### 4.3 Emulsion Analysis

Different concentration solutions of the hybrid nanoparticles in DI-Water were prepared. For the IFT measurements, the method described in section 2.3 was followed. For the purposes of this study, Hexane was used as the oil in IFT measurements.

Following the method described in section 2.3, the following IFT results were obtained for samples D and E in order.

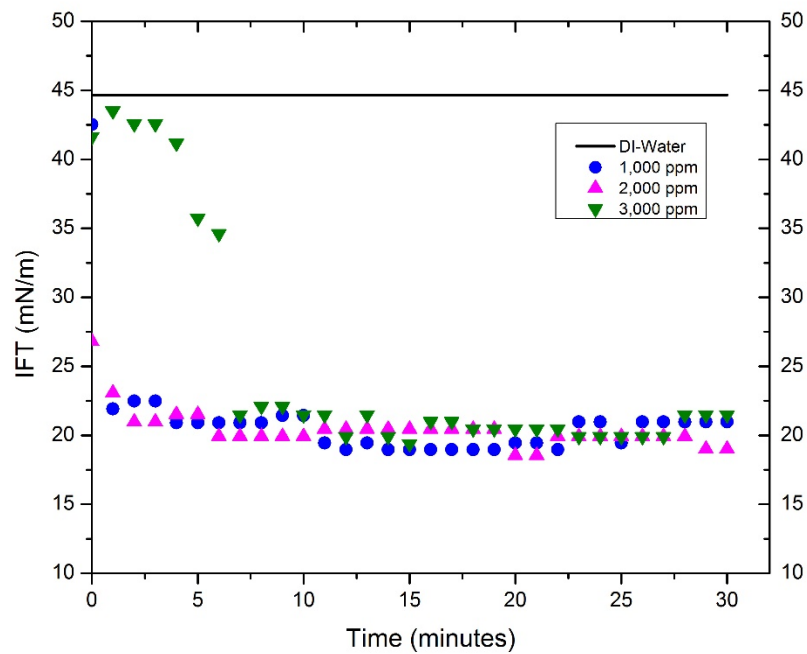


Figure 4. 11: The reduction of the interfacial tension between Hexane and DI-Water using the hybrid nanoparticles of sample D.

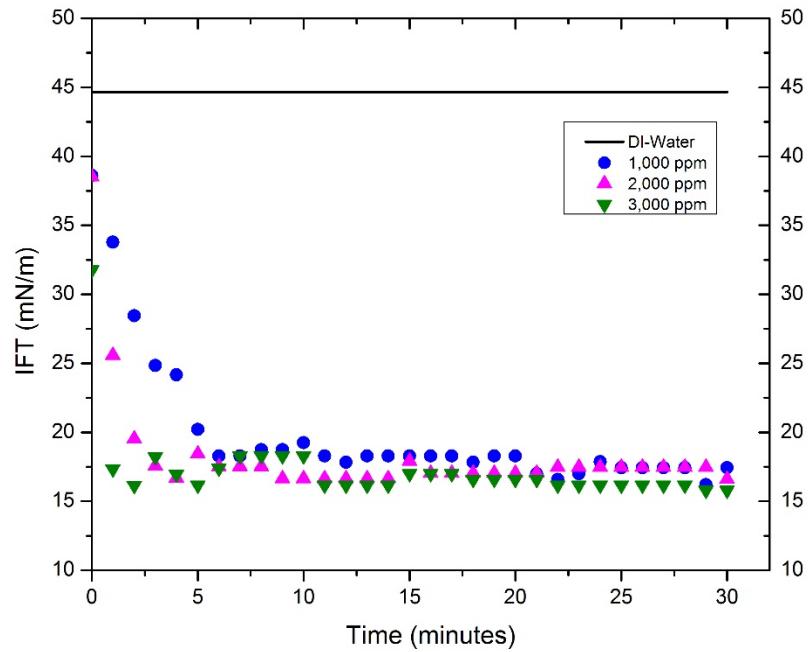


Figure 4. 12: The reduction of the interfacial tension between Hexane and DI-Water using the hybrid nanoparticles of sample E.

The black solid line on the top of each plot corresponds to the IFT between pure DI-Water and Hexane, and has a value of 44.7 mN/m. Also, the plots above show that as the concentration of the sample increases, the IFT is reduced faster and to lower levels.

## 4.4 Summary and Results

Table 4.1, shown below, summarizes the characterization of each of the samples mentioned above.

Table 4. 1: Table summarizing the characterization of the SiO<sub>2</sub>-P(MA-b-OEOMA) samples.

Sample	Reaction Time (hours)	Mn (kDa)	PDI	Grafting Density		Dry State Diameter, d (nm)	Hydrodynamic Diameter, d <sub>h</sub> (nm)
				$\frac{\text{chains}}{\text{SiO}_2}$	$\frac{\text{chains}}{\text{nm}^2}$		
D	1* / 0.5**	6 <sup>†</sup> 204 <sup>‡</sup>	1.0 <sup>†</sup> 2.0 <sup>‡</sup>	8	0.02	18	103
E	3* / 1**	150 <sup>†</sup> 302 <sup>‡</sup>	1.8 <sup>†</sup> 1.5 <sup>‡</sup>	7	0.02	22	60

\* The reaction time for the first synthesis; the SiO<sub>2</sub>-PMA polymerization.

\*\* The reaction time for the second synthesis; the POEOMA chain extension.

† Of the PMA block of the polymer.

‡ Of the overall P(MA-b-OEOMA) polymer.

The molecular weight data obtained using GPC showed an increase in the molecular weight as the polymerization reaction time increased. This is consistent with what we had anticipated. TGA data were also consistent with what we had expected since the polymer weight fraction increased with increasing molecular weight. The figure below

compares the TGA values of the samples discussed above, and shows a clear increase in the polymer weight fraction as the molecular weight of the grafted polymer chains is increased.

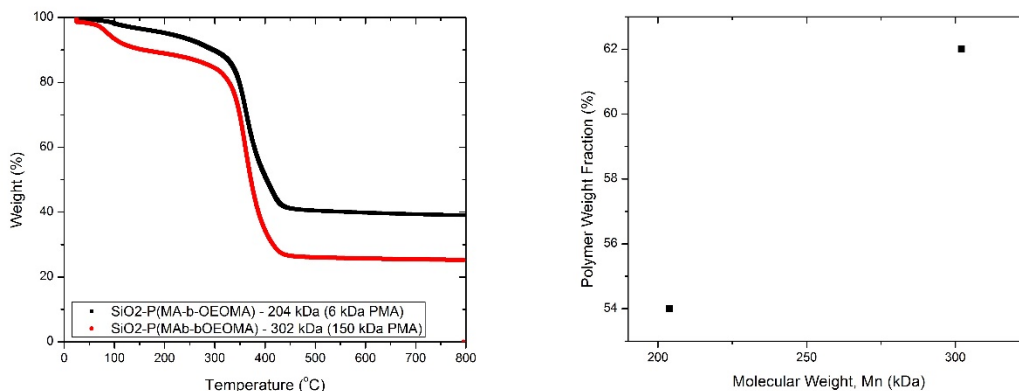


Figure 4. 13: The polymer weight fraction is increasing as the molecular weight of the grafted polymer chains is increased.

When the molecular weight of the polymer chains is increased, the length and weight of those chains are increased. Given that the grafting densities of those samples are almost exactly the same, we have similar amounts of polymer chains in each sample, and so increasing the polymer chain length and weight would increase the polymer weight fraction in the sample. This is precisely what we see in the figure above. As the molecular weight of the polymer chains is increased, the drop in the weight corresponding to the polymer fraction increases reflecting the increase in the polymer weight fraction in the sample. This is only true, however, if the grafting density is relatively similar in the samples. As table 4.1 shows, the number of polymer chains per squared nanometers is exactly the same in both samples. Therefore, increasing the molecular weight would increase the polymer weight fraction.

The dry state diameters obtained using SAXS data are also consistent with the increase in the molecular weight of the polymer chains stemming from increasing the

polymerization reaction times from one sample to the other, as expected. When the molecular weight of the polymer chains is increased, the size of those chains increase, which in turn means that the overall size of the hybrid nanoparticles would also increase. As described earlier, the dry state diameter measured using SAXS is determined by the position of the first peak. As we can see in the figure below, the position of this peak is shifted the left, smaller  $q$  values, as the molecular weight of the polymer chains is increased. The smaller the  $q$  value, the larger the dry state diameter is since the size is inversely proportional to  $q$ .

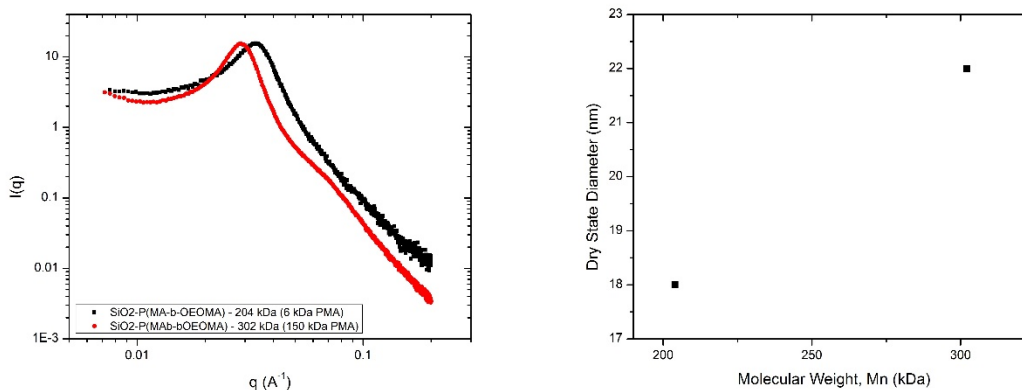


Figure 4. 14: The dry state diameter of the hybrid nanoparticles is increasing as the molecular weight of the grafted polymer chains is increasing.

The polymer investigated in this study is an amphiphilic block copolymer composed of an inner hydrophobic block followed by an outer hydrophilic block. This means that when the polymer is dissolved in DI-Water, we expect the inner block to collapse on itself, while the outer one to extend outward. The extension of the outer block, when considered on its own without regards to the collapse of the inner one, would lead to a hydrodynamic diameter that is larger than the dry state diameter. The collapse of the inner block, on the other hand, when considered on its own without regards to the extension of

the outer block, could possibly lead to a hydrodynamic diameter that is smaller than the dry state diameter.

When the two are combined, the collapse of an inner block and the extension of an outer one, we expect the hydrodynamic diameter to be larger than the dry state diameter, due to the extension of the outer block, but smaller in size than the hydrodynamic diameter of a hydrophilic homopolymer-grafted nanoparticle with the same length of polymer chains as that of the outer hydrophilic block in the amphiphilic block copolymer since the collapse of the inner part would affect the repeat units of the outer part closest to it. Meaning, since the inner part is a hydrophobic block, the outer block would have to cover it and shield it from getting into contact with the water molecular surrounding it. This covering and shielding process would prevent the inner repeat units of the outer hydrophilic block from fully extending outwards. The result is an amphiphilic block copolymer-grafted nanoparticle with a hydrodynamic diameter larger than its dry state diameter, but smaller than the hydrodynamic diameter of a hydrophilic homopolymer-grafted nanoparticle with polymer chains of the same length as the outer hydrophilic block of the amphiphilic block copolymer.

We expect the hydrodynamic diameter of the sample to increase as the molecular weight of the hydrophilic block increases. DLS data showed exactly that. In the case of the amphiphilic block copolymer-grafted nanoparticles, the hydrodynamic diameter increased when we increased the molecular weight of the hydrophilic block. This is shown in the figure below. In this figure, we plot the hydrodynamic diameter vs. the molecular weight of the outer hydrophilic block of the block copolymer instead of the overall molecular weight. This is because, as we had just described, the extension of the chains in water is

due to the hydrophilic nature of the outer block. Therefore, the hydrodynamic diameter depends solely on the length of the hydrophilic chain. This means that the DLS data are also consistent with the increase in the molecular weight.

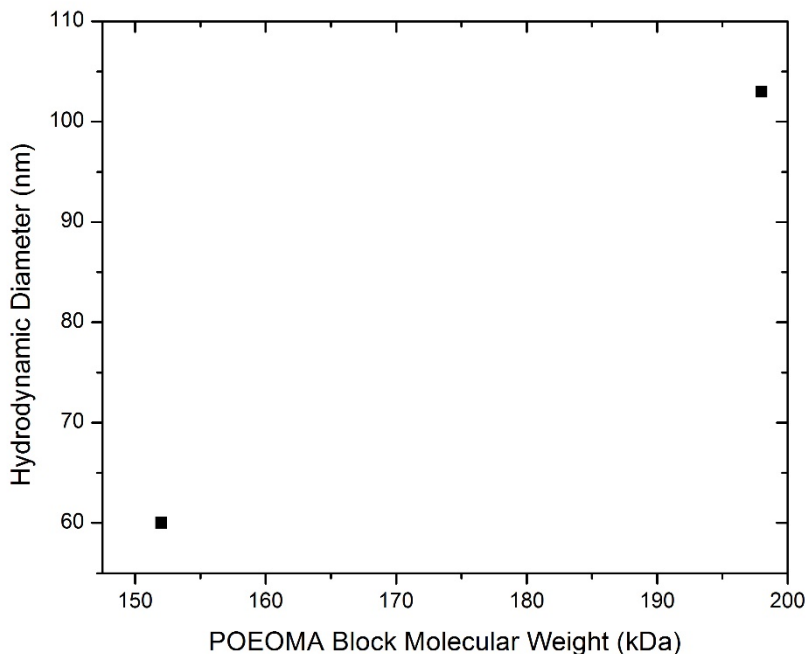


Figure 4. 15: The change in the hydrodynamic diameter as we increase the molecular weight of the hydrophilic part of the grafted polymer chains.

When calculating the hydrodynamic diameters for samples D and E, we calculated the apparent hydrodynamic diameters rather than the actual hydrodynamic diameter. The reason for this is to be consistent with samples A, B, and C. With samples D and E, just as with the other three samples, we used the apparent hydrodynamic diameters based on the data gathered from the 90° angle.

When investigating the IFT measurements, it was shown that the IFT values decreased both faster and to lower values with the concentration of the sample. Since sample D had a larger hydrodynamic radius because it has the longer hydrophilic chain, we expected it to have a better IFT reduction abilities than sample E. This was not the case,

however. Sample E was able to reduce it by 3 mN/m more than sample D. We believe that this small difference can be considered within the experimental error of the study. Therefore, our conclusion that the IFT reduction ability depends on the size of the hybrid nanoparticles, thus on their molecular weight, was not affected. Figures 4.11 and 4.12 show the effect of concentration on the IFT at constant molecular weights. The figure below shows the effect of the molecular weight on the IFT at constant concentrations. Table 4.2 below summarizes the IFT data for the different samples.

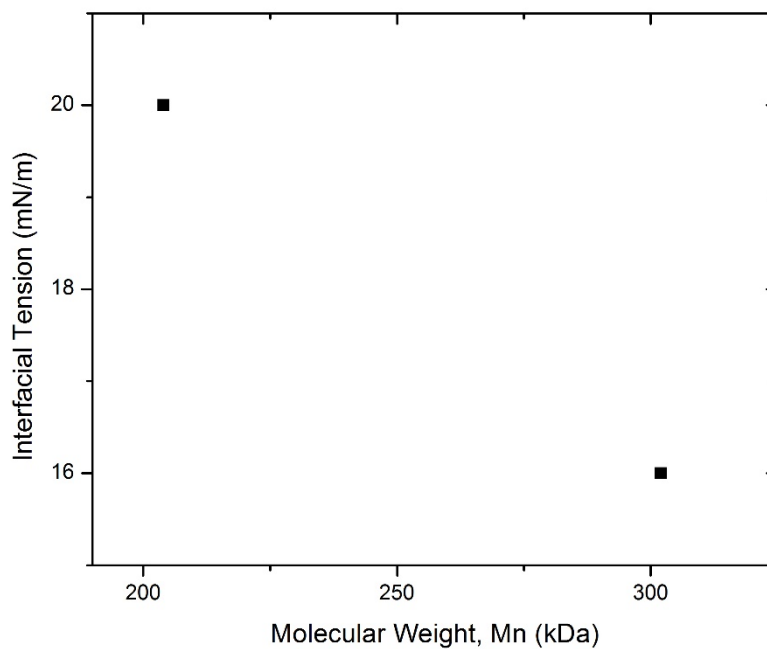


Figure 4. 16: The effect of the SiO<sub>2</sub>-P(MA-*b*-OEOMA) molecular weight (*M<sub>n</sub>*) on the reduction of the interfacial tension between Hexane and DI-Water.

Table 4. 2: Table summarizing the IFT data of the SiO<sub>2</sub>-P(MA-*b*-OEOMA) samples.

Sample	Molecular Weight, Mn (kDa)		Interfacial Tension Between Hexane and DI-Water (mN/m) at		
	PMA	Overall	1,000 ppm	2,000 ppm	3,000 ppm
D	6	204	21	20	20
E	150	302	17	17	16
Pure DI-Water			45		

## Chapter 5 Conclusion

### 5.1 Summary and Conclusion

In this study, we added a hydrophobic block to a hydrophilic block to create amphiphilic block copolymer chains. The hydrophobic block chosen in this study is also lyophobic to alkane oils. The objective was to test the effect this block would have on the reduction of the interfacial tension between an alkane oil and water. As we mentioned earlier, this has been done in a previous study, and the IFT reduction capabilities decreased instead of enhancing due to the use of amphiphilic block copolymer chains. In that study, however, they coated the polymer chains on the colloidal nanoparticles. Our study was conducted to investigate whether this decrease in the IFT reduction capabilities was due to the coating of the polymer chains compared to grafting them, or due to the lack of interactions between the hydrophobic block and the alkane oil. In order to arrive at a definite answer to this question, we used polymers and oils similar to the ones they used in order to imitate, as much as possible, their study.

Therefore, in our study, we used two classes of polymer-grafted nanoparticles. The first class, discussed in chapter 3, was the hydrophilic homopolymer-grafted nanoparticles, and we used poly(p(ethylene glycol) methyl ether methacrylate))-grafted silica nanoparticles, SiO<sub>2</sub>-POEOMA for that. The second class, discussed in chapter 4, was the amphiphilic block copolymer-grafted nanoparticles, and we used poly(methyl acrylate-co-(ethylene glycol) methyl ether methacrylate))-grafted silica nanoparticles, SiO<sub>2</sub>-P(MA-b-OEOMA) for that. The oil used in both cases was Hexane, an alkane oil. The hydrophobic block that's lyophobic to Hexane is the PMA block of the polymer.

Both classes have proven their ability to reduce the interfacial tension very well. During the investigation, it was shown that the ability to reduce the interfacial tension in both depends on the concentration of the nanoparticle solution, and the molecular weight of the polymer chains grafted on the nanoparticles. We believe that there are more parameters that would also affect the ability to reduce the interfacial tension, but they were beyond the scope of this investigation.

As we showed in equations 1.11, 1.14, and 1.15 in section 1.1.2, the adsorption energy of the particles at the interface is proportional to the radius of the particles squared. This means that the larger the particles used are, the better they adsorb to the interface. We also described in that section that the better the adsorption at the interface, the higher their interfacial tension reduction capabilities, which means lower IFT values can be achieved. This has been proven clearly in our study. We explained earlier that the size of the hybrid nanoparticles increase as we increase the molecular weight of the polymer chains grafted to the colloidal silica cores. We also showed that the higher the molecular weight, the better the interfacial tension reduction capabilities of the hybrid nanoparticles were.

We were also able to show in table 3.2 that the dependence of the IFT reduction on the molecular weight is larger than that on the concentration of the hybrid nanoparticles solution. As shown in that table, we were able to reduce the IFT using 1,000 ppm of sample C much better than we were using 3,000 ppm of sample A. The fact that even with a third of the concentration, we were able to achieve better IFT reduction results simply because the molecular weight is larger proves that the dependence on the molecular weight is larger than the dependence on the hybrid nanoparticles solution concentration.

The dependence of the interfacial reduction on the hybrid nanoparticles solution concentration stems from the fact that as we increase the concentration, we are providing more particles that can adsorb at the interface. The more particles we introduce to adsorb at the interface, the more saturation we achieve. Once we achieve saturation of the hybrid nanoparticles at the interface, increasing the concentration further does not make any difference anymore. We believe that this is the only reason behind the dependence on the hybrid nanoparticles concentration.

In this study, we were able to reduce the interfacial tension significantly between Hexane and water; we were able to reduce the IFT from  $\sim 45$  mN/m to  $\sim 24$  mN/m using sample A, to  $\sim 19$  mN/m using sample B, and to  $\sim 17$  mN/m using sample C of the hydrophilic homopolymer-grafted nanoparticles, SiO<sub>2</sub>-POEOMA. This reduction of 21 to 28 mN/m is noteworthy compared to previous efforts mentioned in section 1.3. Those values are also very similar to those gathered by Kim in his investigation of the same polymer-grafted nanoparticles and the same type of oil.<sup>3</sup>

We were also able to reduce the interfacial tension significantly between Hexane and water using the amphiphilic block copolymer-grafted nanoparticles in this study. As mentioned earlier, we were able to reduce the IFT value from  $\sim 45$  mN/m to  $\sim 20$  mN/m using sample D, and to  $\sim 16$  mN/m using sample E. The figure below shows a comparison between the ability to reduce IFT in each class.

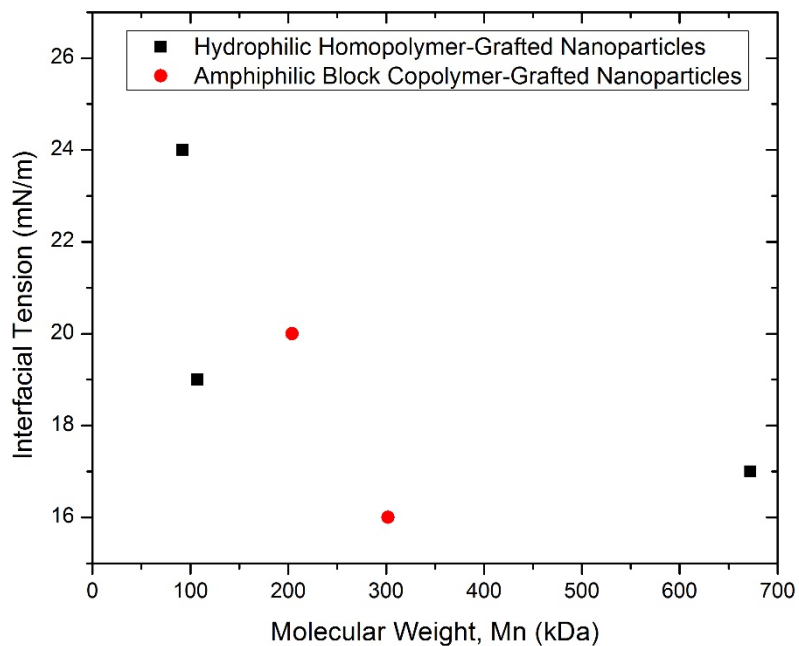


Figure 5. 1: A figure comparing the ability of the two different classes of polymer-grafted nanoparticles to reduce the interfacial tension between hexane and water.

As we can see, the difference between the IFT reduction capabilities of the amphiphilic block copolymer-grafted nanoparticles and the hydrophilic homopolymer-grafted nanoparticles are not different from each other at all. Using SiO<sub>2</sub>-POEOMA, we were able to reduce the IFT to 17 mN/m, while we were able to reduce it to 16 mN/m using SiO<sub>2</sub>-P(MA-b-OEOMA). This difference of 1 mN/m is within the experimental error we had in this investigation. Meaning, there is absolutely no difference in their ability to reduce the IFT between Hexane and water.

The fact that the PMA block is hydrophobic and also lyophobic to the oil used in this study suggest that this block did not interact with either side of the interface. Being hydrophobic prevented it from interacting with the water molecules, and being lyophobic to hexane prevented it from interacting with the hexane molecules. In fact, it was observed that PMA is lyophobic to hexane to the extent that it precipitates when added to it. Meaning,

at the interface, our amphiphilic block copolymer-grafted nanoparticles behaved as hydrophilic homopolymer-grafted nanoparticles.

As mentioned earlier, we purposely grafted our polymer chains to our nanoparticles in order to test whether the cause of the lack of enhancement in the IFT reduction abilities was due to the lack of interactions between PMA and Hexane, or due to the coating vs. grafting. Since we grafted them, yet we still did not achieve any enhancement in the IFT reduction abilities, we can say with confidence that the problem was with the lack of interaction between the hydrophobic block and the alkane oil.

In the case of the study mentioned earlier and done by Yoon *et al.*, not only were they not able to enhance the IFT reduction abilities by converting the hydrophilic homopolymer chains into amphiphilic block copolymer ones, but they actually achieved less IFT reduction. We believe the reason behind that is the fact that they had their hydrophobic PBA block on the outside. As we discussed in this study, the amphiphilic block copolymer chains behaved as hydrophilic homopolymer chains at the interface. This was due to the fact that the PMA block was both hydrophobic and lyophobic to alkane oils. This means that the PMA block would have to be shielded by the POEOMA block so it would not interact with either side of the interface. Had we synthesized the PMA block on the outside, the POEOMA block would not have been able to shield it. In that case, the POEOMA would not have been able to interact with the water molecules as it would have preferred either since the PMA block would collapse and prevent the POEOMA block from interacting freely. This is what we believe to have happened in their study and the cause for the less IFT reduction.

In section 1.3, we also mentioned that when Kim investigated the effect of an amphiphilic block copolymer on the interfacial tension between oil and water, he was able to achieve much lower interfacial tension values, which means he was able to reduce the IFT much more impressively. He was able to achieve 25 fold better IFT reduction capabilities using the amphiphilic block copolymer-grafted nanoparticles compared to hydrophilic homopolymer-grafted nanoparticles using the same oil. We believe the reason behind this is the type of hydrophobic block used, as well as the type of oil used. In his investigation of the amphiphilic block copolymer-grafted nanoparticles capabilities to reduce the interfacial tension, Kim used Toluene as the oil and Polystyrene as his hydrophobic block. Polystyrene consists of a toluene group and a methane group. The similarity in the structure of his hydrophobic block and the oil he used allows for a much higher interfacial activity, which would lead to much better IFT reduction. This led us to the conclusion that the interfacial activity seems to be the far more dominant parameter in the reduction of the interfacial tension.

## **5.2 Future Work**

In this study, we have investigated the effect of two classes of polymer-grafted nanoparticles on the interfacial tension between oil and water; a hydrophilic homopolymer-grafted nanoparticles, and an amphiphilic block copolymer-grafted nanoparticles. The oil used in this investigation was Hexane. Using those polymer-grafted nanoparticles, we were able to successfully reduce the interfacial tension.

Since the applications of this research include the cleaning of oil spills, we believe it is important to look into biodegradable polymer chains instead. As we discussed earlier, the idea of creating emulsions is to allow for accessibility of the hydrocarbons to bacteria

and microorganisms. When they consume the oil molecules through the process of biodegradation, they leave the hybrid nanoparticles behind, and we worry about the effect of leaving those hybrid nanoparticles on the environment. The colloidal silica cores do not pose any threat to the environment since they are basically just sand particles. The problem is with the polymer chains. If we use biodegradable polymer chains, however, we eliminate this problem.

Keeping in mind that natural oil is composed of many different kinds, it is important to test the effect those hybrid nanoparticles would have on reducing the IFT between oil and those other types of oils. It would be highly beneficial to test the effect of different types of polymer chains on different types of oils. The idea behind this is to optimize hybrid nanoparticles that would be effective at reducing the IFT between a wider range of types of oils and water so we can utilize them with natural oil.

In order to optimize the IFT reduction, not only would it be beneficial to look at different types of polymers, but also at the order of the polymer blocks in the case of the amphiphilic block copolymer-grafted nanoparticles. Another way to optimize the IFT reduction would be to look at other parameters that might affect the IFT that were beyond the scope of this investigation. An example of such parameters would be the grafting density of the polymer chains on the colloidal silica cores. During the study, we proposed a method to control the grafting density of the polymer chains, but did not attempt to test it. It would be beneficial to test this proposed method, and investigate the effect of the grafting density on reducing the interfacial tension.

Finally, when discussing the stability of the oil and water emulsions, it is important to come up with quantitative parameters. Using quantitative parameters allows us to truly

compare the different classes of nanoparticles, the different types of polymers, as well as the different parameters discussed above such as grafting density, hybrid nanoparticles solution concentration, molecular weight of grafted polymer chains, etc. Two main quantitative parameters have been discussed in the literature to explain the stability of the emulsions; the volume fraction of the emulsion phase to the overall volume, and for how long the emulsion can remain stable.<sup>3,31</sup> The former is affected by the latter; the stability could change with time, which would mean that the volume fraction could change with time as well. In that case, it would be highly interesting, informative, and beneficial to try to come up with a formula for the stability of the emulsion as a function of time.

## References

1. Katepalli, H. Formation and Stability of Emulsions : Effect of Surfactant- Particle Interactions and Particle. (University of Rhode Island, 2014).
2. Beydoun, D., Guang, D., Chhabra, R. P. & Raper, J. A. Particle settling in oil-in-water emulsions. *Powder Technol.* **97**, 72–76 (1998).
3. Kim, D. NANOPARTICLES FOR OIL DISPERSANTS AND NANO TRACERS. (2015).
4. Shell, M. S. *Thermodynamics and Statistical Mechanics - An integrated approach.* (2014).
5. Bresme, F. & Oettel, M. Nanoparticles at fluid interfaces. *J. Phys. Condens. Matter* **19**, 413101 (2007).
6. Binks, B. P. & Lumsdon, S. O. Influence of Particle Wettability on the Type and Stability of Surfactant-Free Emulsions †. *Langmuir* **16**, 8622–8631 (2000).
7. Foster, L. M., Worthen, A. J., Foster, E. L., Dong, J., Roach, C. M., Metaxas, A. E., Hardy, C. D., Larsen, E. S., Bollinger, J. A., Truskett, T. M., Bielawski, C. W. & Johnston, K. P. High interfacial activity of polymers ‘grafted through’ functionalized iron oxide nanoparticle clusters. *Langmuir* **30**, 10188–10196 (2014).
8. Dickinson, E., Ritzoulis, C., Yamamoto, Y. & Logan, H. Ostwald ripening of protein-stabilized emulsions: Effect of transglutaminase crosslinking. *Colloids Surfaces B Biointerfaces* **12**, 139–146 (1999).
9. Ponnampati, R., Karazincir, O., Dao, E., Ng, R., Mohanty, K. K. & Krishnamoorti, R. Polymer-functionalized nanoparticles for improving waterflood sweep

- efficiency: Characterization and transport properties. *Ind. Eng. Chem. Res.* **50**, 13030–13036 (2011).
10. Alvarez, N. J., Anna, S. L., Saigal, T., Tilton, R. D. & Walker, L. M. Interfacial dynamics and rheology of polymer-grafted nanoparticles at air-water and xylene-water interfaces. *Langmuir* **28**, 8052–8063 (2012).
  11. Cervantes Martinez, A., Rio, E., Delon, G., Saint-jalmes, A., Langevin, D., Binks, B. P., Martinez, A. C., Rio, E., Delon, G., Saint-jalmes, A., Langevin, D. & Binks, B. P. On the origin of the remarkable stability of aqueous foams stabilised by nanoparticles: link with microscopic surface properties. *Soft Matter* **4**, 1531 (2008).
  12. Yoon, K. Y., Li, Z., Neilson, B. M., Lee, W., Huh, C., Bryant, S. L., Bielawski, C. W. & Johnston, K. P. Effect of adsorbed amphiphilic copolymers on the interfacial activity of superparamagnetic nanoclusters and the emulsification of oil in water. *Macromolecules* **45**, 5157–5166 (2012).
  13. Weiss, J., Cancelieri, C. & McClements, D. Mass Transport phenomena in oil-in-water emulsions containing surfactant micelles: Ostwald ripening. *Langmuir* **16**, 6833–6838 (2000).
  14. Binks, B. P. & Fletcher, P. D. I. Particles Adsorbed at the Oil-Water Interface : A Wettability and ‘ Janus ’ Particles. *Langmuir* **17**, 4708–4710 (2001).
  15. Dong, J., Li, J. & Zhou, J. Interfacial and phase transfer behaviors of polymer brush grafted amphiphilic nanoparticles: A computer simulation study. *Langmuir* **30**, 5599–5608 (2014).
  16. Hiemenz, P. & Lodge, T. *Polymer chemistry*. (2007).

17. Gonzalez, J., Figueiras, F. G., Aranguren-Gassis, M., Crespo, B. G., Fernández, E., Morón, X. A. G. & Nieto-Cid, M. Effect of a simulated oil spill on natural assemblages of marine phytoplankton enclosed in microcosms. *Estuar. Coast. Shelf Sci.* **83**, 265–276 (2009).
18. Peterson, C. H., Rice, S. D., Short, J. W., Ester, D., Bodkin, J. L., Ballachey, B. E. & Irons, D. B. Long-Term ecosystem response to the Exxon Valdez oil spill. *Science* (80-. ). **302**, 2082–2086 (2003).
19. Fallis, A. . The Fate of the Oil Spilled from the Exxon Valdez. *J. Chem. Inf. Model.* **53**, 1689–1699 (2013).
20. Mullin, J. V. & Champ, M. A. Introduction/overview to in situ burning of oil spills. *Spill Sci. Technol. Bull.* **8**, 323–330 (2003).
21. Krishnamoorti, R., Bose, A. & John, V. T. Cover for Technical Volume for Effectiveness of Conventional and Novel Dispersant Technologies for Arctic Oil in Slush and Ice Conditions.
22. Buist, I. A., Potter, S. G. & Walker, A. H. *In situ burning in ice-affected waters: a technology summary and lessons from key experts.* (2013).
23. Nedwed, T. & Canevari, G. P. New Dispersant Gel Effective on Cold, Viscous Oils. in (2011). at <<http://www.ioscproceedings.org/doi/abs/10.7901/2169-3358-2011-1-109>>
24. Hamdan, L. J. & Fulmer, P. A. Effects of COREXIT?? EC9500A on bacteria from a beach oiled by the Deepwater Horizon spill. *Aquat. Microb. Ecol.* **63**, 101–109 (2011).
25. Rodd, A. L., Creighton, M. A., Vaslet, C. A., Rangel-mendez, J. R., Hurt, R. H. &

- Kane, A. B. Effects of Surface-Engineered Nanoparticle-Based Dispersants for Marine Oil Spills on the Model Organism *Artemia franciscana*. (2014).  
doi:10.1021/es500892m
26. Ju, B., Fan, T. & Ma, M. Enhanced oil recovery by flooding with hydrophilic nanoparticles. *China Particuology* **4**, 41–46 (2006).
  27. Chengara, A., Nikolov, A. D., Wasan, D. T., Trokhymchuk, A. & Henderson, D. Spreading of nanofluids driven by the structural disjoining pressure gradient. *J. Colloid Interface Sci.* **280**, 192–201 (2004).
  28. Zhang, H., Nikolov, A. & Wasan, D. Enhanced oil recovery (EOR) using nanoparticle dispersions: Underlying mechanism and imbibition experiments. *Energy and Fuels* **28**, 3002–3009 (2014).
  29. Saleh, N., Sarbu, T., Sirk, K., Lowry, G. V, Matyjaszewski, K. & Tilton, R. D. Oil-in-Water Emulsions Stabilized by Highly Charged Polyelectrolyte-Grafted Silica Nanoparticles †. *Langmuir* **21**, 9873–9878 (2005).
  30. Saigal, T., Dong, H., Matyjaszewski, K. & Tilton, R. D. Pickering emulsions stabilized by nanoparticles with thermally responsive grafted polymer brushes. *Langmuir* **26**, 15200–15209 (2010).
  31. Kim, D. & Krishnamoorti, R. Interfacial Activity of Poly[oligo(ethylene oxide)–monomethyl ether methacrylate]-Grafted Silica Nanoparticles. *Ind. Eng. Chem. Res.* **54**, 3648–3656 (2015).
  32. Binks, B. P., Desforges, A. & Duff, D. G. Synergistic stabilization of emulsions by a mixture of surface-active nanoparticles and surfactant. *Langmuir* **23**, 1098–1106 (2007).

33. Katepalli, H., John, V. T. & Bose, A. The response of carbon black stabilized oil-in-water emulsions to the addition of surfactant solutions. *Langmuir* **29**, 6790–6797 (2013).
34. Miller, P. J. & Matyjaszewski, K. Atom Transfer Radical Polymerization of (Meth)acrylates from Poly(dimethylsiloxane) Macroinitiators. *Macromolecules* **32**, 8760–8767 (1999).
35. Stein, J., Lewis, L. N., Gao, Y. & Scott, R. a. In situ determination of the active catalyst in hydrosilylation reactions using highly reactive Pt(0) catalyst precursors. *J. Am. Chem. Soc.* **121**, 3693–3703 (1999).
36. Savin, D. A., Pyun, J., Patterson, G. D., Kowalewski, T. & Matyjaszewski, K. Synthesis and characterization of silica-graft-polystyrene hybrid nanoparticles: Effect of constraint on the glass-transition temperature of spherical polymer brushes. *J. Polym. Sci. Part B Polym. Phys.* **40**, 2667–2676 (2002).
37. Pyun, J., Jia, S., Kowalewski, T., Patterson, G. D. & Matyjaszewski, K. Synthesis and Characterization of Organic / Inorganic Hybrid Nanoparticles : Kinetics of Surface-Initiated Atom Transfer Radical Polymerization and Morphology of Hybrid Nanoparticle Ultrathin Films. **336**, 5094–5104 (2003).
38. Ma, Q. & Wooley, K. L. The preparation oft-butyl acrylate, methyl acrylate, and styrene block copolymers by atom transfer radical polymerization: Precursors to amphiphilic and hydrophilic block copolymers and conversion to complex nanostructured materials. *J. Polym. Sci. Part A Polym. Chem.* **38**, 4805–4820 (2000).
39. Frisken, B. J. *Dynamic Light Scattering: Theory and Practice.* **8**, (2001).

40. Chevigny, C., Dalmas, F., Di Cola, E., Gigmes, D., Bertin, D., Boué, F. & Jestin, J. Polymer-grafted-nanoparticles nanocomposites: Dispersion, grafted chain conformation, and rheological behavior. *Macromolecules* **44**, 122–133 (2011).
41. Gibaud, T., Mahmoudi, N., Oberdisse, J., Lindner, P., Pedersen, J. S., Oliveira, C. L. P., Stradner, A. & Schurtenberger, P. New routes to food gels and glasses. *Faraday Discuss.* **158**, 267 (2012).
42. Frisken, B. J. Revisiting the method of cumulant for the analysis of dynamic light-scattering data. **40**, 4087–4091 (2001).
43. Misak, M. D. Equations for determining  $1/H$  versus  $S$  values in computer calculations of interfacial tension by the pendant drop method. *J. Colloid Interface Sci.* **27**, 141–142 (1968).
44. Rubinstein, M. & Colby, R. H. *Polymer Physics*. (2003). doi:10.1007/978-3-7091-0670-9
45. Aveyard, R., Clint, J. H., Nees, D. & Paunov, V. N. Compression and structure of monolayers of charged latex particles at Air / Water and Octane / Water interfaces. *Langmuir* **16**, 1969–1979 (2000).

